MISCELLANEOUS PAPER C-69-1

STRENGTH AND DEFORMATION PROPERTIES OF GRANITE, BASALT, LIMESTONE AND TUFF AT VARIOUS LOADING RATES

by

R. L. Stowe

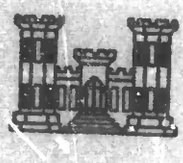

January 1969

Sponsored by

Defense Atomic Support Agency

Conducted by

U. S. Army Engineer Waterways Experiment Station
CORPS OF ENGINEERS
Vicksburg, Mississippi

BLANK PAGES
IN THIS
DOCUMENT
WERE NOT
FILMED

MISCELLANEOUS PAPER C-69-1

STRENGTH AND DEFORMATION PROPERTIES OF GRANITE, BASALT, LIMESTONE AND TUFF AT VARIOUS LOADING RATES

by

R. L. Stowe

January 1969

Sponsored by

Defense Atomic Support Agency

Conducted by

U. S. Army Engineer Waterways Experiment Station
CORPS OF ENGINEERS
Vicksburg, Mississippi

ARMY-MRC VICKSBURG, MISS.

THE CONTENTS OF THIS REPORT ARE NOT TO BE USED FOR ADVERTISING, PUBLICATION, OR PROMOTIONAL PURPOSES. CITATION OF TRADE NAMES DOES NOT CONSTITUTE AN OFFICIAL ENDORSEMENT OR APPROVAL OF THE USE OF SUCH COMMERCIAL PRODUCTS.

ABSTRACT

The objective of the work reported herein was to determine the strength and stress-strain characteristics of rocks of four types under various rates of loading. This was accomplished by conducting slow (specimens loaded at rates of less than 2,251 psi/sec) and rapid (specimens loaded at rates greater than 2,251 psi/sec) unconfined compression tests, tensile splitting tests, and triaxial compression tests utilizing confining pressures ranging from 250 to 5,000 psi. Granite, basalt, limestone, and tuff from the Atomic Energy Commission's Nevada Test Site, Mercury, Nevada, were used in this program. Nondestructive tests such as specific gravity, porosity, and compressional wave velocity were conducted on all specimens to determine homogeneity of each rock. Results of nondestructive tests indicated that the rock within each rock type was quite uniform. Results of the unconfined compressive strength tests on basalt indicated that as the loading rate was increased from 1 to 1.60×10^7 psi/sec, ultimate strength, total axial strain, and Young's modulus of elasticity increased. Total diametral strain decreased as loading rate was increased. Results of triaxial tests indicated that the maximum deviator stress and total axial strain increased as the confining pressure and loading rates were increased. Apparently, loading rates from 1 to 2,250 psi/sec do not have a significant effect on the

angle of internal friction and cohesion of basalt at confining pressures up to 5,000 psi. Compressional wave velocities recorded in the direction of applied stress increased sharply within about one-half of the maximum deviator stress and then generally remained constant to failure. The difference in the unconfined compressive strength between the slow and the rapid rates of loading for the rocks tested varied considerably. The dynamic compressive strength factor for the granite was less than 1; for the basalt, 1.35; for the limestone, 1.52; and for the tuff, 1.74. The compressional wave velocity of rock is affected by increases in both the applied axial stress and confining pressure. Velocities recorded in the direction of applied stress increase sharply within about one-half of the maximum deviator stress and then generally level off until failure.

PREFACE

The study reported herein was sponsored by the Defense Atomic Support Agency and funded under the Nuclear Weapons Effects Research Program Subtask 13.191A, "Rock Mechanics Research Relating to Deep Underground Protective Construction."

The work was conducted during the period October 1965 through October 1967 under the direction of Mr. Bryant Mather, Chief, Concrete Division, U. S. Army Engineer Waterways Experiment Station (WES). The investigation was conducted under the direct supervision of Messrs. J. M. Polatty, Project Officer, W. O. Tynes, and R. L. Stowe. Messrs. J. L. Drake and J. R. Hossley of the Nuclear Weapons Effects Division, WES, conducted the rapid loading tests. Mr. Stowe, who was project leader, prepared this report.

Directors of WES during the conduct of this study and the preparation of this report were COL John R. Oswalt, Jr., CE, and COL Levi A. Brown, CE. Technical Director was Mr. J. B. Tiffany.

CONTENTS

FIGURES

NOTATION

A	Area
c	Cohesion or shearing stress
d	Length of specimen, feet
E	Young's modulus of elasticity
E_t	Tangent Young's modulus at one-half the ultimate compressive strength
f'_{cd}	Dynamic compressive strength factor
G_s	Specific gravity of solids
G_o	Bulk specific gravity
P	Force
t	Pulse traveltime, milliseconds
T	Shearing stress
u	Pore pressure
V	Velocity
V_p	Compressional wave velocity
$\Delta\epsilon_a$	Change in axial strain
$\Delta\sigma$	Change in axial stress
ϵ_a	Axial strain
ϵ_d	Diametral strain
ϵ_v	Unit volumetric change
$\ddot{\epsilon}$	Loading rate, psi/sec

μ Poisson's ratio

σ Applied axial stress, maximum deviator stress, or total normal stress

σ' Effective stresses

σ_1 Major principal stress

σ_2 Intermediate principal stress

σ_3 Confining pressure, lateral pressure, or minor principal stress

ϕ Angle of internal friction

CONVERSION FACTORS, BRITISH TO METRIC UNITS OF MEASUREMENT

British units of measurement used in this report can be converted to metric units as follows.

Multiply	By	To Obtain
inches	2.54	centimeters
feet	0.3048	meters
pounds	0.45359237	kilograms
kips	453.59237	kilograms
pounds per square inch	0.070307	kilograms per square centimeter
pounds per cubic foot	16.0185	kilograms per cubic meter
foot-pounds	0.138255	meter-kilograms
feet per second	0.3048	meters per second

CHAPTER 1

INTRODUCTION

1.1 BACKGROUND

There has been, and still is, a great need for information concerning the strength and stress-strain characteristics of rock under various rates of loading $\dot{\varepsilon}$. This is particularly true for protective-construction purposes. For design purposes, it is necessary to know the mechanical properties of rock since they are used to predict and control the behavior of the in situ rock mass. Past studies of metals, concrete, and, to a small extent, rock have shown considerable strength and deflection changes when the rate of loading was increased.

There are two general approaches to the study of rock properties. The approach used for the work reported herein was one in which intact specimens were extracted from the joint blocks and tested in the laboratory. The results obtained are realized to be an upper (or lower) limit of the in situ strength value that would apply only if the in situ rock had no discontinuities. However, all rocks possess various discontinuities, and a strength reduction factor must be applied to modify appropriately the results obtained in the laboratory. It is understandable that the reduction factor is a function of the kind, spacing, orientation, and physical character of the

natural discontinuities present. There is no reduction factor presented in this report.

The second approach to the study of rock properties is that of field testing the rock in situ. In this testing environment, the test area should be sufficiently large so that the effect of discontinuities enters into the results. This type of testing is necessarily large-scale and expensive. Because of the expense, quite often only a few tests may be conducted, and the results may not be statistically significant. This is a good reason for conducting extensive laboratory testing in which the expense is low and the number of tests large. However, efforts should be made to correlate results of laboratory and in situ tests. If this is not done, the laboratory test results could be meaningless.

1.2 OBJECTIVE AND SCOPE

The objective of the research reported herein was to determine, under a wide range of loading rates, the strengths and stress-strain properties of rock specimens belonging to four rock types. The strength and stress-strain properties were determined in both an unconfined state and a confined state under confining pressures up to 5,000 psi.[1] A laboratory test was devised using a triaxial chamber

---

[1] A table of factors for converting British units of measurement to metric units is presented on page 12.

and sonic equipment in an effort to simulate the field in situ stress conditions. This test will be discussed in detail later. The objective was accomplished by: (1) a literature survey that consisted of a review of a collection of available experimental rock property data from tests on rock and information regarding details of the particular testing techniques used; and (2) a laboratory study that consisted of nondestructive and destructive testing of four rocks from the Atomic Energy Commission's Nevada Test Site (NTS) at Mercury, Nevada; the rocks were granite from the Operation Flint Lock, Shot Pile Driver Experiment, dense basalt from Buckboard Mesa, limestone from the Flat Top Experiment, and tuff from the Red Hot-Deep Well Experiment. The nondestructive tests run on all rocks consisted of bulk dry specific gravity, specific gravity of solids, porosity, and compressional wave velocity tests. The destructive tests consisted of tensile splitting strength, slow[2] unconfined compressive strength, Young's modulus of elasticity, Poisson's ratio, triaxial compressive strength, and rapid[3] unconfined compressive strength tests. A few direct tension tests were run on the granite only.

---

2 "Slow loading" in this report denotes that specimens were loaded at rates less than 2,251 psi/sec.

3 "Rapid loading" denotes that specimens were loaded at rates greater than 2,251 psi/sec.

During the literature survey, particular attention was given to those articles and papers that pertained to the following: (1) the effect of loading rate on stress-strain properties, strength, and strain at failure; (2) the effect of confining pressure on stress-strain properties, strength, and strain at failure; and (3) the effect of confining pressures on the compressional wave velocity of rock.

1.3 LITERATURE SURVEY

From the available literature, it is evident that not many previous investigators have been concerned with the effect of loading rate on the stress-strain properties, strength, and strain at failure of rock. The articles found concerning this effect (References 1 through 3) generally indicated that an increase in the loading rate increased the ultimate unconfined compressive strength and increased the Young's modulus of elasticity (a stress-strain property). Data from other tests with increased loading, such as impact and sonic tests, show that the strength and Young's modulus of elasticity can increase by as much as a factor of two (Reference 4). Figure 1.1 is a plot of stress rate versus ultimate strength that shows a considerable increase in ultimate strength when the stress rate is increased from 10 to about 10^{11} psi/sec. The maximum stress rate used for the rapid testing reported herein was about 10^{7} psi/sec. Figure 1.2 shows the

dependence of the stress-strain curve on time of loading and shows a decrease in strain at failure when the stress rate is increased (Reference 4). Results of the research reported herein show that this is not always true.

There were many articles found during the literature survey that dealt with the effect of confining pressure on stress-strai· properties, strength, and strain at failure for a wide range of rock (References 5 through 15).

References 5 and 6 present the works of some of the first investigators who attempted to determine the effect of confining pressure on the strength of rock. These early investigators applied axial loads to rock samples that were encased by a very tight-fitting steel jacket. A drawback to this method of confining samples was that the steel jacket restricted the lateral expansion of the rock, and a pressure normal to the axis of loading was created at the rock-steel boundary. The results of these investigations can be summarized by stating that the ultimate strength and ductility of rock increase with increased confinement (Reference 7). However, due to the type of constrainment of the samples, no exact relation between confining pressure and increased strength could be established.

In 1911, the inherent inadequacies of steel-jacketed testing of rock samples were recognized and worthwhile improvements were made, both to the testing apparatus and the method of constraining the rock

(Reference 8). From tests on marble and sandstone, a relation between confining pressure and rock strength was established. The results of these tests were presented in terms of Mohr's circles, from which it was concluded in Reference 8 that: (1) rock strength is greatly increased by a lateral confining pressure, and (2) Mohr's theory can be used to represent triaxial test data on rock. Since the early 1900's, investigators have made extensive refinements both in testing apparatus and method of jacketing samples; however, the conclusions drawn in Reference 8 remain basically unchanged. In almost all the work referred to in References 5 through 15, it was found that both axial and lateral strain increased with increasing confining pressure on rock samples. The increase of compressive strength caused by confining pressure is many times higher than that caused by increased stress rates (Reference 4).

Many investigators have been concerned with the effect of confining pressures on the compressional wave and shear wave velocities of various rocks (References 16 through 31). Most of the early work was conducted in the interest of geophysical problems in which the interpretation of seismic velocities in petroleum exploration was most important. However, in the late 1930's, laboratory measurements were made of elastic waves in rock (Reference 16). In the 1950's, new developments in pulse circuitry, fast-writing oscilloscopes, and other electronic equipment were used to investigate wave velocities in rock

as well as in many other materials (References 18 through 24).

One way to investigate wave velocities in rock as affected by pressure is to record velocities in three different orientations at right angles to one another. This adequately indicates the degree and variations of anisotropy of the material. In some of the more homogeneous rocks, the three velocities are within a few percentage points of one another; this is true for equigranular rocks. In schistose and bedded rocks, velocities can vary up to 25 percent, depending on orientation. The greatest controlling variable of velocity appears to be the density of the material (Reference 25). It is stated in Reference 25 that, except for the most compact rocks, little significance should be attached to the velocities for pressures below 500 bars (7,250 psi); they are not reliably reproducible to better than 10 percent.

The velocities recorded in the direction of applied stress for almost all rocks increase toward failure and usually remain constant at failure. Velocities recorded normal to the applied stress in most rocks increase sharply, level off, and then decrease toward failure. A logical reason for this is given in Reference 27. When a specimen begins to fail, internal vertical cracking normally develops. Although the velocities parallel to the load are not affected by the cracks, the velocities normal to the cracks must travel around the cracks and are, therefore, slower. Figure 1.3 shows the variation of

wave velocities with stress in the axial and the transverse directions under various confining pressures.

In the literature search, a considerable amount of rock property data was found concerning a wide range of physical properties of different rock types. A tabulation of these properties has been compiled and will be published separately from this report. The tabulation contains 58 different physical properties along with some ratios of physical properties. This table was compiled as a reference source for those working in the field of rock mechanics.

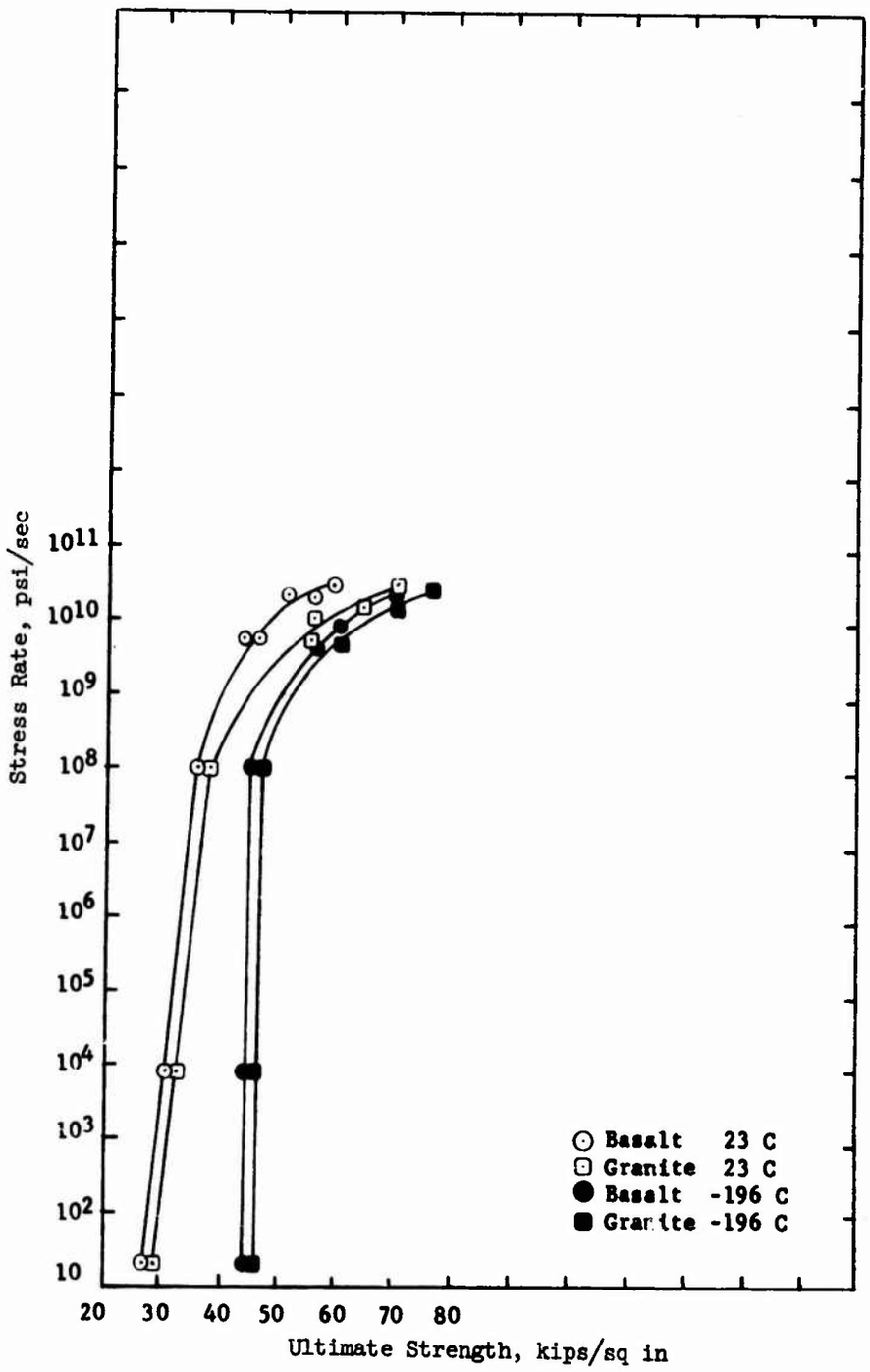

Figure 1.1 Effect of loading rate on ultimate compressive strength (after Reference 1).

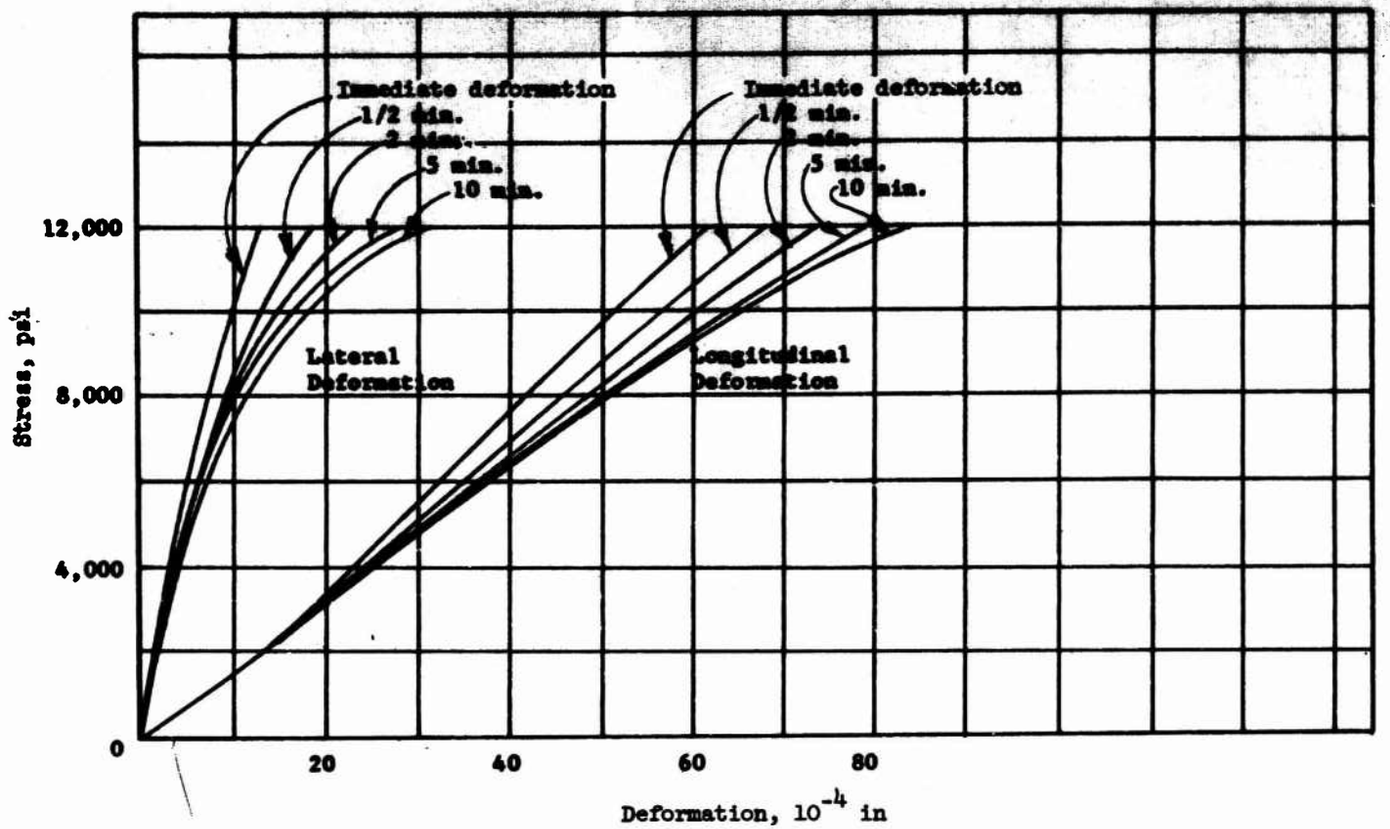

Figure 1.2 Effect of time of loading on stress-strain diagram, compression (after Reference 4).

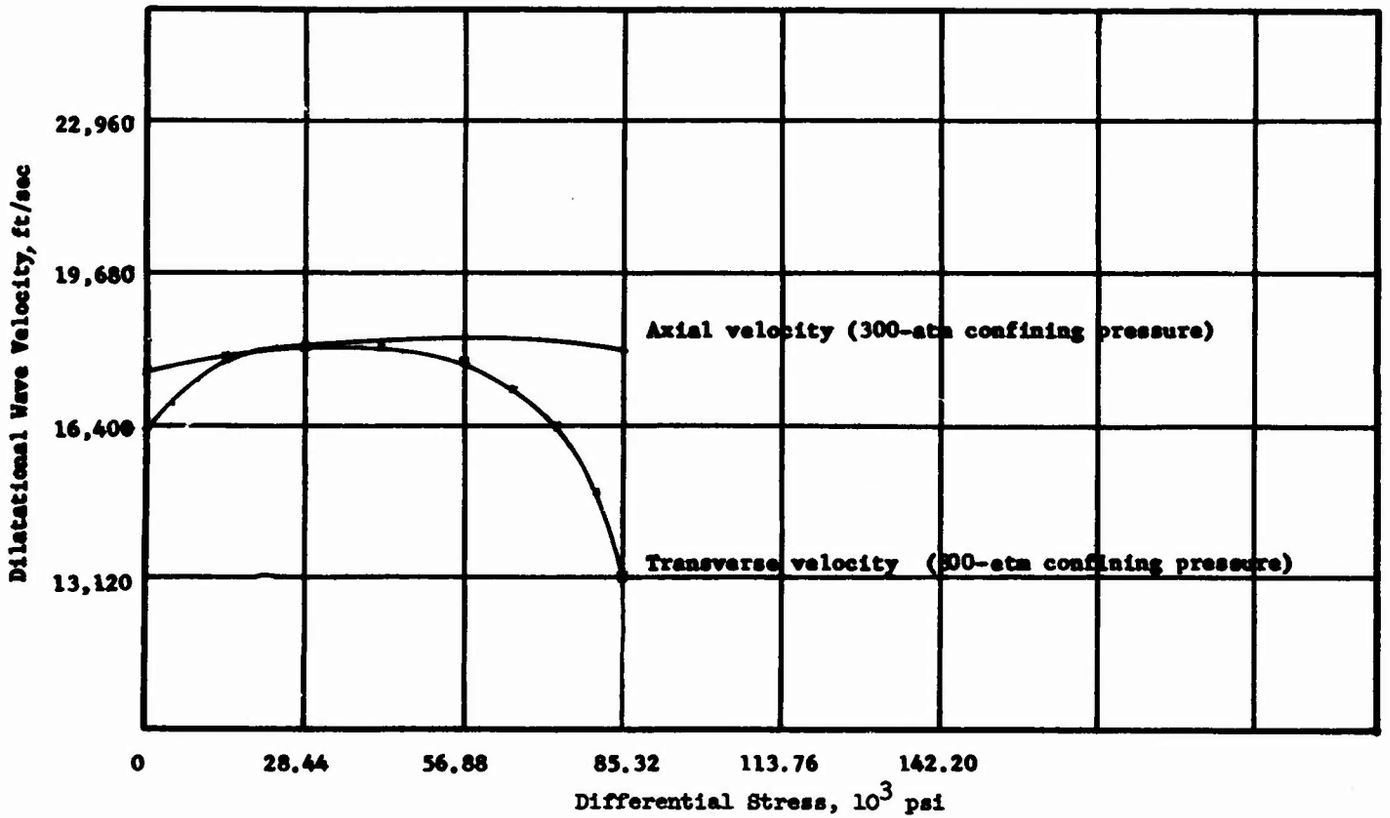

Figure 1.3 Effect of compressional stresses on the wave velocity in the axial and transverse directions under confining pressures.

CHAPTER 2

MATERIALS AND TEST METHODS

2.1 ROCK TYPES

The four rock types used in this program were to meet the following criteria: (1) they were to be taken from sites where weapons tests had been performed or were to be performed, and (2) they were to fit roughly into the strength classification system (Engineering Classification of Intact Rock) developed at the University of Illinois (Reference 32). The rocks are classified according to their unconfined compressive strength into five groups. Group A is for very high strength rocks, above 32,000 psi; Group B is for high strength rocks, which range from 16,000 to 32,000 psi; Group C is for medium strength rocks, which range from 8,000 to 16,000 psi; Group D is for low strength rocks, which range from 4,000 to 8,000 psi; and Group E is for very low strength rocks, which range from zero to 4,000 psi.

Granodiorite (granite) from the Operation Flint Rock, Shot Pile Driver Experiment at the NTS, taken from depths of 11.1 to 1,759.9 feet, was used for both Groups A and B. The unconfined compressive strength of the rock varied from about 19,000 to 34,000 psi; this made it necessary to classify the rock under both Groups A and B. The rock was a light gray, dense, coarse-grained, unweathered granodiorite. According to the classification system presented in

Reference 33, this rock is called a granodiorite or granite. The rock will be referred to as a granite in this report. Plagioclase feldspar having an average composition in the high oligoclase-low andesine range, orthoclase, and quartz were the most abundant constituents. Biotite, some of which was in the process of altering to chlorite, was present in moderate amounts. Accessory minerals present in very minor amounts were sphene, an amphibole, an epidote-group mineral, pyrite, and magnetite. Small patches of pyrite were disseminated throughout the rock and were present, along with quartz, in sealed fractures.

Dense basalt from Buckboard Mesa, NTS, taken from depths of 13.2 to 157.1 feet was used for Group B rocks. The rock was a light gray, dense, fine-grained, unweathered basalt or subandesite, and was composed of plagioclase feldspar, with lesser amounts of pyroxene, olivine, and magnetite.

Limestone from the Flat Top Experiment, NTS, taken from depths of 5.5 to 82.0 feet, was used for Group C rocks. The rock was a light olive-gray, dense, very fine-grained limestone containing some stylolite seams. The seams were not planes of weakness within the rock but were areas of concentration of the relatively insoluble part of the limestone; X-ray diffraction analysis indicated that the material was composed of clay mica (illite) and quartz. In thin

sections, the rock consisted of fine-grained calcite and coarser dolomite. The rock contained 30 to 40 percent dolomite, and was tightly cemented.

Tuff from the Red Hot-Deep Well Experiment, NTS, taken from depths of 0.0 to 76.0 feet, was used for Group E rocks. The rock varied in color from a light greenish-yellow, to a brownish-red, to a dark red. It was composed of volcanic ash and was fairly well welded.

2.2 SAMPLE PREPARATION

The rock cores used for this program were NX (2-1/8-inch diameter) in size. The cores were cut to have a length-to-diameter (L/D) ratio equal to two using a diamond-blade, masonry-rock saw. After the cores had been cut to proper size, the ends were surface ground with a machine shop surface grinder. The core ends were then hand lapped with No. 320 Carborundum abrasive to obtain plane end surfaces; the end surfaces were within 0.001 inch planeness, were parallel to each other within 0.006 inch, and were perpendicular to the sides within 0.5 degree.

2.3 STRAIN GAGES

The rock cores tested in unconfined and confined compression had six 13/16-inch-long electrical-resistance strain gages bonded to the core; three gages were placed vertically 120 degrees apart, and three

were placed horizontally 120 degrees apart. All gages were located at the midpoint of the core, and had a resistance of 120.4 $\pm$ 0.2 ohm, and a gage factor of 2.01 $\pm$ 0.01 percent.

2.4 NONDESTRUCTIVE TEST METHODS

In order to obtain nearly homogeneous specimens for destructive testing, a series of nondestructive tests was performed on all rock cores. The tests included bulk specific gravities, specific gravities of solids, porosities, and compressional wave velocities. The bulk specific gravity of a rock core is the ratio of the weight in air of its volume of permeable material at a stated temperature to the weight in air of an equal volume of distilled water at a stated temperature. The specific gravities determined for the granite, basalt, and limestone were ovendry determinations; the tuff specific gravity was an as-received determination. The specific gravity of solids in rock is the ratio of the weight in air of a given volume of solids at a stated temperature to the weight in air of an equal volume of distilled water at a stated temperature. The rock porosity value was obtained by using the specific gravity values as follows:

$$\frac{G_s - G_o}{G_s} \times 100\%$$

where,

G_s is the specific gravity of solids, and

G_o is the bulk specific gravity.

A through-sample method is used to measure compressional wave velocity. A transducer is coupled to each end of the sample by a film of silicone grease. The transducers used in this investigation were barium titanite with a lower resonant frequency of 1 Mc/sec. A pressure impulse is imparted to the sample from the expansion of a transducer caused by a step in voltage being applied to the transducer. The incidence of the transmitted pressure impulse on the receiving transducer generates a voltage signal indicating this arrival. These signals are displayed on an oscilloscope and compared with a signal from a crystal-controlled, time-mark generator for determining the transit time through the sample. From this measurement of time and the known transmissive-path length, the compressional wave velocity can be computed.

2.5 DESTRUCTIVE TEST METHODS

The slow tests consisted of tensile splitting, direct tensile, unconfined compressive strength, and triaxial compressive strength tests using compressional wave velocity equipment. The tensile splitting tests were conducted in accordance with Test Method CRD-C 77-61 of Reference 34. The unconfined compressive strength tests were conducted in accordance with Test Method CRD-C 19-65, except that the specimen ends had closer tolerances. Three specimens each of granite, basalt, limestone, and tuff were loaded at a rate of 50. psi/sec.

Based on nondestructive and destructive test results, the basalt rock was selected for extensive confined and unconfined compressive testing; that is, loading rates of 1, 500, and 2,250 psi/sec for confined tests and 1, 500, 2.00×10^5, 3.00×10^6, and 1×10^7 psi/sec for unconfined tests. The triaxial compressive strength tests were conducted in accordance with Test Method CRD-C 93-64, except that compressional wave velocity equipment was used to determine the effect of axial and lateral pressures on compressional wave velocities through the long axes of the samples.

The principle of triaxial testing is summarized briefly as follows. A cylindrical specimen encased in a flexible membrane is placed in a triaxial chamber, subjected to a constant lateral fluid pressure, then loaded axially to failure. The flexible membrane excludes the fluid from the specimen, thereby maintaining a constant degree of saturation of the specimen during the test. At least three specimens, each under a different lateral pressure, are tested to failure to establish the relation between shear strength and normal stress. During the application of axial load, the major principal stress σ_1 is equal to the applied axial stress $\sigma (\sigma = P/A)$ where P equals force and A equals area plus the lateral pressure σ_3. The applied stress is termed the deviator stress. The intermediate principal stress σ_2 and the minor principal stress σ_3 are assumed to be identical and are equal to the lateral pressure used in the test.

Confining pressures of 250, 1,000, and 5,000 psi were selected as reasonable pressures for the triaxial testing.

The method of using wave velocity apparatus in conjunction with triaxial equipment is relatively new. Figure 2.1 is a sketch showing the triaxial chamber and the accessories used inside the chamber for velocity determinations. The measurement of velocity through the rock sample is accomplished in a manner similar to the measurement described for the unconfined samples. However, in the chamber it is necessary to use end plates (housing the transducers) and bearing plates, which allow for a size reduction to the NX size samples. In this study, aluminum end plates and bearing plates were used because the impedance of aluminum is closer to that of most dense rock than any other material available. The traveltime through the end plates and the bearing plates is accurately measured prior to testing; this traveltime is the delay time that is subtracted from the traveltime through the plates and rock sample. The equation $V = \frac{d}{t}$ was used to obtain the compressive velocity where V is the velocity, d is the length of the specimen in feet, and t is the pulse traveltime through the sample in milliseconds.

Commercially available barium titanite transducers were used with no change except for light hand lapping of the flat surfaces to ensure even contact. A light film of oil was applied to the core end surfaces to fill any small irregularities that may have

been present on the specimen ends. The aluminum plates were the wrought-type No. 14 S-T having a yield strength in compression of 60,000 psi and a modulus of elasticity of 10.6×10^6 psi. Connections between the transducers and the recording equipment were made with coaxial cables; 50-ohm cables about 0.08 inch in diameter were used.

A Hewlett-Packard 212-A square-wave voltage generator was altered to produce a peak voltage of 200 volts. This was needed for the longer transmission path. The oscilloscope used was a Tektronix, Type 551, dual beam, with a Tektronix 1121 amplifier. This system was sufficient for detection of the low-level signals produced at the receiving transducer over the increased transmission length. A Tektronix 181 time-mark generator was used to measure pulse length.

The rapid tests were accomplished using two separate testing apparatuses, a drop-tower facility and a hydraulic-operated 200-kip loader. The drop-tower facility had a capability of 2,012 ft-lb of energy, and consisted of a falling mass weighing 384 pounds guided by two cylindrical steel columns. The mass was remotely triggered and allowed to fall free from a predetermined height. Friction brakes built into the falling mass prevented any rebound of the mass after impact. A 200,000-pound-capacity SR 4 type load cell, two single-sweep dual-beam oscilloscopes, and two Polariod cameras were used to record the stress-strain traces. A 0.5-inch-thick piece of Celotex

was placed on top of the rock sample to mitigate the pulse. The tuff rock was tested using the drop-tower apparatus.

The 200-kip loader consisted of a large hydraulic actuator and a rigid support system as shown in Figure 2.2. The actuator is pressurized with a low-volume, high-pressure multiplier. The actuator has three pressure chambers producing pressure above the piston, below the piston, and between the rupture disks. The rupture disks perform the task of a rapid-opening valve. The machine is pressurized by slow buildup of pressure above and below the piston while a slight preload on the specimen is maintained. Concurrently, pressure is built up in the volume between the two rupture disks; the pressure between the rupture disks is maintained at exactly one-half the pressure below the ram, thereby enabling half the total pressure below the piston to be supported by the first rupture disk and the remaining half of this total pressure to be supported by the second rupture disk. When the machine is triggered, the rupture disks burst and move the loading ram onto the specimen, which is positioned below the ram.

This loader is capable of applying a 200,000-pound force to a rigid specimen with rise times of approximately 1.5 msec; longer rise times can be created by placing a suitable orifice upstream of the rupture disk assembly. The slowest loading rates obtained to date have been about 2.0×10^5 psi/sec. Total stroke of the ram is 4 inches.

The load is measured above and below the test specimen by means of strain-gage type load cells. Accelerations are measured above and below the specimen by means of commercial-type accelerometers. The outputs of all the sensing devices are recorded simultaneously on a multichannel, magnetic tape recorder and later played back using a light-beam galvanometer oscillograph.

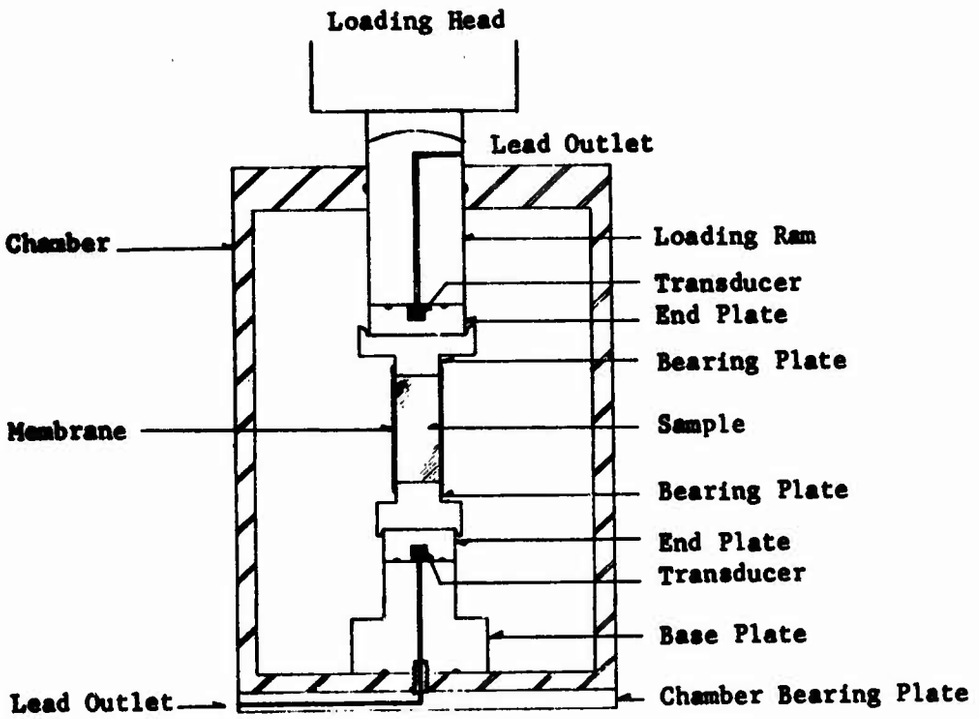

Figure 2.1 Triaxial chamber with transducers.

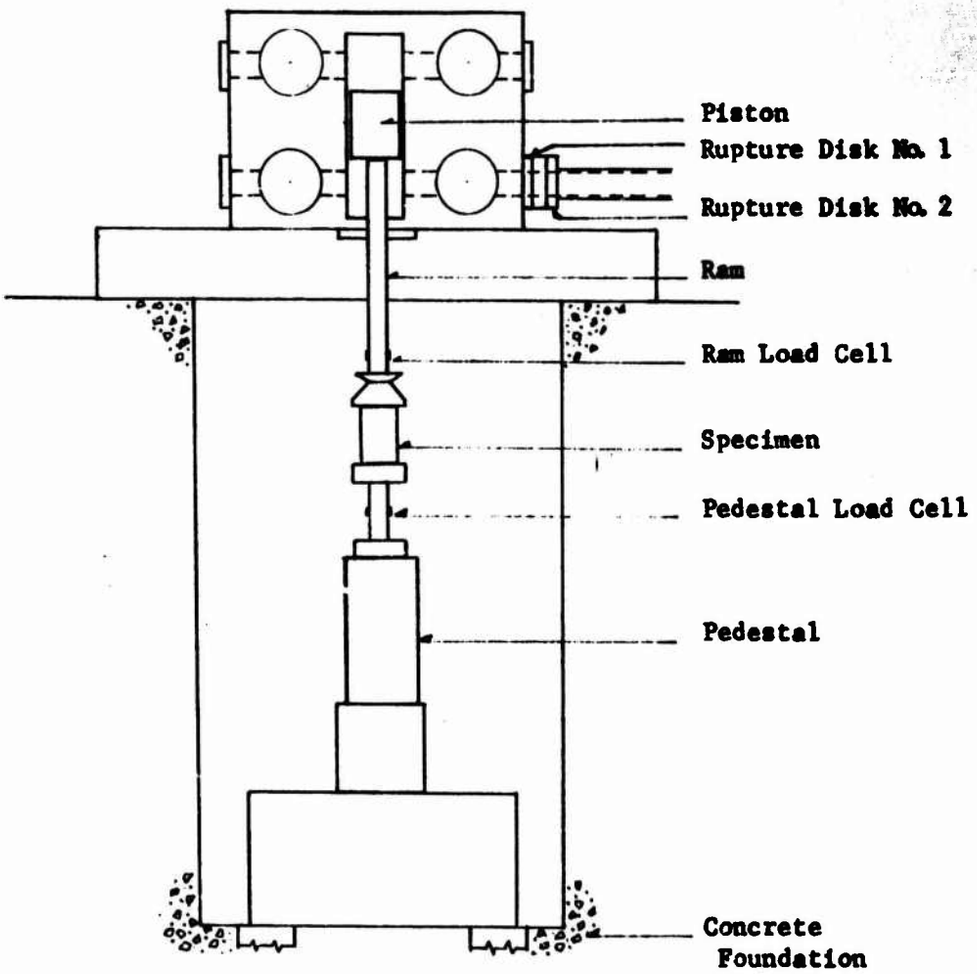

Figure 2.2 200-kip dynamic loader.

CHAPTER 3

PRESENTATION AND DISCUSSION OF RESULTS

Visual appearance and physical test results, particularly the nondestructive results, indicated that within each rock type the rocks were reasonably uniform. The variations in test data within a rock type are best explained by (1) the slight change in mineral content and inherent structure from one sample to the next; (2) the difference in specific gravities; (3) the difference in porosity; and (4) the chance for human error in sample preparation and in conducting the tests.

Due to the limited supply of granite rock cores, it was necessary to use cores from six different boreholes. The basalt cores were obtained from eight different boreholes; however, the depth interval from which they were taken was small. Based on a visual examination and an analysis of the nondestructive properties, the basalt cores were deemed very nearly the same. The limestone cores were taken from three separate boreholes, and the tuff cores were taken from one borehole.

Forty pieces of granite core were visually examined, and based on texture, presence or absence of fractures, gross grain size, and whether the cores were weathered or altered, 25 pieces were selected for nondestructive testing. Based on an analysis of the nondestructive

properties of the cores, 13 samples were used for destructive testing. Thirty-nine basalt samples were selected for nondestructive testing, from which 31 samples were selected for destructive testing. Twenty samples of limestone were tested for nondestructive properties, from which 12 were used for destructive testing. Thirty-one tuff samples were tested for nondestructive properties, from which 12 samples were used for destructive testing. Tables 3.1 through 3.4 list the nondestructive and destructive properties of the granite, basalt, limestone, and tuff, respectively. A summary of the nondestructive physical properties is given in the following paragraphs.

3.1 NONDESTRUCTIVE TESTS

The range in bulk specific gravity, the difference between the low and high specific gravity values, the average specific gravities, and the density difference are given in the following tabulation for the four rock types tested. Similar data with regard to specific

Rock Type	Range of Bulk Specific Gravity	Difference	Average Bulk Specific Gravity	Density Difference
				pcf
Granite	2.66 to 2.71	0.05	2.69	3.11
Basalt	2.65 to 2.77	0.12	2.70	7.35
Limestone	2.68 to 2.72	0.04	2.70	2.55
Tuff	1.89 to 1.98	0.09	1.92	5.73

gravity of solids are given below for the four rock types tested.

Rock Type	Range of Specific Gravity of Solids	Difference	Average Specific Gravity of Solids	Density Difference
				pcf
Granite	2.68 to 2.71	0.03	2.69	2.18
Basalt	2.81 to 2.84	0.03	2.83	1.68
Limestone	2.70 to 2.73	0.03	2.72	1.93
Tuff	2.33 to 2.49	0.16	2.39	9.90

The range in the calculated porosity for the granite was 0.10 to 0.75 percent or a difference of 0.65 percent; the average porosity for the 20 samples selected for destructive testing was 0.30 percent. The range in the calculated porosity for the basalt was 3.07 to 5.37 percent; the average porosity for the 16 samples selected for destructive testing was 4.60 percent. The range in the calculated porosity for the limestone was 0.18 to 0.85 percent; the average porosity for the 13 samples selected for destructive testing was 0.46 percent. The range in the calculated porosity for the tuff was 15.90 to 23.30 percent; the average porosity for the 12 samples selected for destructive testing was 19.82 percent.

The compressional wave velocity was the only nondestructive physical property that varied greatly for the four rock types. The

following tabulation gives the range in velocity, the difference, and the average velocity for those rock samples that were destructively tested.

Rock Type	Range in Compressional Wave Velocity	Difference	Average Compressional Wave Velocity
	ft/sec	ft/sec	ft/sec
Granite	17,400 to 19,440	2,040	18,450
Basalt	15,270 to 17,760	2,490	16,630
Limestone	19,885 to 22,320	2,435	20,710
Tuff	6,597 to 8,810	2,213	7,890

The reproducibility of the compressional wave velocity through the aluminum transducer holders and of the electronic components used in conjunction with the transducers was checked and found to be very good. The difference in the velocity, later referred to as the delay velocity, of the aluminum holders for a series of nine readings was less than one percent.

Prior to testing the cores for compressional wave velocities, a granite and a basalt sample were tested for reproducibility of wave velocities. A series of six velocities was recorded for each sample; this was accomplished by placing the core between the transducers, recording the velocity, and then removing the core. The difference in the velocities for the granite was 2.6 percent and for the basalt was

3.0 percent. This difference is attributed to the fact that the first signal arrival is not sharply defined on the oscilloscope trace. In most cases, however, the signal was fairly sharp. Figures 3.1 and 3.2 are typical photographs of the wave velocity trace recorded for the four rock types used in this work. The signal arrival for the tuff samples was less distinct than that for the other three rock types.

3.2 DESTRUCTIVE TESTS

The average results of three tensile splitting tests for the four rock types are given below.

Rock Type	Average Tensile Splitting Strength	Direct Tension	Range in Strength	Ratio of Compressive Strength to Tensile Strength at 50-psi/sec Loading Rate
	psi	psi	psi	
Granite	1,700	1,700	380	12:1
Basalt	1,900	--	300	13:1
Limestone	1,210	--	390	9:1
Tuff	170	--	120	10:1

Direct tension tests (pull tests) were conducted on the granite in order to compare direct tension results with the results of the tensile splitting test (see Figure 3.3 for stress-strain test results). A comparison of the average strengths obtained from these two tests

shows that the average strengths are identical; however, the range of individual data is greater for the tensile splitting test than for the direct tension test There is very little data from which to conclude any distinct advantage of one method of tensile testing over the other; however, the test results indicate that the direct pull method is more consistent. Logically, the direct method should give a truer tensile strength because when the sample is pulled, it will fail along its weakest plane, wherever that plane may be. In the tensile splitting test, the plane selected for testing need not necessarily be the weakest. The modulus of elasticity in tension is quite close to the modulus calculated for specimens tested in unconfined compression.

There were three static unconfined compressive strength tests conducted for each of the four rock types at a loading rate of 50 psi/sec. The basalt was then tested at 1, 500, 2.00×10^5, 3.13×10^6, 1.29×10^7, 1.34×10^7, and 1.60×10^7 psi/sec. A modulus of elasticity E and a Poisson's ratio μ were calculated for each unconfined compression specimen tested. The modulus of elasticity is a value calculated at one-half the ultimate strength, i.e., $E = \frac{\Delta\sigma}{\Delta\epsilon_a}$, where $\Delta\sigma$ is the change in axial stress, and $\Delta\epsilon_a$ is the change in axial strain. Poisson's ratio is also calculated at one-half the ultimate strength, i.e., $\mu = \frac{\epsilon_d}{\epsilon_a}$, where ϵ_a is the axial strain and ϵ_d is the diametral strain. The modulus of elasticity and Poisson's

ratio calculated for the twelve unconfined compression tests are given in Tables 3.1 through 3.4.

The modulus of elasticity values calculated for the static unconfined compression tests run on the granite rock compare quite closely with the in situ values reported in Reference 35. The work in Reference 35 was conducted on rock similar to that tested in this investigation. The average modulus values for Sites 1 and 2 of Reference 35 were 8.91×10^6 and 9.73×10^6 psi, respectively. The average modulus for the granite cores tested during this project was 10.70×10^6 psi.

The unit volumetric strain was also calculated for the unconfined compression and the triaxial compression tests reported herein. This value was plotted with the stress versus axial and diametral strain curves to determine at what stress level the instantaneous rate of change of volumetric change is zero; the volumetric change is zero when the slope of the volumetric strain curve changes sign. Unit volumetric strain was also plotted to determine if it could be correlated with a significant change in compressional wave velocity on the deviator stress versus compressional wave velocity curve. It was felt that when the volumetric strain was constant, possibly indicating that internal microcracks were closed, the compressional wave velocity might be at its highest level. The results of this comparison will be given with the discussion of triaxial testing. According to the theory of elasticity, the unit volumetric change is given by:

$$\epsilon_v = \frac{1 - 2\mu}{E} (\sigma_1 + \sigma_2 + \sigma_3) \qquad (3.1)$$

where μ is the Poisson's ratio and E is the modulus of elasticity taken at one-half the ultimate compressive strength.

The tuff samples tested in unconfined compression at natural water content had compressional wave velocities V_p recorded parallel to the applied stress at various increments of applied stress. These tests were conducted in order to compare the change in velocity in the unconfined state with the change in velocity in the confined state, i.e., in the triaxial compression test. Figure 3.4 shows the change in compressional wave velocity with a change in the axial stress for the tuff samples, and Figure 3.5 shows the V_p data obtained from triaxial testing. A comparison of Figures 3.4 and 3.5 shows that the compressional wave velocity of tuff is affected more by combined stresses σ_1 and σ_3 than by axial stress alone. The average initial velocity for samples tested in unconfined compression (Figure 3.4) was 6,980 ft/sec, while the average velocity for these samples at failure was 8,300 ft/sec. This was an increase due to axial loading of 1,320 ft/sec. The average initial velocity for samples tested under combined stresses was 7,340 ft/sec, while the average velocity at failure up to 1,500 psi, σ_3, was 9,130 ft/sec. This was a 1,790-ft/sec increase. The compressional wave velocity increased faster under combined stresses than under axial stress only. This was due to the fact

that a confining pressure tends to consolidate the specimen uniformly, thereby closing internal cracks and causing V_p to increase more sharply.

Generally the granite specimens tested in unconfined compression at both slow and rapid rates of loading failed in shear; however, a few failed by vertical splitting. Two basalt specimens tested at a loading rate of 50 psi/sec failed on high-angle planes of approximately 70 degrees, and one failed by vertical splitting.

The three limestone specimens failed by vertical splitting, while the tuff specimens failed on planes approximately 65 degrees from the horizontal. The high shear angle, approximately 65 degrees for the granite and the basalt, was probably caused by localized stress concentrations within the constrained regions of the specimens. If the specimen length-to-diameter ratio were increased from 2 to about 2.5, then possibly the failure angle would develop in the specimen midsection outside the constrained regions. Typical basalt shear breaks are shown in Figure 3.6.

Most of the available rock mechanics literature that was received showed that brittle rock, such as granite and basalt, fails by vertical splitting when tested in unconfined compression. This has been the case at the WES laboratory in the past. However, it was found that when the specimen ends of brittle rocks were surface ground, hand lapped, and tested without a capping material, higher unconfined

compressive strengths and pronounced shear failures were obtained. This was found to be true at various rates of loading when the samples were held within close tolerances; the ends were ground plane to 0.001 inch, were perpendicular to the side of the specimen within 0.5 degrees, and were parallel to within 0.006 inch.

Figures 3.7 through 3.31 show the relation of stress to axial, diametral, and volumetric strains of rock specimens tested in unconfined compression. The slow stress-strain curves for the granite, basalt, and limestone rocks behave elastically to failure, and the mode of failure is brittle. The rapid stress-strain curve for the granite behaves elastically to about 90 percent of ultimate strength. The rapid stress-strain curves for the basalt behave elastically to about 45 percent of ultimate strength, then behave plastically to failure. The rock is characterized by a slight ductile failure. The dynamic stress-strain curves for the limestone are highly irregular; however, there is no clear explanation for this. Both the slow and rapid stress-strain curves for the tuff rock behave plastically, then elastically, and then plastically again towards failure; the mode of failure is ductile.

Results of the slow and the rapid unconfined compression tests show a significant difference in ultimate strength and total axial strain with the exception of the granite. The granite (Operation Flint Lock, Shot Pile Driver, NTS) used for the unconfined compressive

strength tests was weaker than the same granite tested in the past at the Concrete Division, WES, and at the Missouri River Division Laboratory, Omaha, Nebraska. Previous tests have shown that the slow compressive strength of the Pile Driver granite ranges from about 19,000 to about 31,000 psi, with an average of 25,000 psi (Reference 36). Evidently, the granite cores used for testing in this program were at the lower end of the strength range. The dynamic compressive strength factor f'_{cd} for granite was less than one.

Both strength and total axial strain at failure for the limestone and the tuff increased under rapid loading. The f'_{cd} for the limestone was 1.52, and the axial strain at failure under rapid loading was approximately 2.6 times greater than the strain under slow loading. The f'_{cd} for the tuff was 1.74, and the increase in axial strain at failure was about 2,267 μin, or about 1.6 times greater under rapid loading. The tuff f'_{cd} appears to be quite high compared with that of the other two rock types; however, additional rapid testing would have to be done to determine the validity of this factor.

As stated earlier, the basalt rock was selected for further confined and unconfined compressive testing. Additional triaxial tests were run at loading rates of 1, 500, and 2,250 psi/sec, and additional unconfined tests were run at loading rates of 1, 500, and 2.06×10^5 psi/sec. In summary, the loading rates for the basalt

rock ranged from 1 to 1.60×10^7 psi/sec. The average slow compressive strength of the basalt was 21,460 psi, and the rapid compressive strength was 29,020 psi. This is an increase of 7,560 psi for a compressive strength factor f'_{cd} of 1.35. The difference between the average rapid and the average slow axial strain at failure was 2,940 μin/in, with the rapid strain being greater. Slow diametral strain at failure was slightly greater than the rapid strain at failure, i.e., 140 μin/in greater. Figures 3.32 and 3.33 show the effects of increased rates of load on the unconfined compressive strength and total axial strain at failure of the basalt specimens. It can be seen from these graphs that loading rates up to 500 psi/sec do not have a pronounced effect on total axial strain and only a slight effect on the compressive strength. However, at higher rates of loading both strength and axial strain increase considerably. Figure 3.32 is a plot of the relation between loading rates and ultimate compressive strength. This plot definitely shows a considerable increase in strength with an increase in rate of loading. The curve of best fit for the data is very good for both ends of the curve; however, the center portion of the curve could be improved considerably if additional data were obtained between decades 10^3 and 10^6. The data were fitted with a least-squares polynomial curve fit program taken to the third order, GE program No. CD 225H6.004, with the form $y = a + bx + cx^2 + dx^3$.

Intuitively one might expect that total axial strain at failure would decrease with an increase in rate of loading. This is graphically shown in Figure 1.1 for relatively low rates of loading. However, the test data presented herein show this not to be true at faster loading rates. Reference 37 reports that similar results were observed during testing of concrete cylinders utilizing stressing rates ranging from 7.1 to 1.7×10^6 psi/sec. Results of tests reported in Reference 38 also indicated an increase in axial strain at failure with an increase in stressing rates.

One explanation for the increase in rapid axial strain at failure over slow axial strain at failure may be the fact that as the rock begins to fail under dynamic loading, the rock midsection on which the strain gages are bonded breaks away intact and continues to strain. High-speed movies taken at WES of rock cores failing under rapid loads show that the core fails in a cone break. This type of break normally leaves the midsection intact after failure.

A curve of best fit for the strength-strain data shown in Figure 3.33 was judged to be in the form of a curvilinear equation of form $y = ax^b$. The solution for the equation coefficients, a and b, and other pertinent statistical parameters was handled by a computer program, OCE No. 04-G1-Z5-002 (Reference 39). This program uses the method of least squares for a curvilinear regression to determine the

equation coefficients of the line of best fit for the input data.

Figure 3.34 shows the relation of loading rate and total axial strain at failure for basalt. Figure 3.35 shows that with an increase in loading rate, the total diametral strain at failure decreases slightly. Figure 3.36 shows the relation of loading rate and modulus of elasticity taken at one-half the ultimate compressive strength. The variation in modulus at a given loading rate is quite wide, and additional data should be developed to verify the increase in modulus with increased rates of loading. Curves of best fit were obtained by using the previously mentioned OCE computer program.

Figures 3.37 through 3.58 show the relation of deviator stress $(\sigma_1 - \sigma_3)$ to axial, diametral, and volumetric strains. Figures 3.59 through 3.61 and Figure 3.5 give results of the compressional wave velocity tests and show the relation between wave velocity and deviator stress. Figures 3.62 through 3.68 are plots of Mohr circles that show the relation of normal stress to shearing stress; the angle of internal friction ϕ and the shearing stress c are given for each rock type. These figures also show the observed failure plane in the core. Data from basalt rock tested in triaxial compression at loading rates of 1, 50, 500, and 2,250 psi/sec are interesting in regard to the loading rates at a specific confining pressure σ_3. Figure 3.52 shows that at σ_3's of 250 and 1,000 psi the maximum deviator stress σ increased with increased loading rate except for the

specimens loaded at 50 psi/sec. At a σ_3 of 5,000 psi, σ increased throughout the full range of loading rates used. Total axial strain increased in all cases with an increase in loading rate at each of the σ_3's used except at a σ_3 of 250 psi and a loading rate of 50 psi/sec.

From the data presented for the unconfined compression tests (Figure 3.69) and the above-described triaxial compression tests, it is evident that at least the basalt rock behaves consistently under various rates of loading, i.e., both strength and axial strain increase.

The tuff rock was the only one tested that showed a decrease in deviator stress with increased confining pressures. The rock was tested at a natural moisture content of approximately 21 percent and in the undrained state. The pore pressure buildup due to confining pressure and axial loading probably caused the pore pressure to break down some of the rock structure, thereby causing lower strengths at increased confining pressure. This fact is cited a number of times in the literature that was reviewed. Should additional triaxial testing be done, the effect of pore pressure should definitely be accounted for in terms of effective stresses $\sigma' = \sigma - u$, where σ' = effective stresses, σ = applied axial stress, and u = pore pressure.

The results of the compressional wave velocity tests, which were conducted along with the triaxial compression tests, agree quite well

with the test results found in the literature search. There were twelve tests run, and in all cases except one the compressional wave velocity increased sharply when the axial stress was increased to about one-half of the ultimate stress. The velocities then leveled off until just before failure; at failure, they either remained constant or decreased slightly. Velocities also increased with increased confining pressure. The increases in velocity from zero to maximum deviator stress for the rocks tested are given below:

Rock	Factor by Which Velocities Increased at Indicated Confining Pressures					
	250 psi	500 psi	1,000 psi	1,500 psi	4,000 psi	5,000 psi
Granite	1.09	--	1.10	--	1.04	--
Basalt	1.03	--	1.06	--	--	1.12
Limestone	1.10	--	1.04	--	--	1.10
Tuff	--	1.23	1.21	1.27	--	--

No distinct correlation could be made between the compressional wave velocity versus deviator stress and the volumetric strain versus deviator stress curves. Generally though, the compressional wave velocity curve was at a constant level, or at its highest value when the volumetric curve was expanding, i.e., just after the volumetric change was constant.

For all practical purposes, the straight-line relation described by Mohr's criterion $T = c + \sigma \tan \phi$ where T is the shearing stress, c is referred to as cohesion, σ is normal stress on the failure plane, and ϕ is the angle of internal friction, fits most of the stress circles presented for the granite and basalt. A curvilinear analysis would best fit the stress circles presented for the limestone rock. No envelope was drawn for the results of the tuff rock due to the decrease in deviator stress with increased σ_3. Nearly all the observed shear failure planes did approach those predicted from Mohr's criterion ($\phi = 90 - 2\alpha$). This can be seen in the following tabulation.

Rock	Loading Rate	σ_3	Observed Failure Angle	Predicted Failure Angle $\phi = 90 - 2\alpha$	Envelope
	psi/sec	psi	degrees	degrees	degrees
Granite	50	250	52	72	54
Granite	50	4,000	50	72	54
Basalt	1	1,000	61	77	--
Basalt	1	5,000	--	--	--
Basalt	50	250	60	72	54
Basalt	50	1,000	63	72	54
Basalt	50	5,000	63	72	54
Basalt	500	250	71	70	50

(Continued)

Rock	Loading Rate	σ_3	Observed Failure Angle	Predicted Failure Angle $\phi = 90 - 2\alpha$	Envelope
	psi/sec	psi	degrees	degrees	degrees
Basalt	500	1,000	75	70	50
Basalt	500	5,000	70	70	50
Basalt	2,250	1,000	74	73	55
Basalt	2,250	5,000	72	73	55

Figure 3.70 shows Mohr envelopes for the basalt rock at loading rates of 1, 50, 500, and 2,250 psi/sec. There is very little difference in ϕ at the lower σ_3's and at the higher σ_3's with the exception of the envelope developed from specimens loaded at a rate of 50 psi/sec. The ϕ's of envelopes at the tangent point of the 1,000- and the 5,000-psi σ_3 stress circles are presented below.

1,000-psi σ_3 Circle		5,000-psi σ_3 Circle	
Loading Rate	ϕ	Loading Rate	ϕ
psi/sec	degrees	psi/sec	degrees
1	--	1	--
50	54	50	16
500	50	500	47
2,250	55	2,250	46

The data on the previous page indicate that basalt under triaxial stresses is not greatly affected by loading rates ranging from 1 to 2,250 psi/sec with regard to ϕ, and that Mohr's criterion of failure fits the basalt rock quite well. Generally, the observed angles of failure do increase with increased rates of load at a given confining pressure; however, the method of measuring these angles is rather crude and not taken as very accurate. The cohesion values for the loading rates used are presented below:

Loading Rate	Cohesion (c)
psi/sec	psi
1	--
50	3,800
500	3,900
2,250	3,700

Here again there is no clear indication that loading rates significantly affect cohesion of basalt at rates up to 2,250 psi/sec.

Figures 3.71 through 3.73 are charts showing the engineering classification for the intact rock specimens tested during the project. This classification system is the one referred to earlier in Reference 32. Generally, the data reported herein fell very close to similar rock data plotted in Reference 32.

Figures 3.74 and 3.75 show the relation of axial stress to

lateral stress at failure in triaxial compression at various loading rates for the rock tested during this program. The data shown in Figure 3.34 are consistent with data found in the literature search. However, there were no data found during the literature search on any one rock that had been subjected to triaxial loading at different loading rates. The results of this investigation show that as the rate of loading is increased, for a set of confining pressures, a straight-line equation exists; the samples tested at a loading rate of 50 psi/sec are an exception to this statement.

TABLE 4.1 TEST RESULTS FOR SALT

Specimen No.	Hole No.	Depth	Specific Gravity		Porosity	Compressional Wave Velocity	Direct Tension	Tensile Splitting Strength	Unconfined Compressive Strength Test				Slow C
			Bulk Dry	Solids					Loading Rate	Strength	Young's Modulus	Poisson's Ratio	Strength Pressur 1,000, 250
		feet			pct	ft/sec	psi	psi	psi/sec	psi	10^6 psi		psi
G-1	U-1501-U2	11.1 to 11.7	2.69	2.70	0.33	18,840	--	1,540	--	--	--	--	--
G-2	U-1501-U2	73.2 to 74.4	2.69	2.70	0.33	18,590	--	--	50	19,790	10.20	0.22	--
G-4	U-15-17	52.6	2.71	2.71	0.10	18,820	--	--	--	--	--	--	--
G-5	U-1501-U1	728.0 to 730.2	2.68	2.70	0.63	18,270	--	1,630	--	--	--	--	--
G-6	U-15-27	121.0	2.69	2.70	0.29	18,550	1,770	--	--	--	--	--	--
G-7	U-15E-01	99.4	2.68	2.70	0.63	18,000	--	--	--	--	--	--	--
G-8	U-1501-U1	728.0 to 730.2	2.68	2.69	0.33	17,500	1,770	--	--	--	--	--	--
G-10	U-1501-U1	728.0 to 730.2	2.68	2.69	0.29	19,230	--	--	50	20,140	11.60	0.22	--
G-11	U-1501-U1	1709.0 to 1710.7	2.70	2.70	0.11	19,220	--	--	--	--	--	--	--
G-13	U-1501-U1	1709.0 to 1710.7	2.66	2.68	0.75	17,400	--	--	--	--	--	--	--
G-15	U-1501-U1	1759.9 to 1760.9	2.70	2.71	0.11	19,440	--	--	50	22,290	10.30	0.22	--
G-16	U-15-27	178.0	2.68	2.69	0.37	18,720	--	1,920	--	--	--	--	--
G-17	U-15E-01	106.5	2.70	2.70	0.11	17,860	--	--	--	--	--	--	--
G-18	U-1501-U1	1759.9 to 1760.9	2.70	2.71	0.11	18,380	--	--	--	--	--	--	--
G-19	U-1501-U1	--	2.69	2.69	0.22	18,660	--	--	--	--	-	--	--
G-20	U-1501-U1	--	2.68	2.69	0.47	18,250	--	--	--	--	--	--	24,120
G-21	U-1501-U1	--	2.70	2.70	0.03	18,270	--	--	--	--	--	--	--
G-22	U-15-27	121.0	2.69	2.70	0.29	18,500	--	--	--	--	--	--	--
G-23	U-1501-U1	--	2.68	2.69	0.46	18,260	--	--	--	--	--	--	--
G-24	U-1501-U1	--	2.66	2.69	0.37	18,470	--	--	--	--	--	--	--
		Average	2.69	2.69	0.30	18,450	1,770	1,770		20,740	10.70	0.22	

A

Slow Compression											Rapid Compression		
Unconfined Compressive Strength Test				Triaxial Compressive Strength with Compressional Wave Velocity (V_p)							Unconfined Compressive Strength Test		
Loading Rate	Strength	Young's Modulus	Poisson's Ratio	Strength at Confining Pressures of 250, 1,000, and 4,000			Young's Modulus	Poisson's Ratio	Initial V_p	High V_p	Loading Rate	Strength	Young's Modulus
				250	1,000	4,000							
psi/sec	psi	10^6 psi		psi	psi	psi	10^6 psi		ft/sec	ft/sec	psi/sec	psi	10^6 psi
--	--	--	--	--	--	--	--	--	--	--	--	--	--
50	19,790	10.20	0.22	--	--	--	--	--	--	--	--	--	--
--	--	--	--	--	--	52,540	10.00	0.29	20,660	21,840	--	--	--
--	--	--	--	--	--	--	--	--	--	--	--	--	--
--	--	--	--	--	--	--	--	--	--	--	--	--	--
--	--	--	--	--	29,320	--	11.30	0.22	18,000	19,940	--	--	--
--	--	--	--	--	--	--	--	--	--	--	--	--	--
50	20,140	11.60	0.22	--	--	--	--	--	--	--	--	--	--
--	--	--	--	--	--	--	--	--	--	--	6.03×10^6	18,070	10.51
--	--	--	--	--	--	--	--	--	--	--	6.95×10^6	20,960	10.03
50	22,290	10.30	0.22	--	--	--	--	--	--	--	--	--	--
--	--	--	--	--	--	--	--	--	--	--	--	--	--
--	--	--	--	--	--	--	--	--	--	--	--	--	--
--	--	--	--	--	--	--	--	--	--	--	--	--	--
--	--	--	--	--	--	--	--	--	--	--	--	--	--
--	--	--	--	24,120	--	--	10.70	0.25	18,250	20,050	--	--	--
--	--	--	--	--	--	--	--	--	--	--	--	--	--
--	--	--	--	--	--	--	--	--	--	--	--	--	--
--	--	--	--	--	--	--	--	--	--	--	--	--	--
--	--	--	--	--	--	--	--	--	--	--	--	--	--
	20,740	10.70	0.22									19,510	10.27

B

TABLE [illegible] TEST RESULTS ON BASALT

Specimen No.	Hole No.	Depth	Specific Gravity		Porosity	Compressional Wave Velocity	Tensile Splitting Strength	Slow Compression								
			Bulk Dry	Solids				Unconfined Compressive Strength Test				Triaxial Compressive Strength with Comp Wave Velocity (V_p)				
								Loading Rate	Strength	Young's Modulus	Poisson's Ratio	Loading Rate	Strength at Confining Pressures of 250, 1,000, and 5,000 psi			Young's Modulus	Poisson's Ratio
													250	1,000	5,000		
		feet			pct	ft/sec	psi	psi/sec	psi	10^6 psi		psi/sec	psi	psi	psi	10^6 psi	
B-1	DA-1	75.3 to 76.5	2.70	2.83	--	16,640	--	1	21,370	4.66	0.26	--	--	--	--	--	--
B-2	NCG-38	--	2.68	2.83	5.26	15,650	1,820		--	--	--	--	--	--	--	--	--
B-3	DA-1	138.2 to 140.0	2.67	2.82	5.35	16,350	--	500	21,010	4.80	0.29	--	--	--	--	--	--
B-4	DA-1	138.2 to 140.0	2.67	2.82	5.35	16,370	--	--	--	--	--	50	30,000	--	--	4.60	0.22
B-5	NCG-42A	68.5	2.66	2.82	5.37	16,090	--	--	--	--	--	50	--	34,980	--	4.90	0.17
B-6	NCG-45	73.9	2.73	2.84	3.47	15,270	--	500	21,410	5.37	0.32	--	--	--	--	--	--
B-7	Calex	--	2.69	--	--	16,430	--	500	22,310	4.00	0.25	--	--	--	--	--	--
B-8	Calex	--	2.71	--	--	16,990	--	--	--	--	--	--	--	--	--	--	--
B-9	--	156.8	2.73	2.84	3.79	15,670	--	50	22,740	4.17	0.29	--	--	--	--	--	--
B-10	--	157.1	2.73	2.84	3.99	16,490	--	--	--	--	--	--	--	--	--	--	--
B-11	Calex	--	2.70	--	--	16,730	--	--	--	--	--	--	--	--	--	--	--
B-12	NCG-23	49.0	2.74	2.83	3.07	17,700	1,790	--	--	--	--	--	--	--	--	--	--
B-13	DA-2	95.0 to 96.5	2.74	2.83	3.11	17,760	--	--	--	--	--	500	39,670	--	--	4.46	0.31
B-14	--	13.2	2.68	2.83	5.26	17,050	--	--	--	--	--	1	31,840	--	--	5.18	0.41
B-15	NCG-40	61.3	2.68	2.83	5.26	15,440	--	--	--	--	--	--	--	--	--	--	--
B-16	NCG-40	61.3	2.68	2.83	5.26	15,610	--	--	--	--	--	--	--	--	--	--	--
B-17	NCG-38	64.4	2.69	2.82	4.61	17,550	--	--	--	--	--	--	--	--	--	--	--
B-18	NCG-38	64.4	2.69	2.82	4.61	17,650	--	--	--	--	--	--	--	--	--	--	--
B-19	DA-2	67.8	2.68	2.82	5.20	17,360	--	--	--	--	--	50	--	--	46,280	6.08	0.16
B-20	DA-2	67.8	2.68	2.82	5.24	17,200	--	50	20,730	4.26	--	--	--	--	--	--	--
B-21	Calex	--	2.70	--	--	16,800	--	1	22,580	4.71	0.33	--	--	--	--	--	--
B-22	Calex	--	2.70	--	--	16,550	--	1	18,920	3.48	0.47	--	--	--	--	--	--
B-23	Calex	--	2.70	--	--	16,500	--	--	--	--	--	1	--	27,880	--	4.19	0.43
B-24	Calex	--	2.69	--	--	16,100	--	--	--	--	--	1	--	--	33,430	4.62	0.22
B-25	Calex	--	2.68	--	--	16,250	2,090	--	--	--	--	--	--	--	--	--	--
B-26	Calex	--	2.69	--	--	16,950	--	--	--	--	--	500	--	31,290	--	3.94	0.27
B-27	Calex	--	2.71	--	--	15,100	--	--	--	--	--	500	--	--	49,430	4.42	0.31
B-28	Calex	--	2.70	--	--	16,940	--	--	--	--	--	2,740	28,700	--	--	4.00	0.25
B-29	Calex	--	2.69	--	--	15,990	--	50	21,250	5.00	0.28	--	--	--	--	--	--
B-30	Calex	--	2.72	--	--	16,980	--	--	--	--	--	2,250	--	35,010	--	4.71	0.25
B-31	Calex	--	2.70	--	--	16,890	--	--	--	--	--	2,250	--	--	94,000	5.03	0.15
		Average	2.69	2.83	4.60	17,140	1,900		21,460	5.06	0.32						

Slow Compression											Rapid Compression				Mode of Failure
Unconfined Compressive Strength Test			Triaxial Compressive Strength with Compressional Wave Velocity (V_p)								Unconfined Compressive Strength Test				
Strength	Young's Modulus	Poisson's Ratio	Loading Rate	Strength at Confining Pressures of 250, 1,000, and 5,000 psi			Young's Modulus	Poisson's Ratio	Initial V_p	Highest V_p	Loading Rate	Strength	Young's Modulus	Poisson's Ratio	
				250	1,000	5,000									
psi	10^6 psi		psi/sec	psi	psi	psi	10^6 psi		ft/sec	ft/sec	psi/sec	psi	10^6 psi		
21,370	4.66	0.26	--	--	--	--	--	--	--	--	--	--	--	--	--
--	--	--	--	--	--	--	--	--	--	--	--	--	--	--	--
21,810	4.80	0.29	--	--	--	--	--	--	--	--	--	--	--	--	Shear at 60 degrees from horizontal
--	--	--	50	30,000	--	--	4.60	0.22	16,060	16,510	--	--	--	--	Shear at 63 degrees from horizontal
--	--	--	50	--	36,980	--	4.90	0.17	16,020	17,130	--	--	--	--	--
21,410	5.37	0.32	--	--	--	--	--	--	--	--	--	--	--	--	--
22,310	4.00	0.25	--	--	--	--	--	--	--	--	--	--	--	--	--
--	--	--	--	--	--	--	--	--	--	--	2.06×10^5	24,970	3.62	0.27	--
22,740	4.17	0.29	--	--	--	--	--	--	--	--	--	--	--	--	--
--	--	--	--	--	--	--	--	--	--	--	3.13×10^6	28,170	5.00	0.45	--
--	--	--	--	--	--	--	--	--	--	--	2.06×10^5	27,520	3.42	0.39	--
--	--	--	--	--	--	--	--	--	--	--	--	--	--	--	--
--	--	--	500	25,620	--	--	4.46	0.37	--	--	--	--	--	--	Shear at 71 degrees from horizontal
--	--	--	1	21,240	--	--	5.18	0.41	--	--	--	--	--	--	Vertical splitting
--	--	--	--	--	--	--	--	--	--	--	2.06×10^5	23,340	3.71	0.35	--
--	--	--	--	--	--	--	--	--	--	--	1.60×10^7	32,120	4.73	0.23	--
--	--	--	--	--	--	--	--	--	--	--	1.29×10^7	32,390	4.68	0.20	--
--	--	--	--	--	--	--	--	--	--	--	1.34×10^7	34,580	4.66	0.25	--
--	--	--	50	--	--	4	6.08	0.1	16,670	16,750	--	--	--	--	Shear at 63 degrees from horizontal
20,730	4.25	--	--	--	--		--	--	--	--	--	--	--	--	--
22,580	4.71	0.34	--	--	--	--	--	--	--	--	--	--	--	--	--
18,920	3.48	0.47	--	--	--	--	--	--	--	--	--	--	--	--	--
--	--	--	1	--	27,880	--	4.19	0.43	--	--	--	--	--	--	Shear at 61 degrees from horizontal
--	--	--	1	--	--	33,430	4.65	0.22	--	--	--	--	--	--	Vertical splitting
--	--	--	--	--	--	--	--	--	--	--	--	--	--	--	--
--	--	--	500	--	31,250	--	3.94	0.27	--	--	--	--	--	--	Shear at 75 degrees from horizontal
--	--	--	500	--	--	29,330	4.42	0.31	--	--	--	--	--	--	Shear at 70 degrees from horizontal
--	--	--	2,740	25,700	--	--	4.00	0.25	--	--	--	--	--	--	Vertical splitting
21,250	5.00	0.28	--	--	--	--	--	--	--	--	--	--	--	--	--
--	--	--	2,250	--	35,000	--	4.71	0.25	--	--	--	--	--	--	Shear at 74 degrees from horizontal
--	--	--	2,250	--	--	34,400	5.03	0.15	--	--	--	--	--	--	Shear at 72 degrees from horizontal
21,460	4.06	0.32										25,010	4.40	0.31	

TABLE 3.3 TEST RESULTS FOR LIMESTONE

Specimen No.	Hole No.	Depth	Specific Gravity		Porosity	Compressional Wave Velocity	Tensile Splitting Strength	Unconfined Compressi Strength Test		
			Bulk Dry	Solids				Loading Rate	Strength	Young' Modulu
		feet			pct	ft/sec	psi	psi/sec	psi	10^6 ps
L-2	FT-1.3	5.5 to 6.5	2.68	2.70	0.81	19,890	--	50	9,500	10.42
L-4	FT-1.1	12.1 to 12.8	2.71	2.73	0.69	20,580	--	--	--	--
L-6	FT-1	68.0	2.72	2.73	0.43	20,990	--	--	--	--
L-7	FT-1	69.0	2.72	2.73	0.40	20,690	--	50	12,750	12.00
L-8	FT-1	82.0	2.70	2.71	0.22	20,760	--	50	11,300	11.28
L-10	--	--	2.70	2.71	0.33	21,580	--	--	--	--
L-12	FT-1.0	8.4 to 9.1	2.71	2.73	0.55	20,250	--	--	--	--
L-13	FT-1.0	13.6 to 14.8	2.68	2.70	0.85	19,700	1,460	--	--	--
L-14	FT-1.1	8.0 to 8.8	2.71	2.73	0.55	20,490	1,100	--	--	--
L-15	FT-1.3	5.5 to 6.5	2.70	2.71	0.29	19,890	1,070	--	--	--
L-17	FT-1	18.6	2.70	2.71	0.40	22,320	--	--	--	--
L-18	FT-1	62.8	2.71	2.72	0.29	20,930	--	--	--	--
L-20	FT-1	27.8	2.71	2.72	0.18	21,150	--	--	--	--
		Average	2.70	2.72	0.46	20,710	1,210		11,180	11.23

Slow Compression											Ra
Unconfined Compressive Strength Test				Triaxial Compressive Strength with Compressional Wave Velocity (V_p)							Uncon Stren
Loading Rate	Strength	Young's Modulus	Poisson's Ratio	Strength at Confining Pressures of 250, 1,000, and 4,000 psi			Young's Modulus	Poisson's Ratio	Initial V_p	Highest V_p	Loading Rate
				250	1,000	4,000					
psi/sec	psi	10^6 psi		psi	psi	psi	10^6 psi		ft/sec	ft/sec	psi/sec
50	9,500	10.42	0.19	--	--	--	--	--	--	--	--
--	--	--	--	15,140	--	--	10.80	0.35	20,220	22,250	--
--	--	--	--	--	--	--	--	--	--	--	--
50	12,750	12.00	0.29	--	25,200	--	11.80	0.32	21,060	21,960	--
50	11,300	11.28	0.30	--	--	--	--	--	--	--	--
--	--	--	--	--	--	--	--	--	--	--	--
--	--	--	--	--	--	31,630	9.82	0.32	19,880	21,930	--
--	--	--	--	--	--	--	--	--	--	--	--
--	--	--	--	--	--	--	--	--	--	--	--
--	--	--	--	--	--	--	--	--	--	--	--
--	--	--	--	--	--	--	--	--	--	--	1.87×10^7
--	--	--	--	--	--	--	--	--	--	--	5.80×10^6
--	--	--	--	--	--	--	--	--	--	--	1.49×10^6
	11,180	11.23	0.26								

mpression						Rapid Compression			
Triaxial Compressive Strength with Compressional Wave Velocity (V_p)						Unconfined Compressive Strength Test			
at Confining of 250, d 4,000 psi		Young's Modulus	Poisson's Ratio	Initial V_p	Highest V_p	Loading Rate	Strength	Young's Modulus	Poisson's Ratio
,000	4,000								
psi	psi	10^6 psi		ft/sec	ft/sec	psi/sec	psi	10^6 psi	
--	--	--	--	--	--	--	--	--	--
--	--	10.80	0.35	20,220	22,250	--	--	--	--
--	--	--	--	--	--	--	--	--	--
5,200	--	11.80	0.32	21,060	21,960	--	--	--	--
--	--	--	--	--	--	--	--	--	--
--	--	--	--	--	--	--	--	--	--
--	31,630	9.82	0.32	19,880	21,930	--	--	--	--
--	--	--	--	--	--	--	--	--	--
--	--	--	--	--	--	--	--	--	--
--	--	--	--	--	--	--	--	--	--
--	--	--	--	--	--	1.87×10^7	37,290	12.03	0.40
--	--	--	--	--	--	5.80×10^6	29,000	11.76	0.35
--	--	--	--	--	--	1.49×10^6	14,930	7.61	0.46
							27,070	10.46	0.40

TABLE 3.4 TEST RESULTS FOR TUFF

Specimen No.	Hole No.	Depth	Specific Gravity		Porosity	Natural Water Content		Compressional Wave Velocity	Tensile Splitting Strength	
			Bulk Dry	Solids		Before Test	After Test			Loading Rate
		feet			pct			ft/sec	psi	psi/sec
T-7	U12 GO 6U4	10.0 to 12.0	1.93	2.39	19.38	23.2	17.4	6,600	--	50
T-11	U12 GO 6U4	31.5 to 37.0	1.85	2.34	21.77	22.4	16.6	8,640	--	--
T-13	U12 GO 6U4	31.5 to 37.0	1.92	2.44	21.10	21.0	17.1	7,190	210	--
T-14	U12 GO 6U4	41.4 to 42.9	1.94	2.35	17.60	19.7	15.7	8,810	--	--
T-15	U12 GO 6U4	41.4 to 42.9	1.94	2.43	20.30	19.7	15.6	7,470	130	--
T-20	U12 GO 6U4	67.7 to 72.0	1.92	2.35	18.39	20.4	17.1	7,610	--	--
T-21	U12 GO 6U4	67.7 to 72.0	1.92	2.40	20.29	17.1	14.1	7,670	--	--
T-23	U12 GO 6U4	67.7 to 72.0	1.98	2.35	15.90	24.7	20.6	8,060	250	--
T-24	U12 GO 6U4	67.7 to 72.0	1.89	2.33	18.95	23.5	17.6	8,190	--	--
T-25	U12 GO 6U4	67.7 to 72.0	1.91	2.49	23.30	20.2	16.3	8,190	--	50
T-26	U12 GO 6U4	67.7 to 72.0	1.91	2.44	21.80	20.2	16.5	8,000	--	50
T-27	U12 GO 6U4	67.7 to 72.0	1.91	2.36	19.06	21.9	19.1	8,280	--	--
		Average	1.92	2.39	19.82	21.1	16.9	7,891	197	

Tensile Splitting Strength	Slow Compression											
	Unconfined Compressive Strength Test				Triaxial Compressive Strength with Compressional Wave Velocity (V_p)							
	Loading Rate	Strength	Young's Modulus	Poisson's Ratio	Strength at Confining Pressures of 250, 1,000, and 1,500 psi			Young's Modulus	Poisson's Ratio	Initial V_p	Highest V_p	Load Rate
					250	1,000	1,500					
psi	psi/sec	psi	10^6 psi		psi	psi	psi	10^6 psi		ft/sec	ft/sec	psi/
--	50	1,560	0.43	0.13	--	--	--	--	--	--	--	
--	--	--	--	--	--	--	--	--	--	--	--	8.4
210	--	--	--	--	--	--	--	--	--	--	--	
--	--	--	--	--	--	--	3,560	0.878	0.19	7,575	9,644	
130	--	--	--	--	--	--	--	--	--	--	--	
--	--	--	--	--	--	3,610	--	0.333	0.17	6,944	8,413	
--	--	--	--	--	4,910	--	--	0.947	0.25	7,532	9,859	
250	--	--	--	--	--	--	--	--	--	--	--	
--	--	--	--	--	--	--	--	--	--	--	--	1.6
--	50	1,670	0.77	0.24	--	--	--	--	--	--	--	
--	50	1,680	0.40	0.19	--	--	--	--	--	--	--	
--	--	--	--	--	--	--	--	--	--	--	--	3.1
197		1,640	0.53	0.19								

Slow Compression							Rapid Compression			
Triaxial Compressive Strength with Compressional Wave Velocity (V_p)							Unconfined Compressive Strength Test			
Strength at Confining Pressures of 250, 1,000, and 1,500 psi			Young's Modulus	Poisson's Ratio	Initial V_p	Highest V_p	Loading Rate	Strength	Young's Modulus	Poisson's Ratio
250	1,000	1,500								
psi	psi	psi	10^6 psi		ft/sec	ft/sec	psi/sec	psi	10^6 psi	
--	--	--	--	--	--	--	--	--	--	--
--	--	--	--	--	--	--	8.46×10^5	4,230	0.91	0.36
--	--	--	--	--	--	--	--	--	--	--
--	--	3,560	0.878	0.19	7,575	9,644	--	--	--	--
--	--	--	--	--	--	--	--	--	--	--
--	3,610	--	0.333	0.17	6,944	8,413	--	--	--	--
4,910	--	--	0.947	0.25	7,532	9,859	--	--	--	--
--	--	--	--	--	--	--	--	--	--	--
--	--	--	--	--	--	--	1.68×10^5	1,850	0.33	0.42
--	--	--	--	--	--	--	--	--	--	--
--	--	--	--	--	--	--	--	-	--	--
--	--	--	--	--	--	--	3.11×10^5	2,490	0.41	0.49
								2,860	0.55	0.42

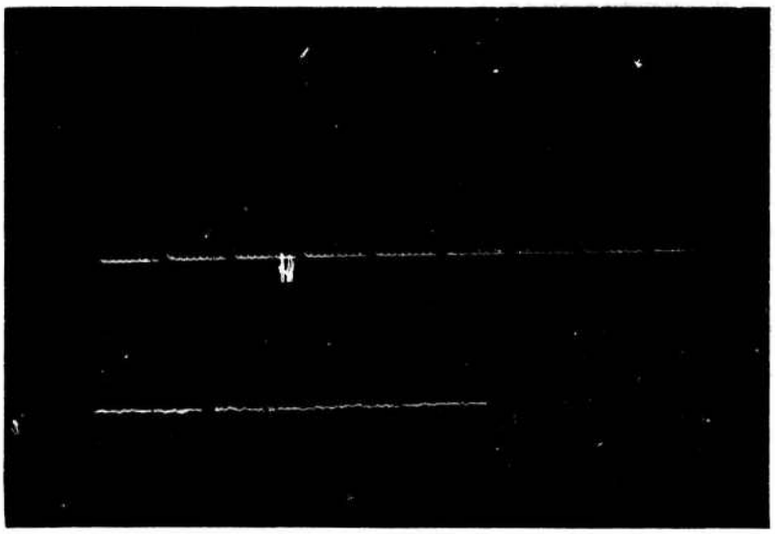

a. Granite.

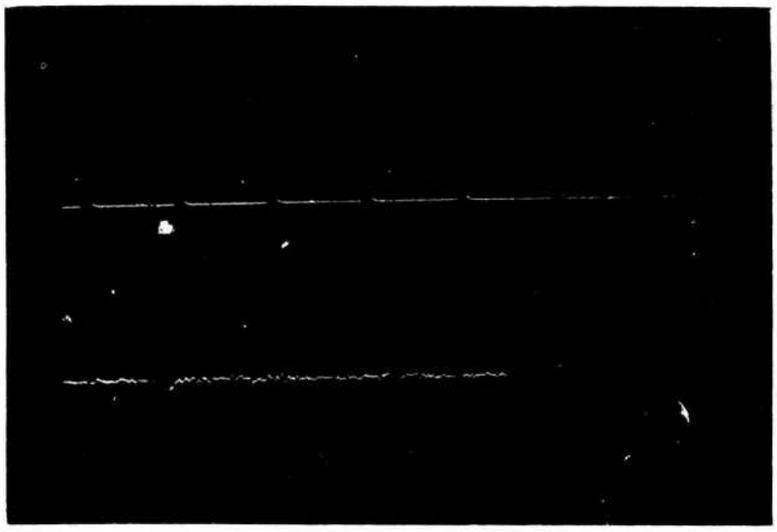

b. Basalt.

Figure 3.1 Photographs showing traces of compressional wave velocity for granite and basalt. The top trace is the time-mark generator trace with one large division equal to 10 μsec. The bottom trace is the compressional wave velocity signal initiating at 1.5 time marks (zero time) and arriving 41.5 μsec later.

a. Limestone.

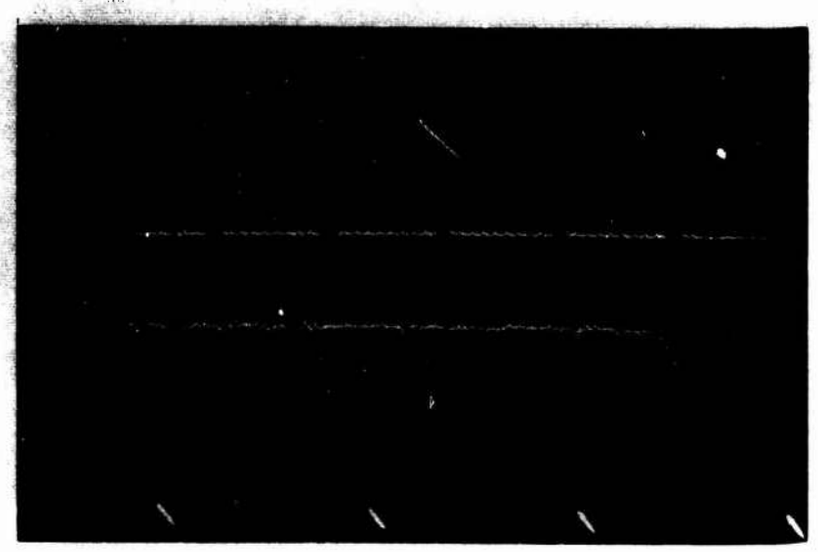

b. Tuff.

Figure 3.2 Photographs showing traces of compressional wave velocity for limestone and tuff.

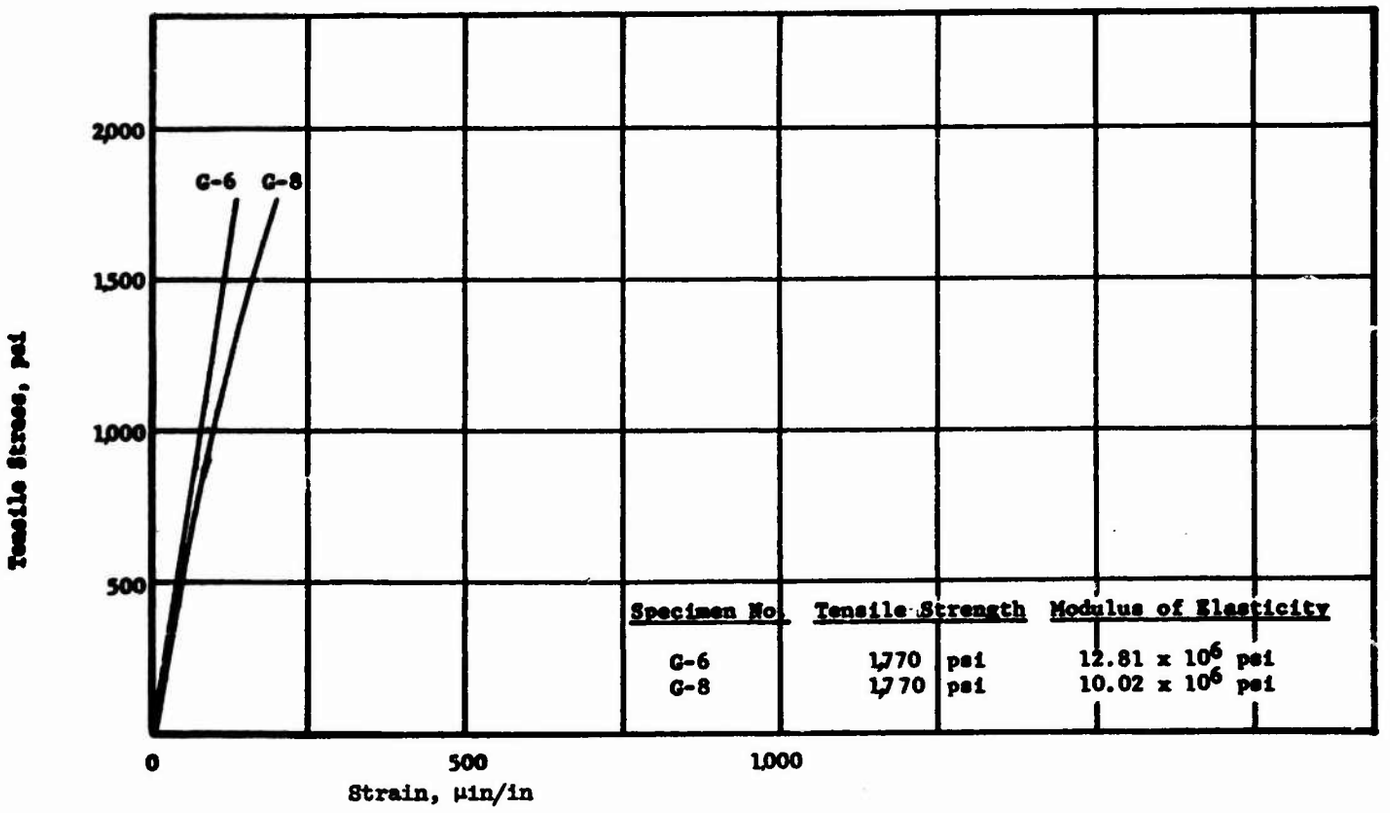

Figure 3.3 Direct tensile stress versus axial strain, granite.

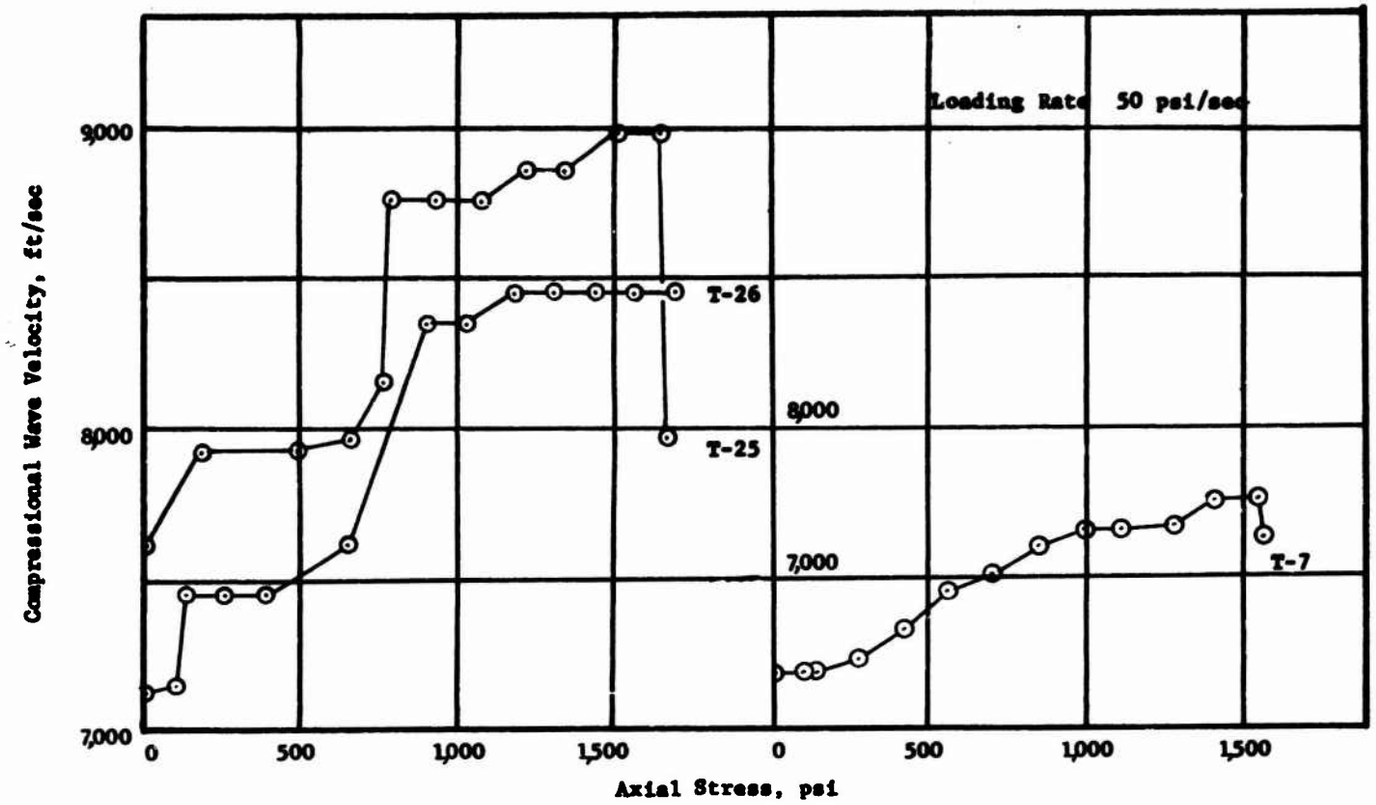

Figure 3.4 Compressional wave velocity versus axial stress, tuff in unconfined compression.

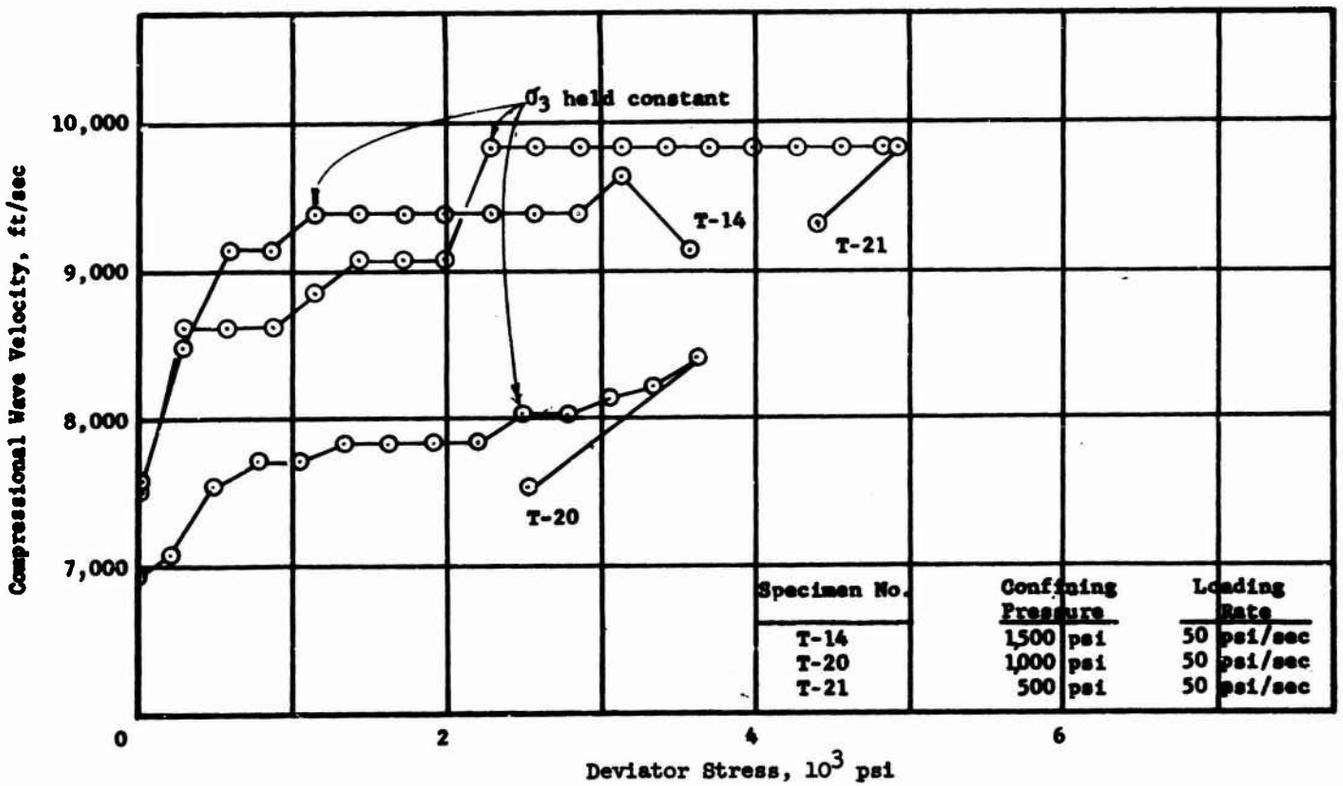

Figure 3.5 Compressional wave velocity versus deviator stress, tuff.

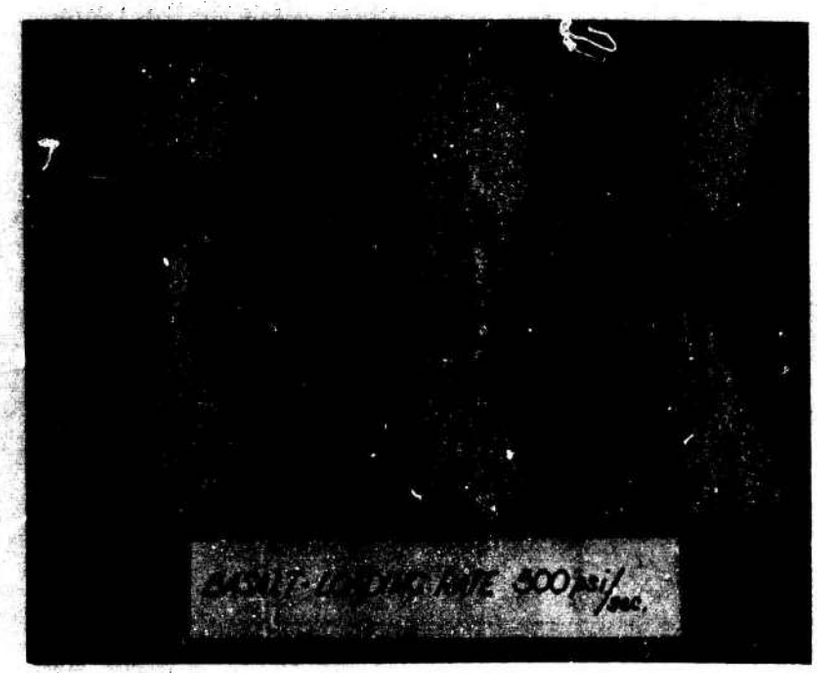

Figure 3.6 Typical basalt shear breaks.

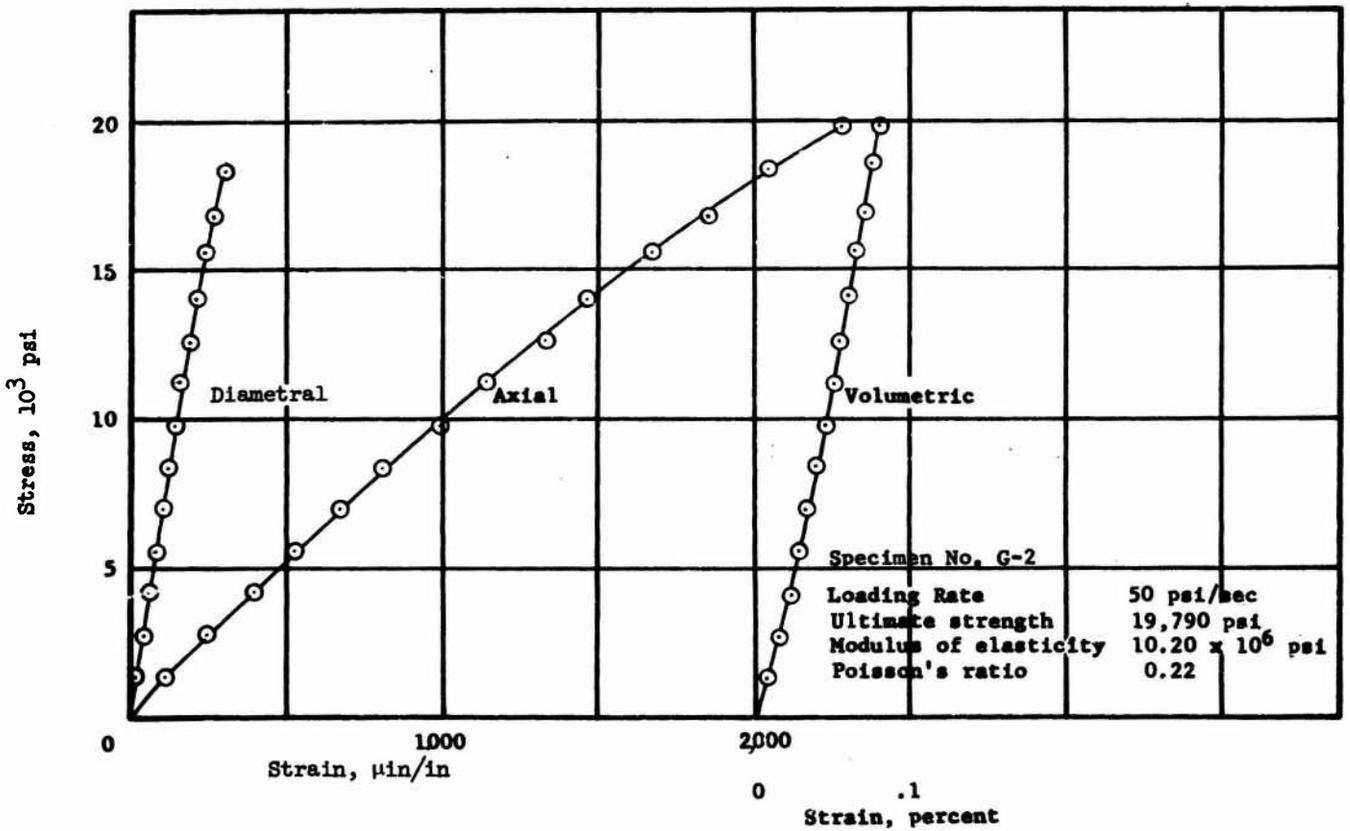

Figure 3.7 Stress versus strain curves for granite Specimen G-2.

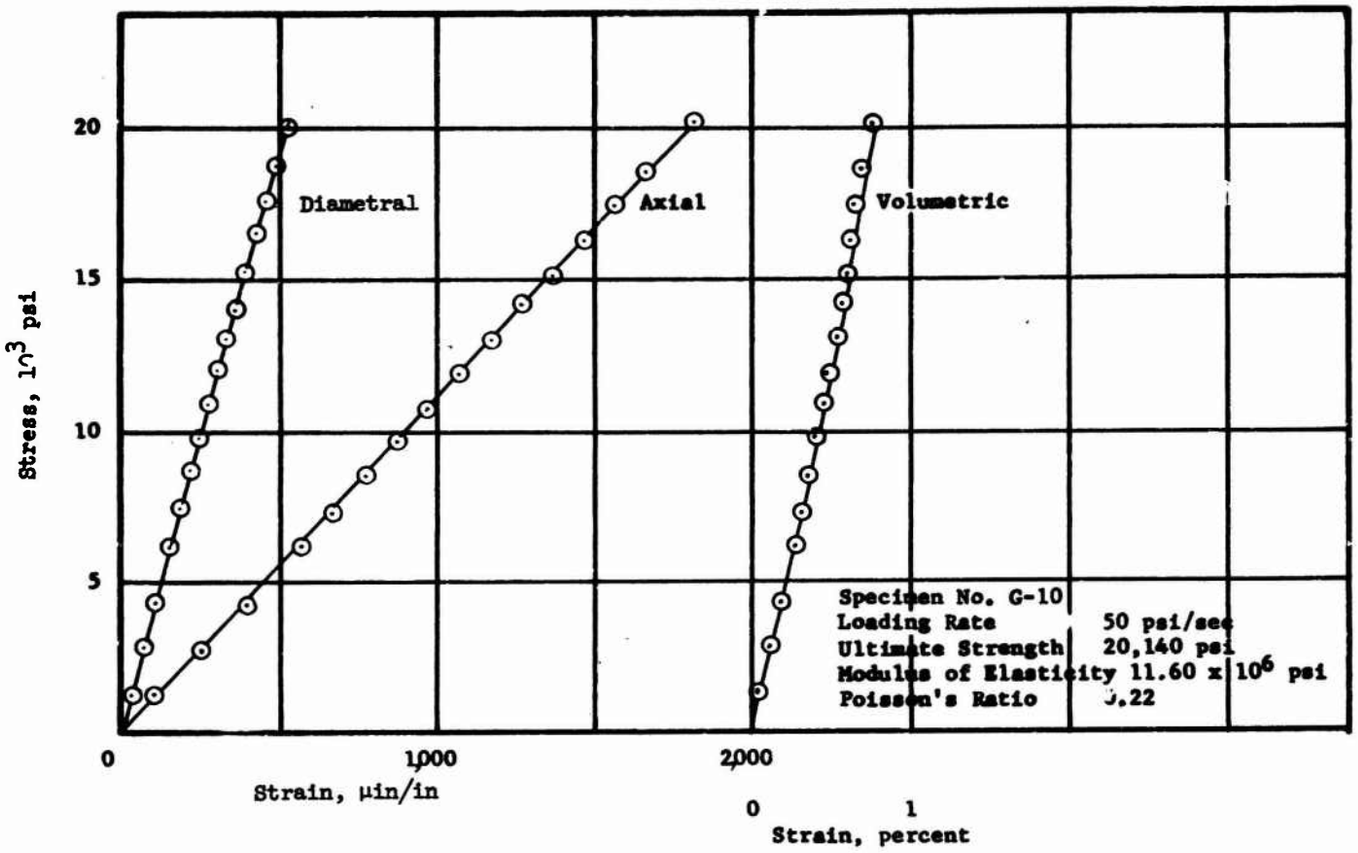

Figure 3.8 Stress versus strain curves for granite Specimen G-10.

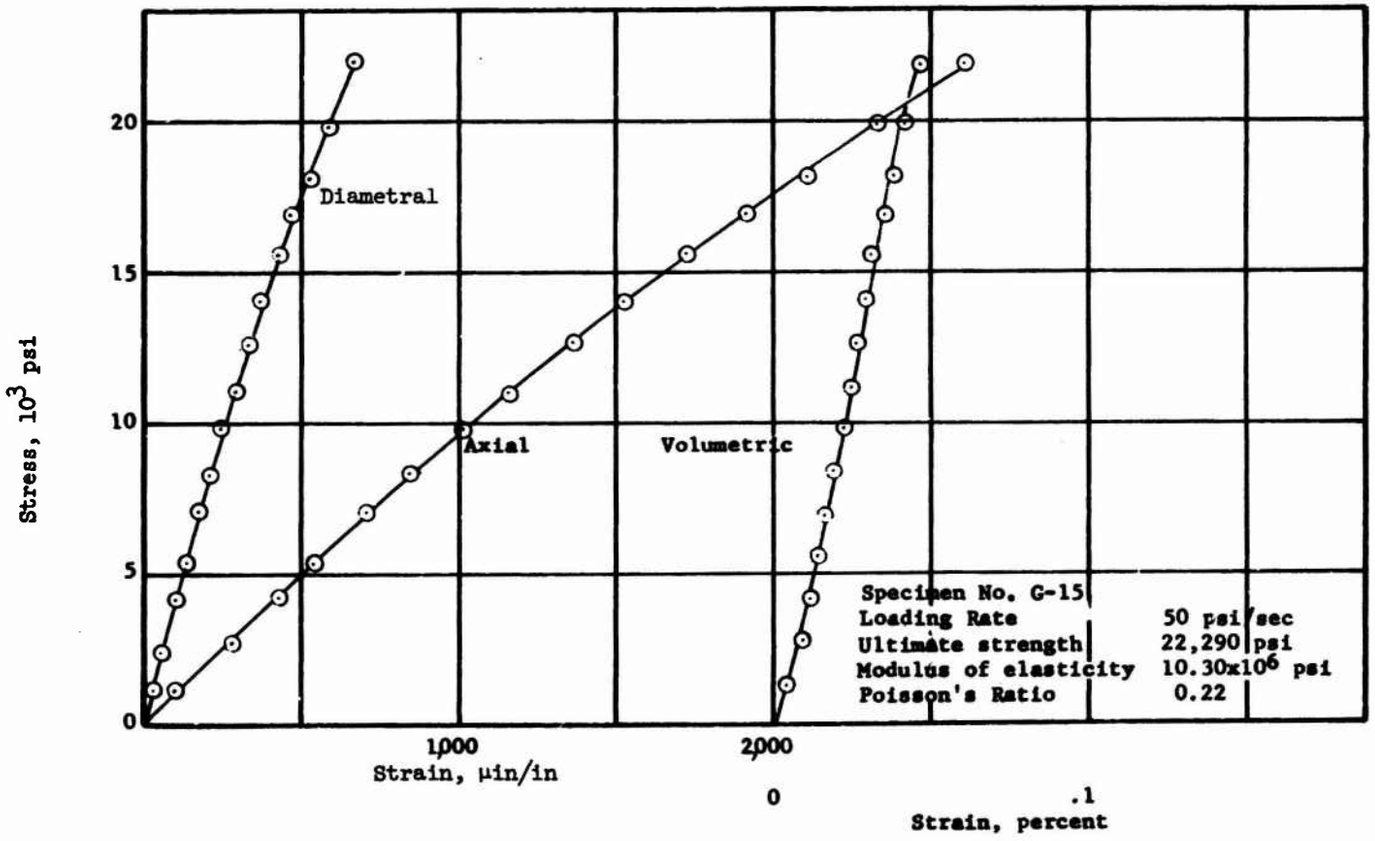

Figure 3.9 Stress versus strain curves for granite Specimen G-15.

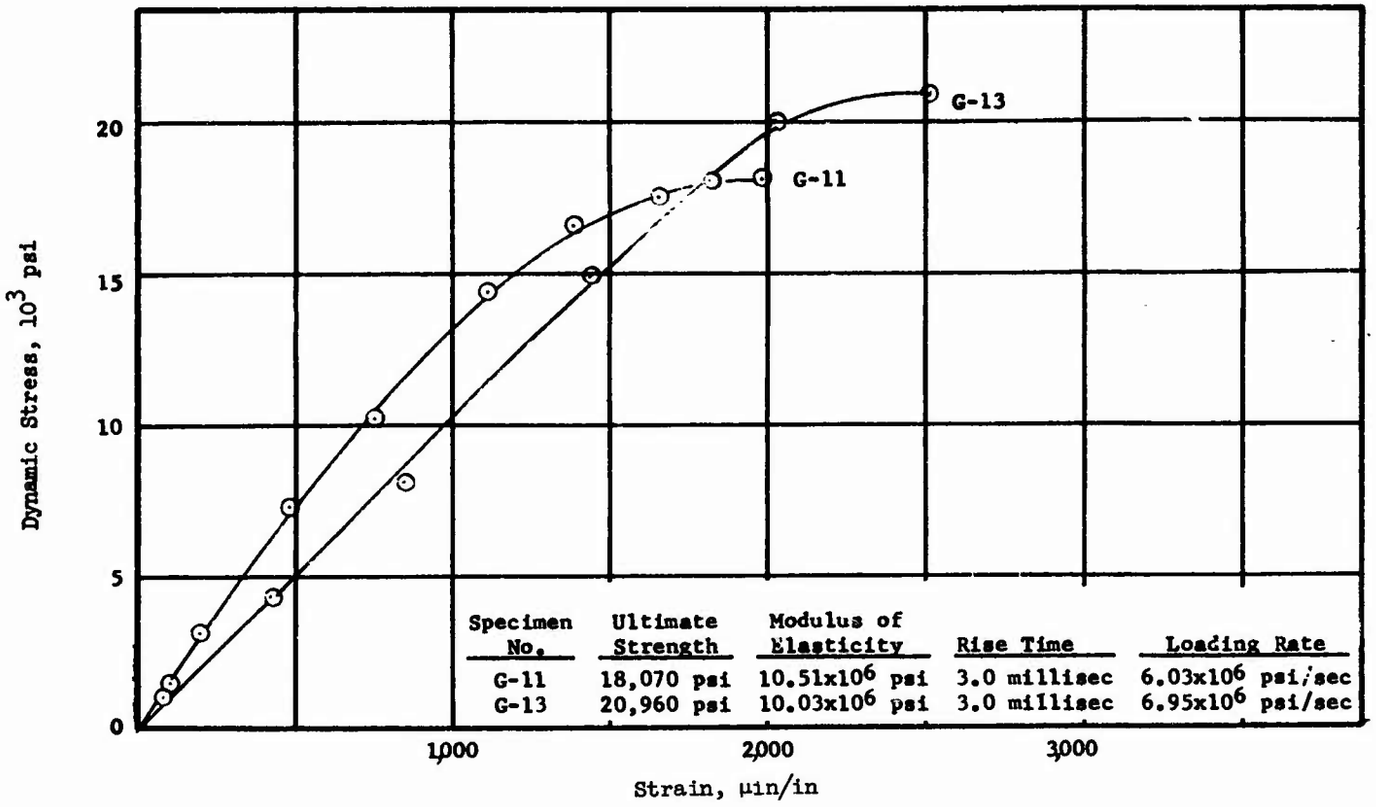

Figure 3.10 Dynamic stress versus strain curves for granite (200-kip loader) Specimens G-11 and G-13.

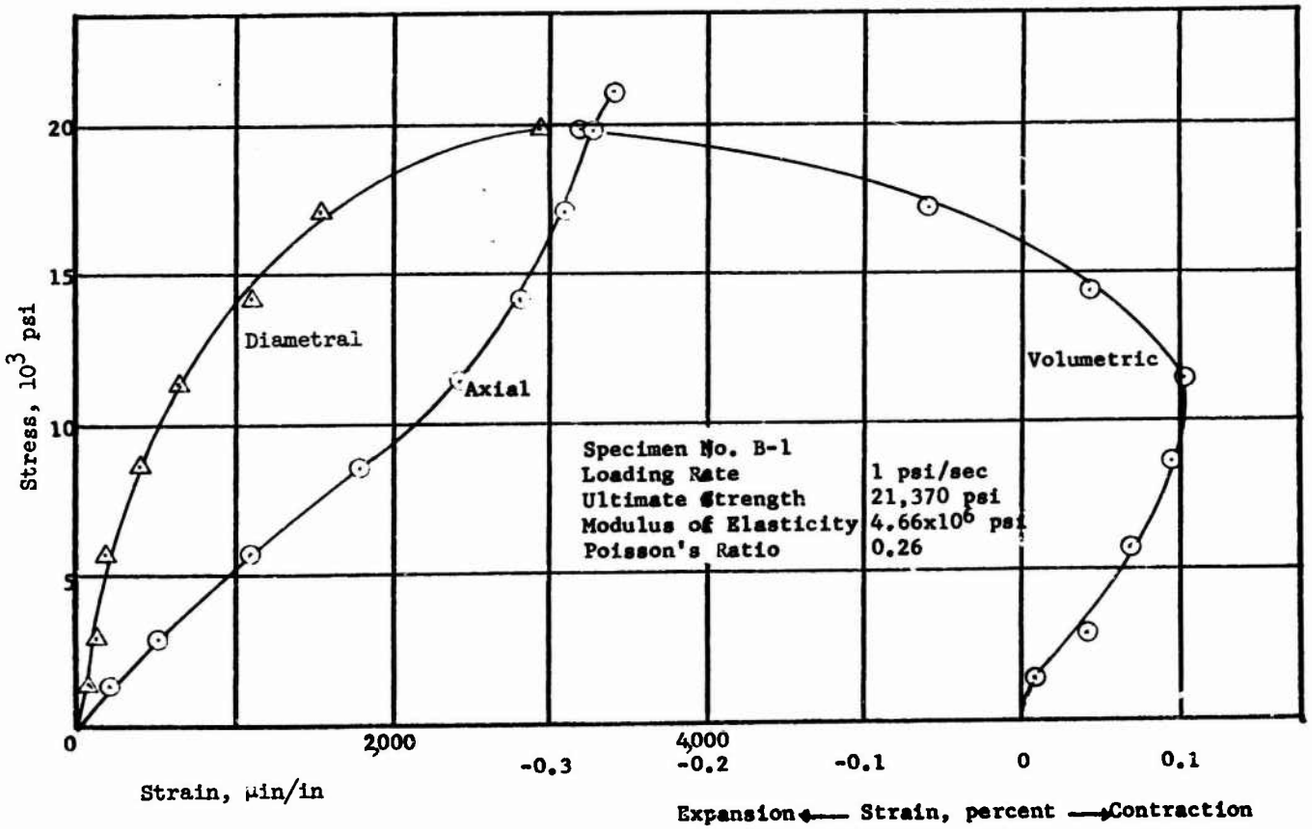

Figure 3.11 Stress versus strain curves for basalt Specimen B-1.

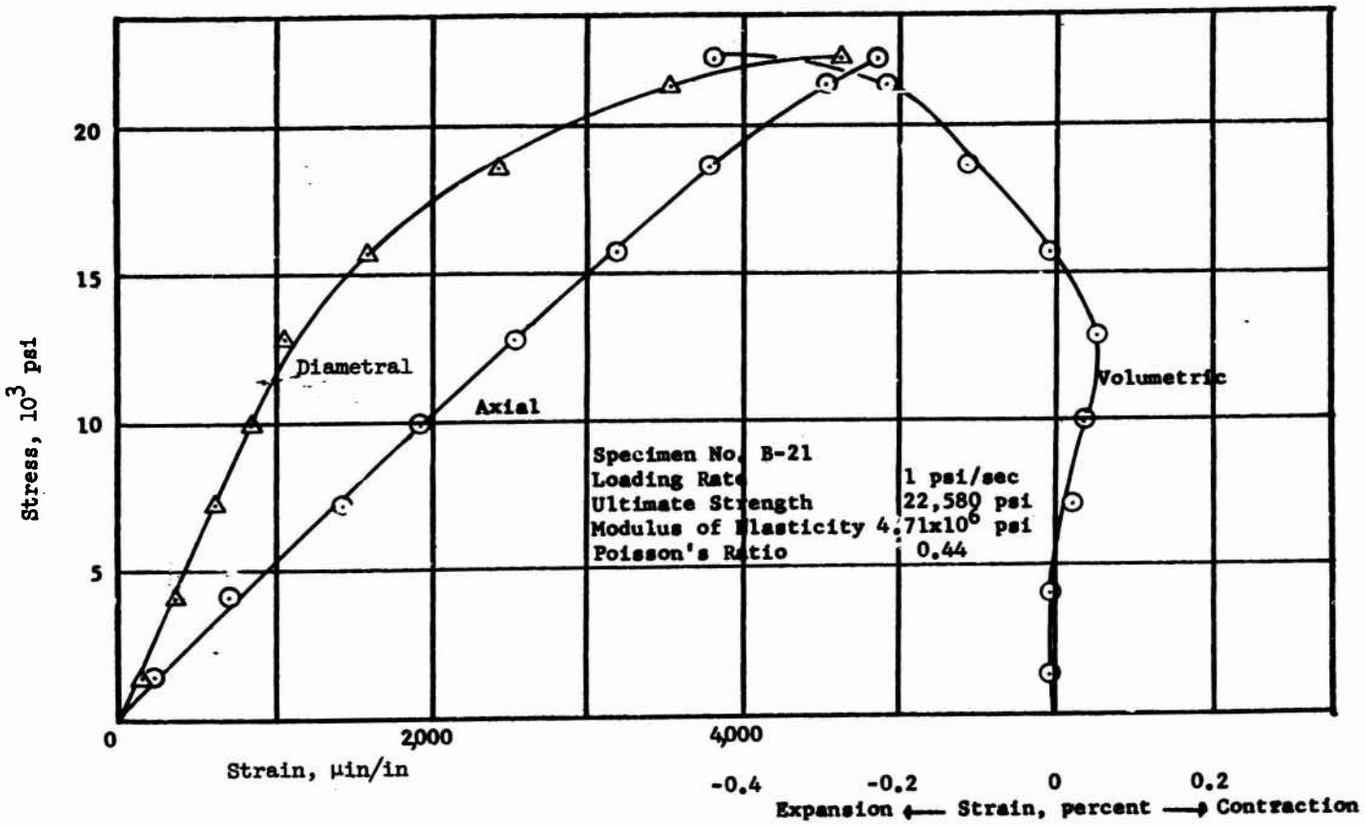

Figure 3.12 Stress versus strain curve for basalt Specimen B-21.

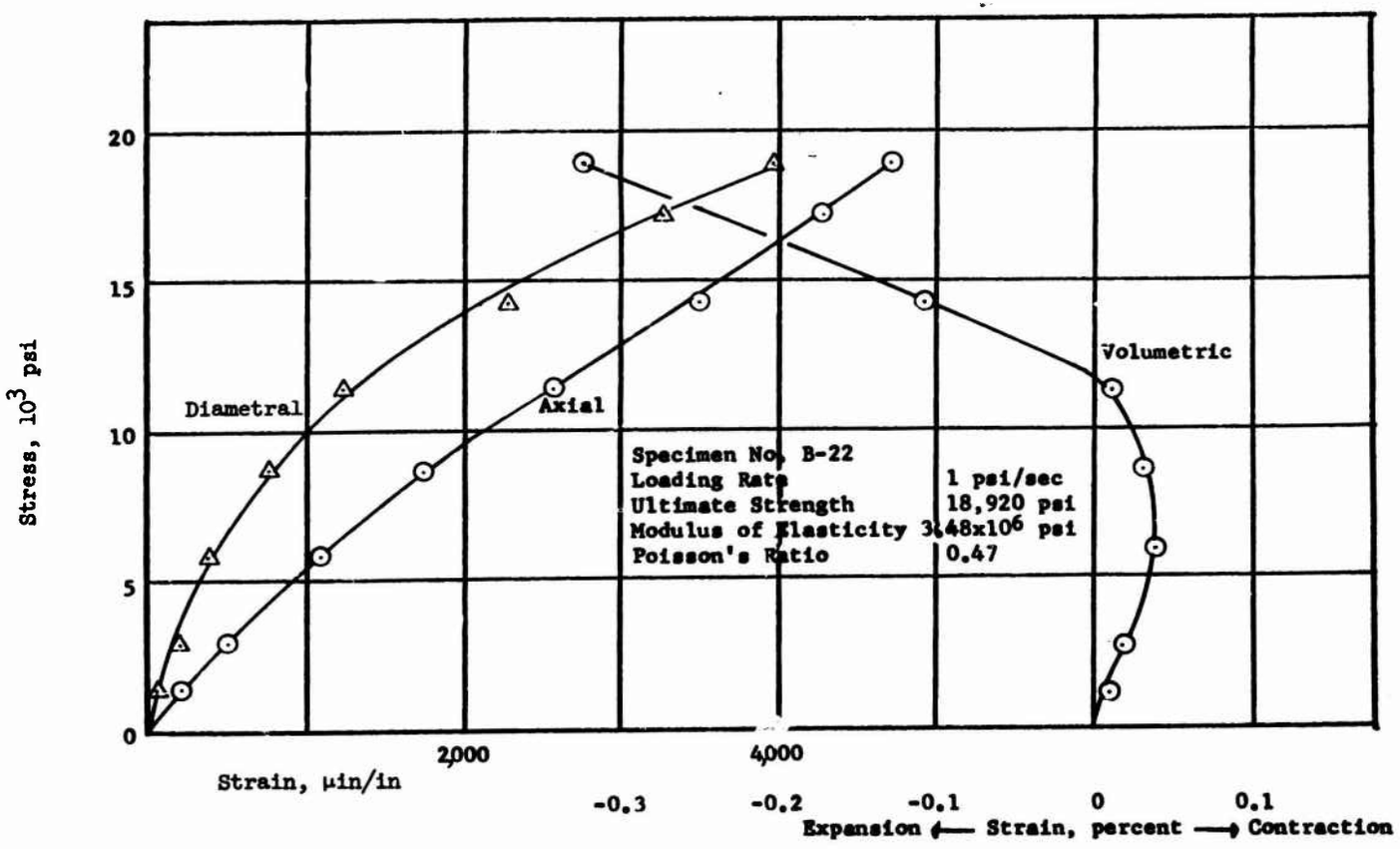

Figure 3.13 Stress versus strain curves for basalt Specimen B-22.

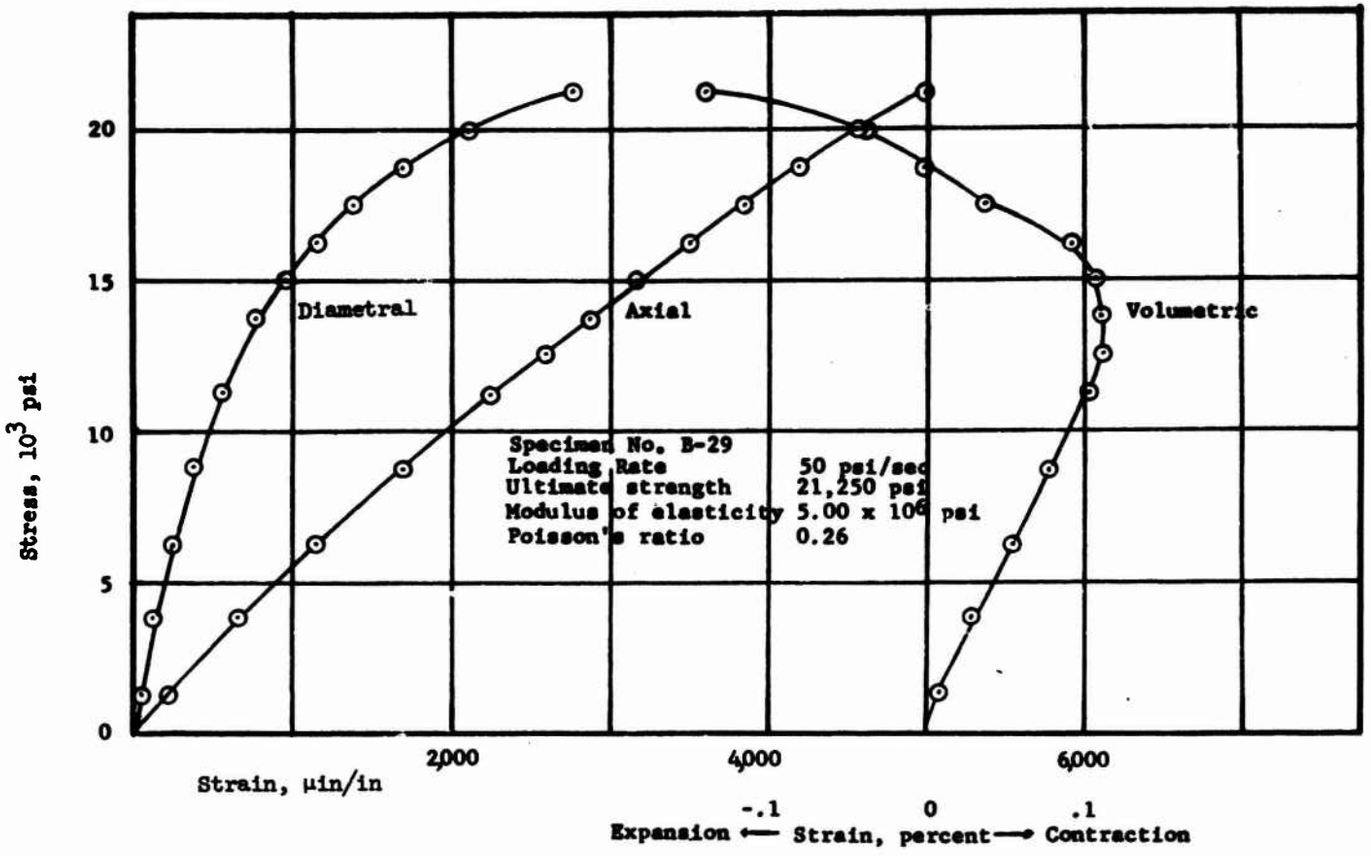

Figure 3.14 Stress versus strain curves for basalt Specimen B-29.

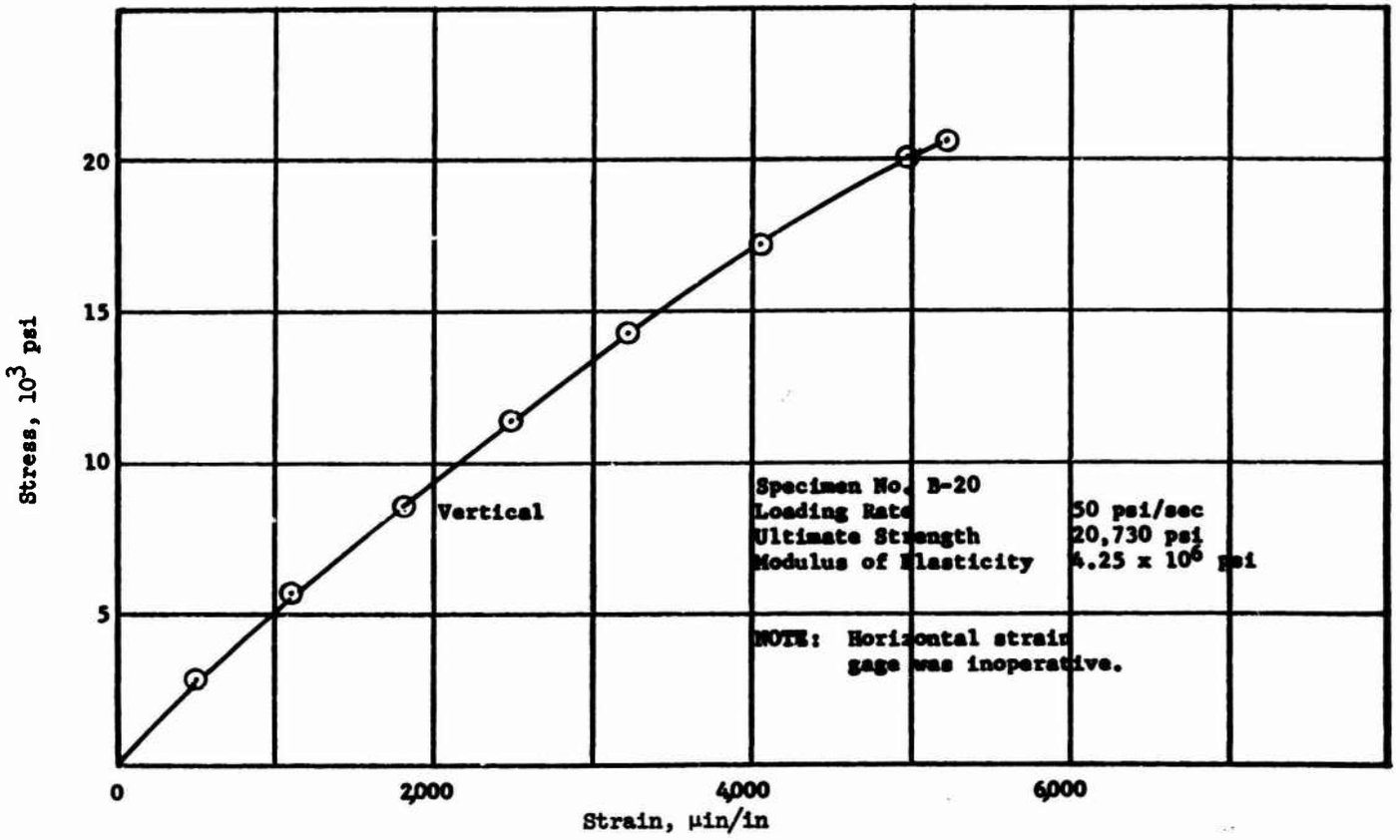

Figure 3.15 Stress versus strain curves for basalt Specimen B-20.

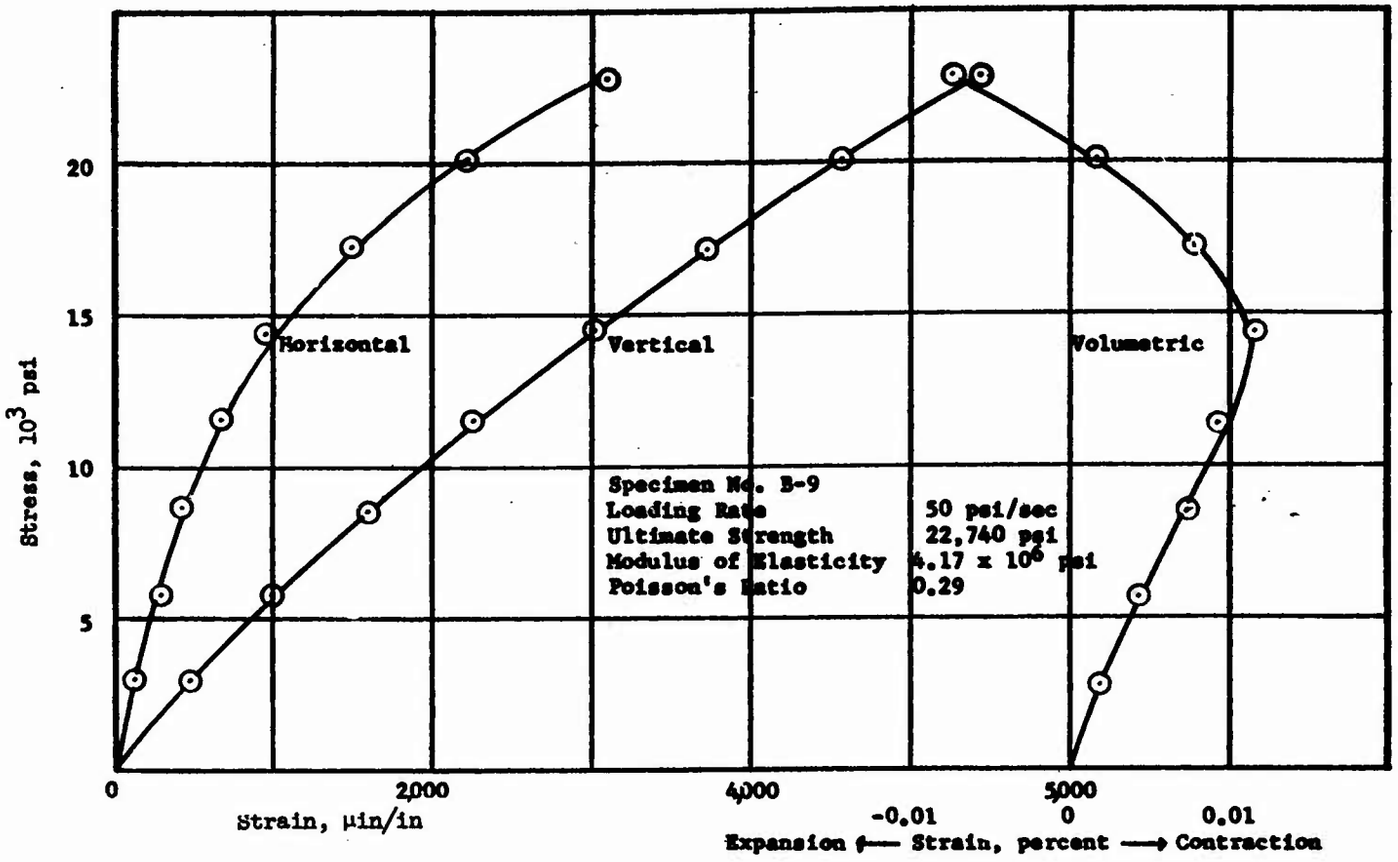

Figure 3.16 Stress versus strain curves for basalt Specimen B-9.

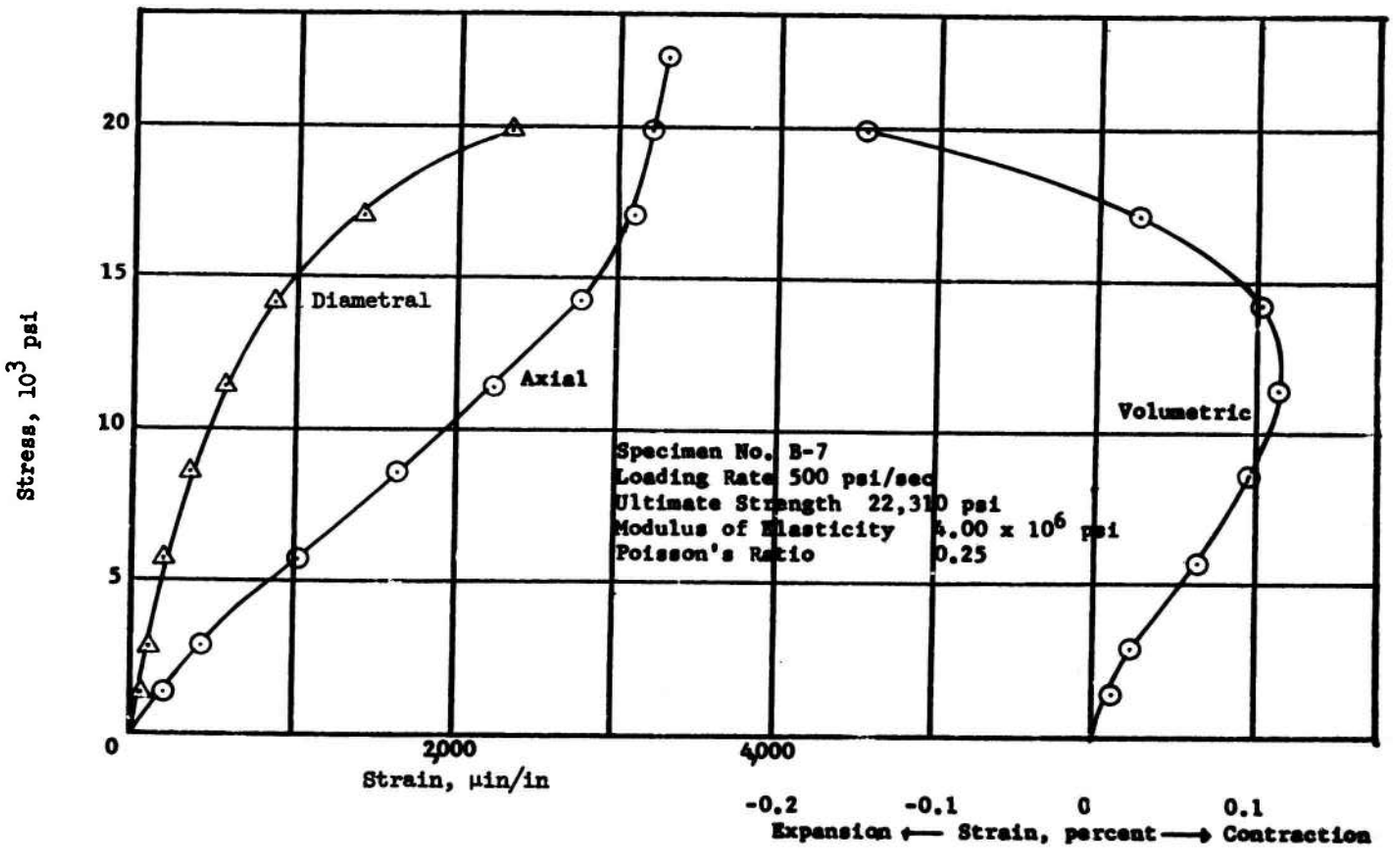

Figure 3.17 Stress versus strain curves for basalt Specimen B-7.

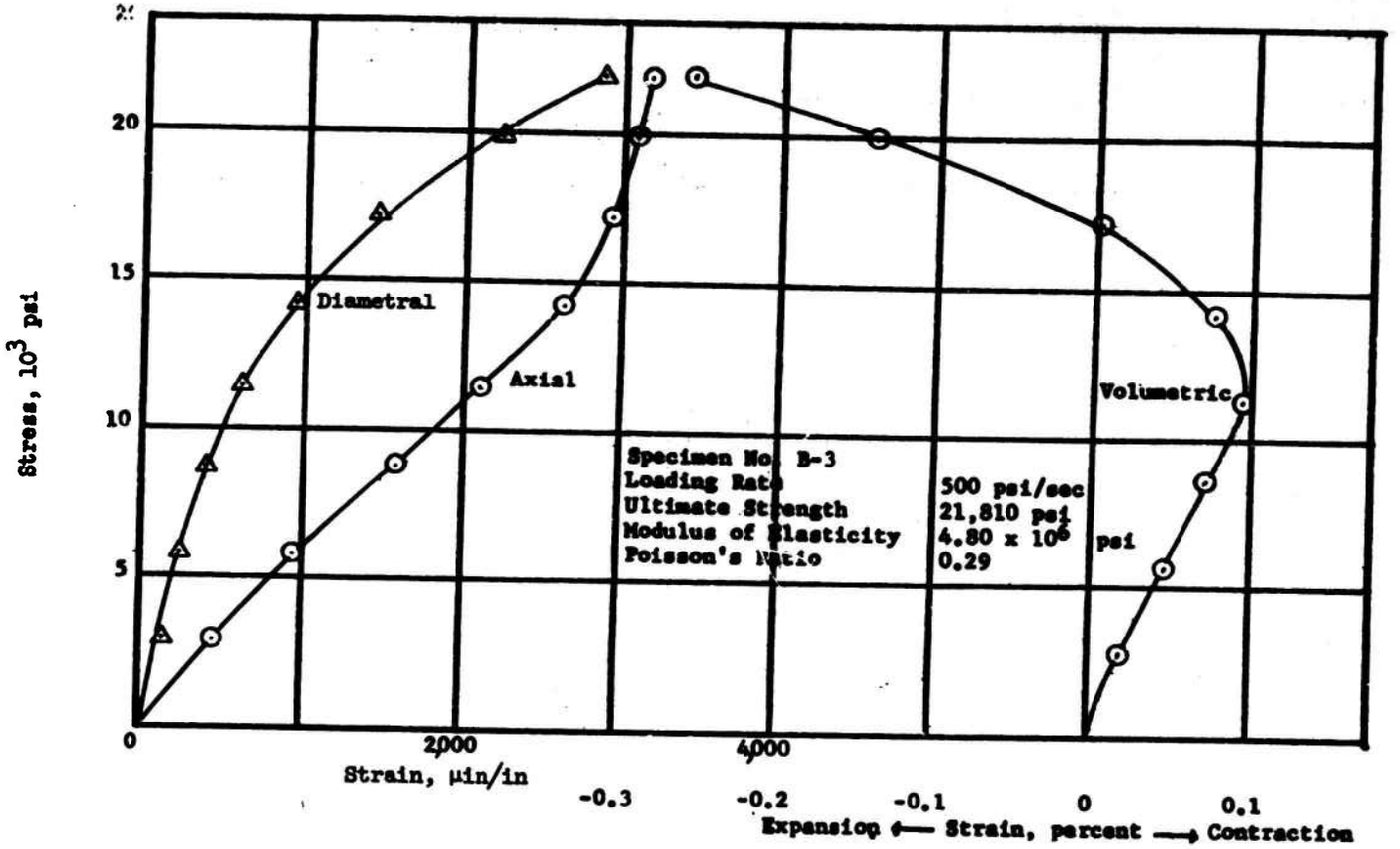

Figure 3.18 Stress versus strain curves for basalt Specimen B-3.

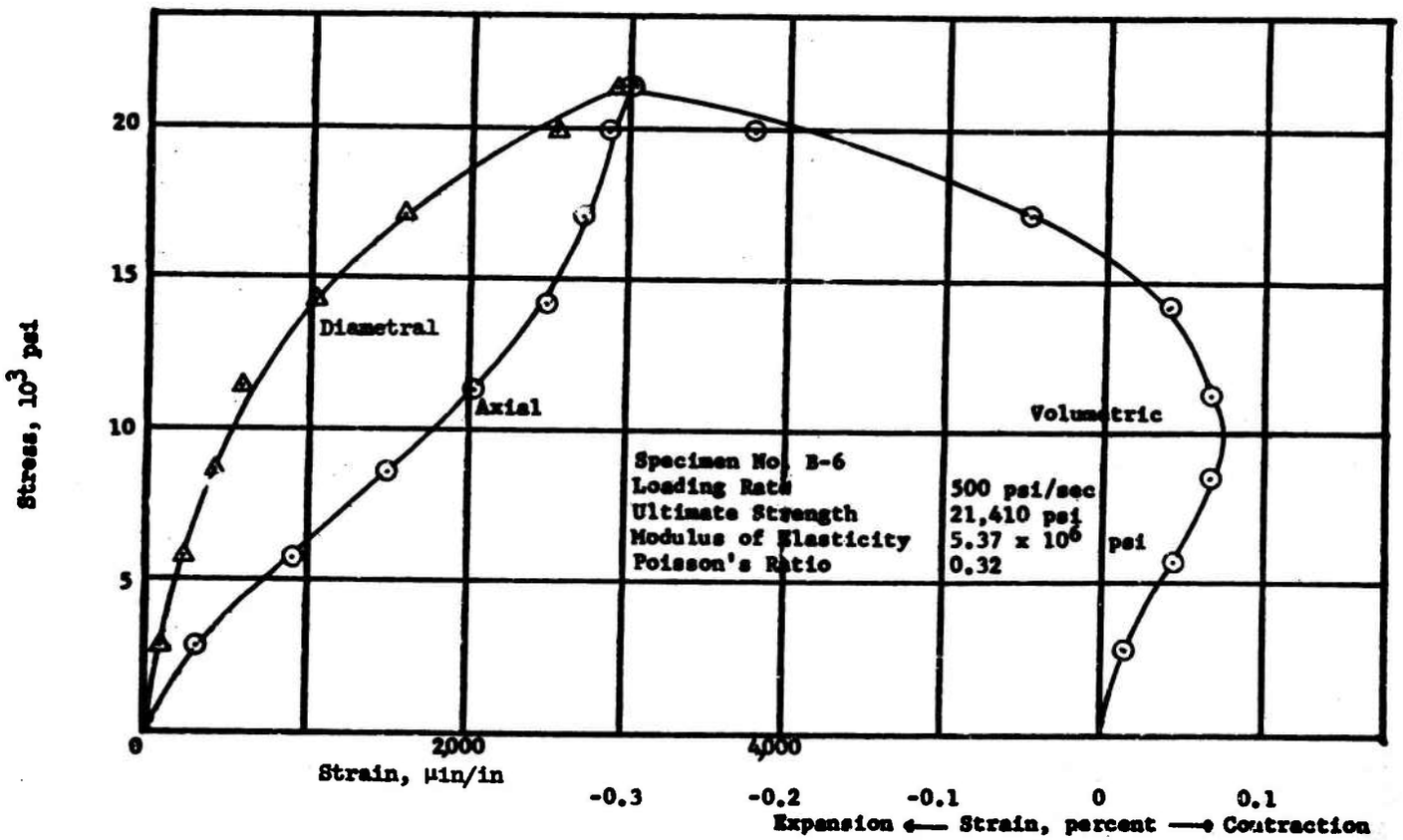

Figure 3.19 Stress versus strain curves for basalt Specimen B-6.

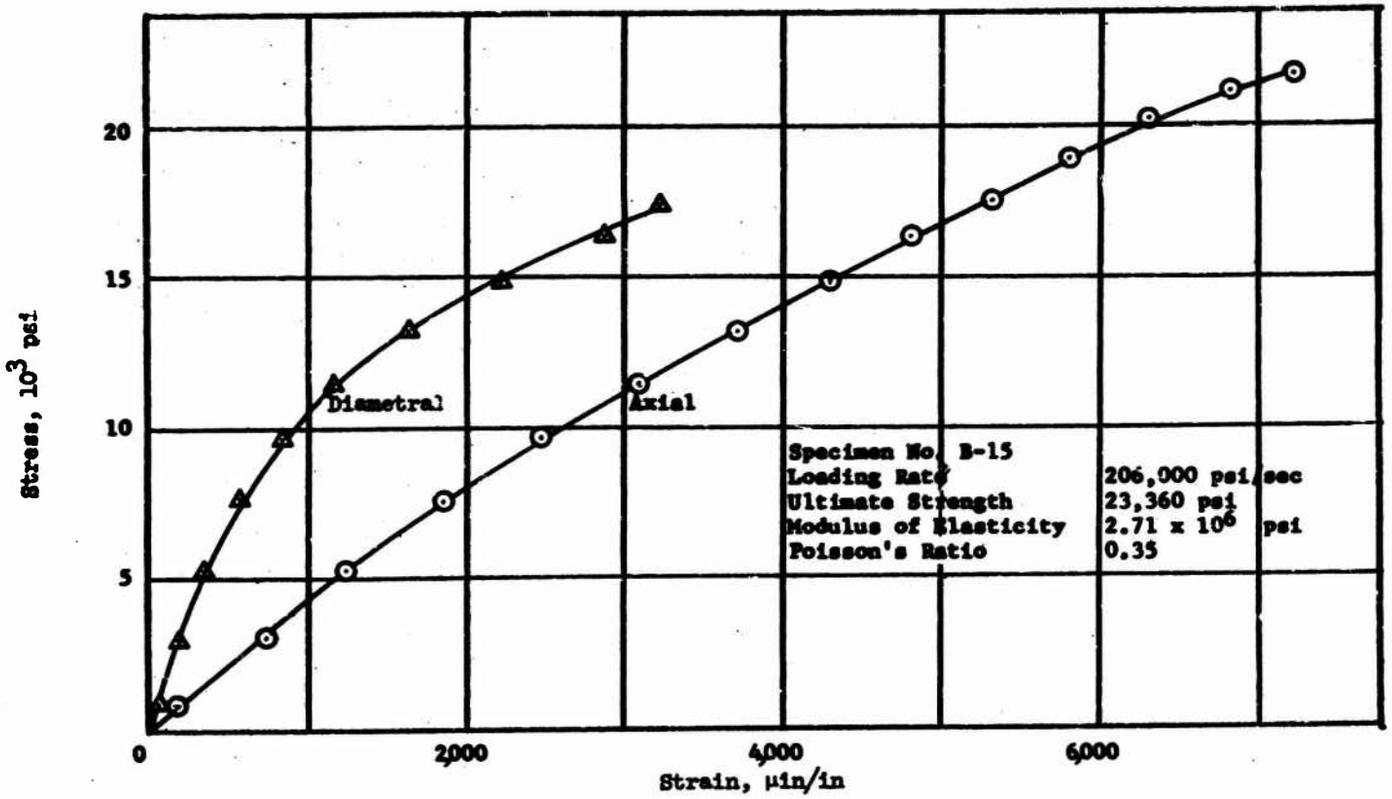

Figure 3.20 Stress versus strain curves for basalt Specimen B-15.

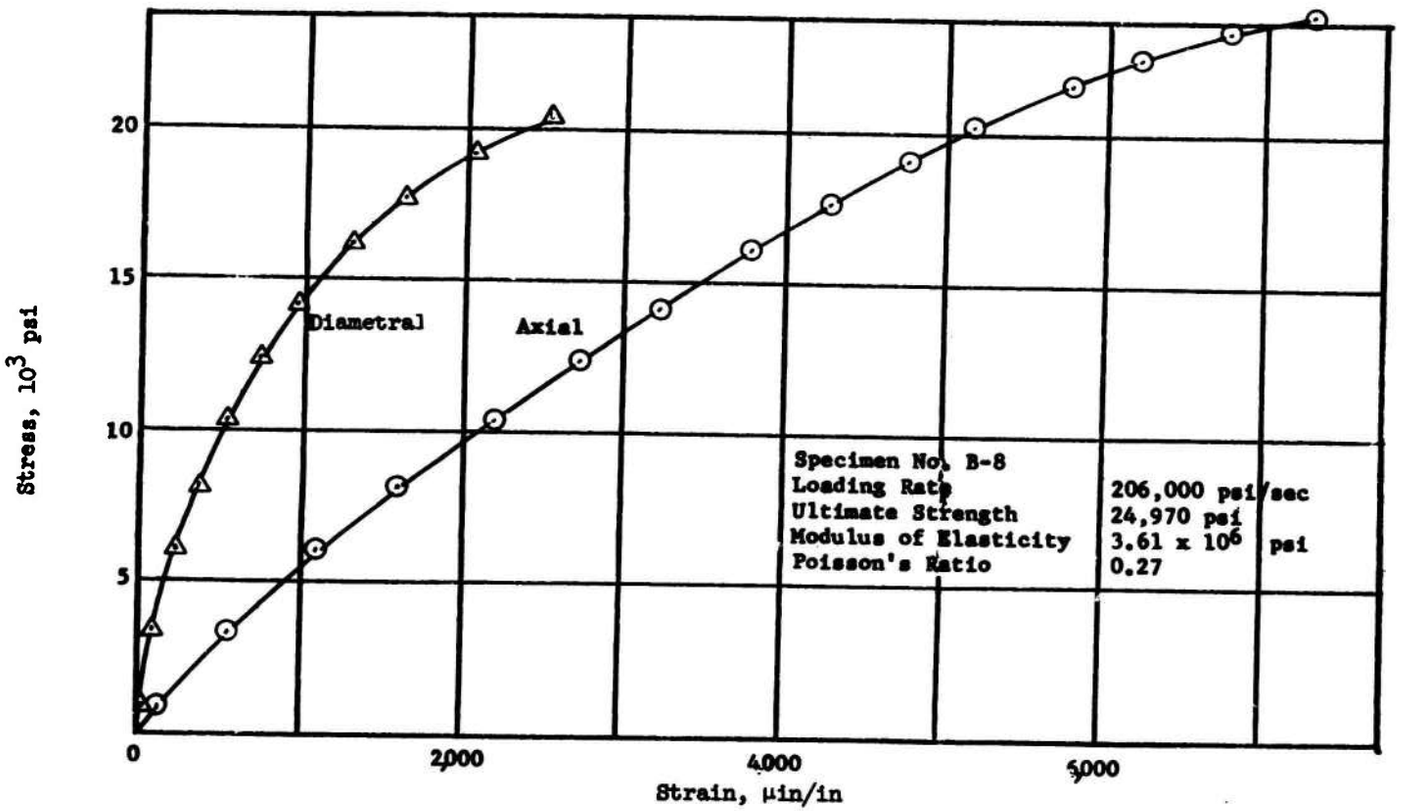

Figure 3.21 Stress versus strain curves for basalt Specimen B-8.

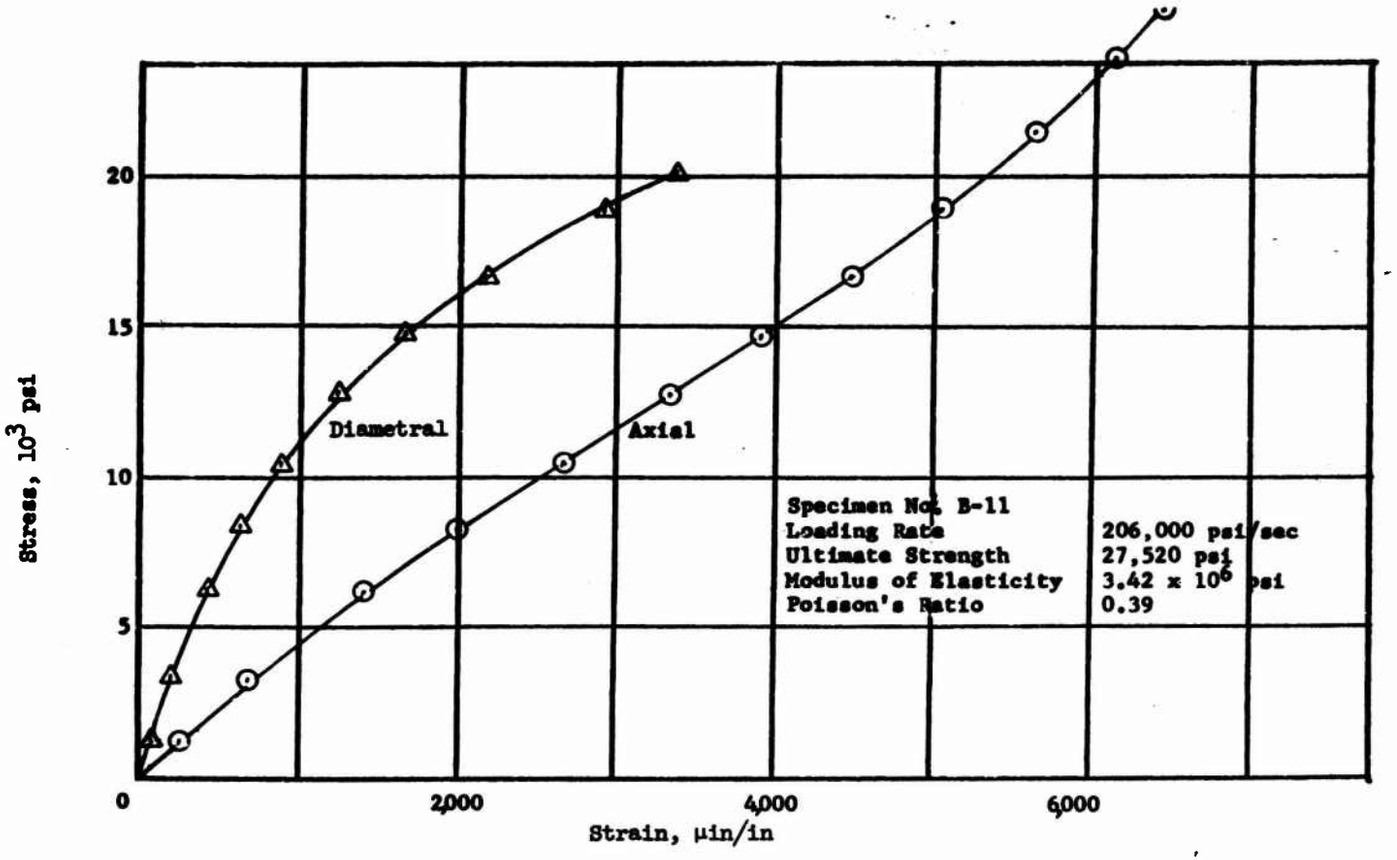

Figure 3.22 Stress versus strain curves for basalt Specimen B-11.

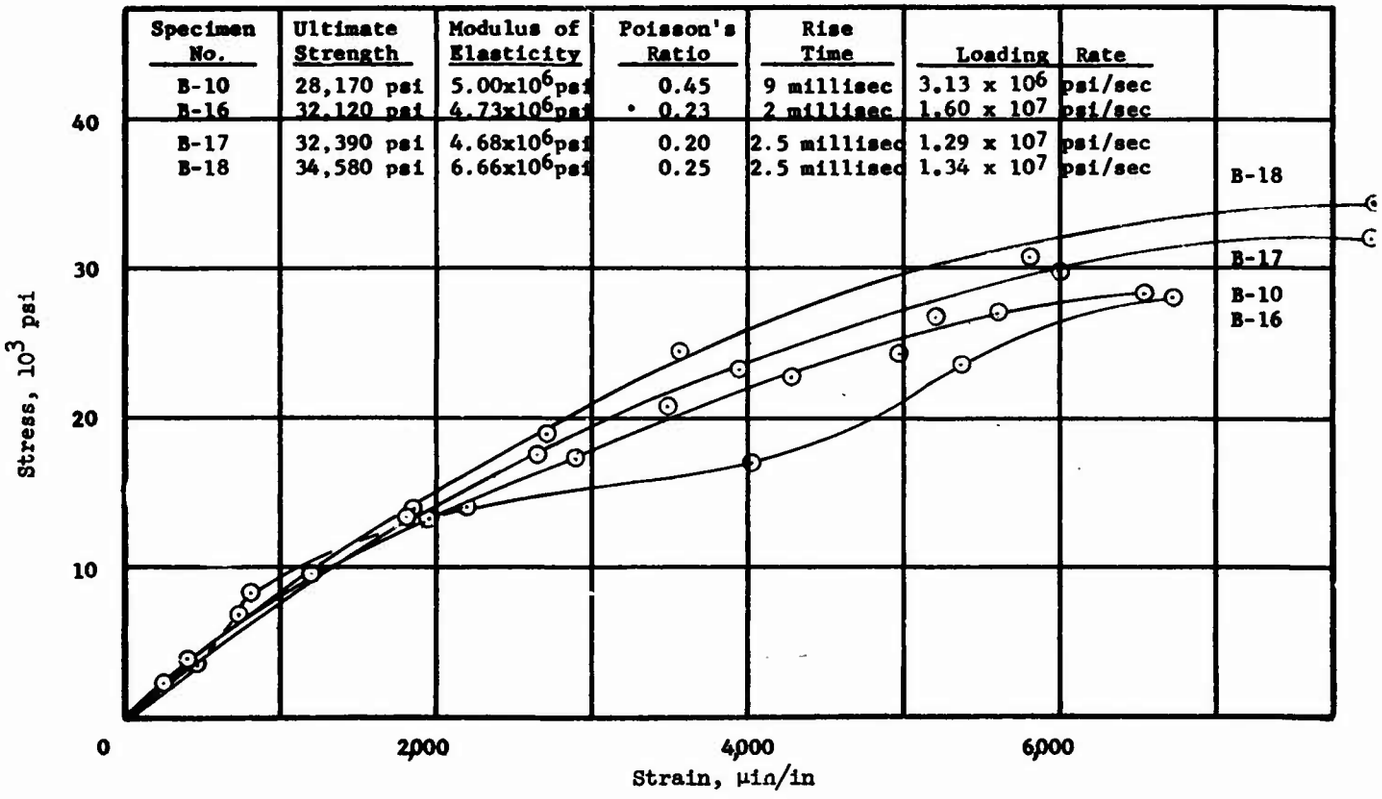

Figure 3.23 Dynamic stress versus strain curves for basalt (200-kip loader) Specimens B-10, B-16, B-17, and B-18.

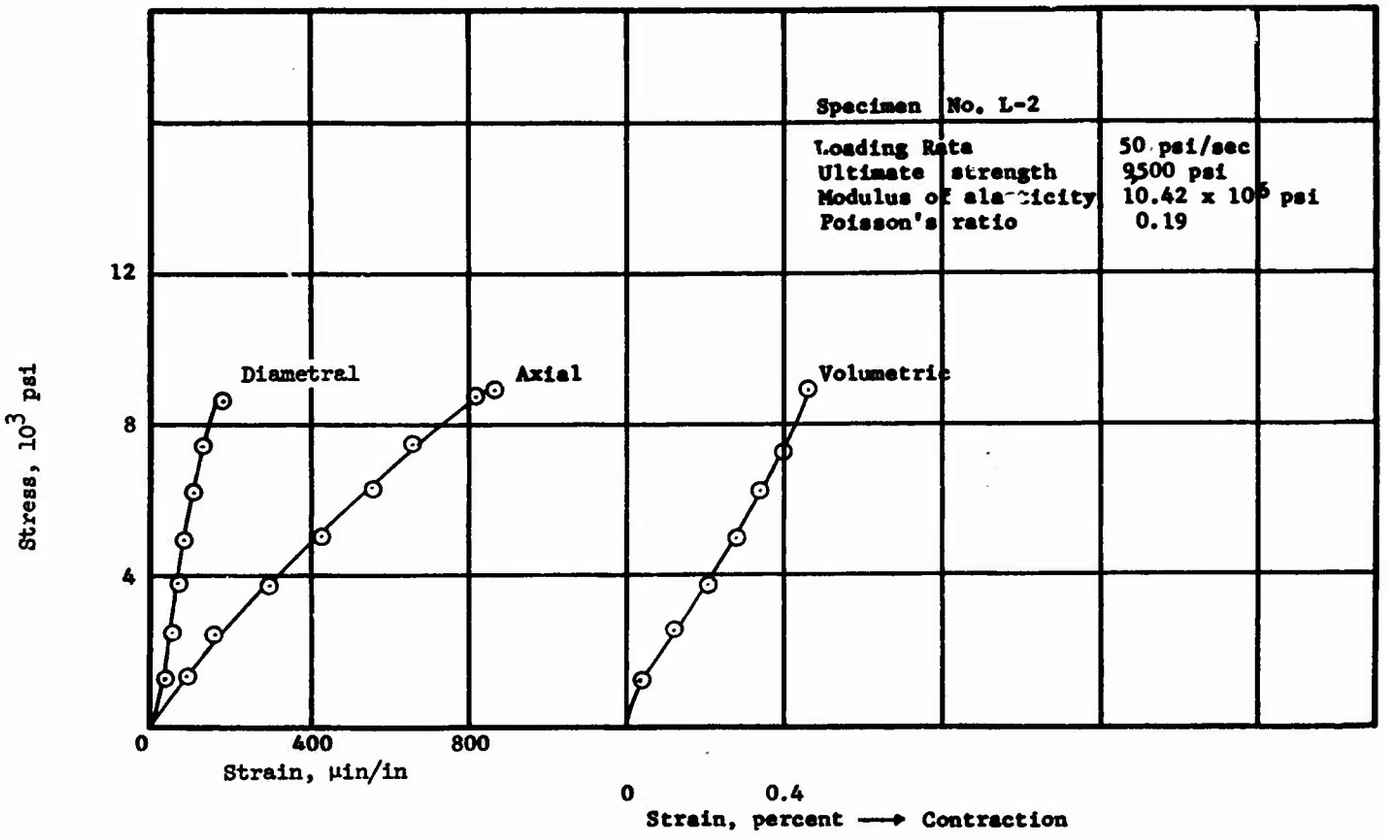

Figure 3.24 Stress versus strain curves for limestone Specimen L-2.

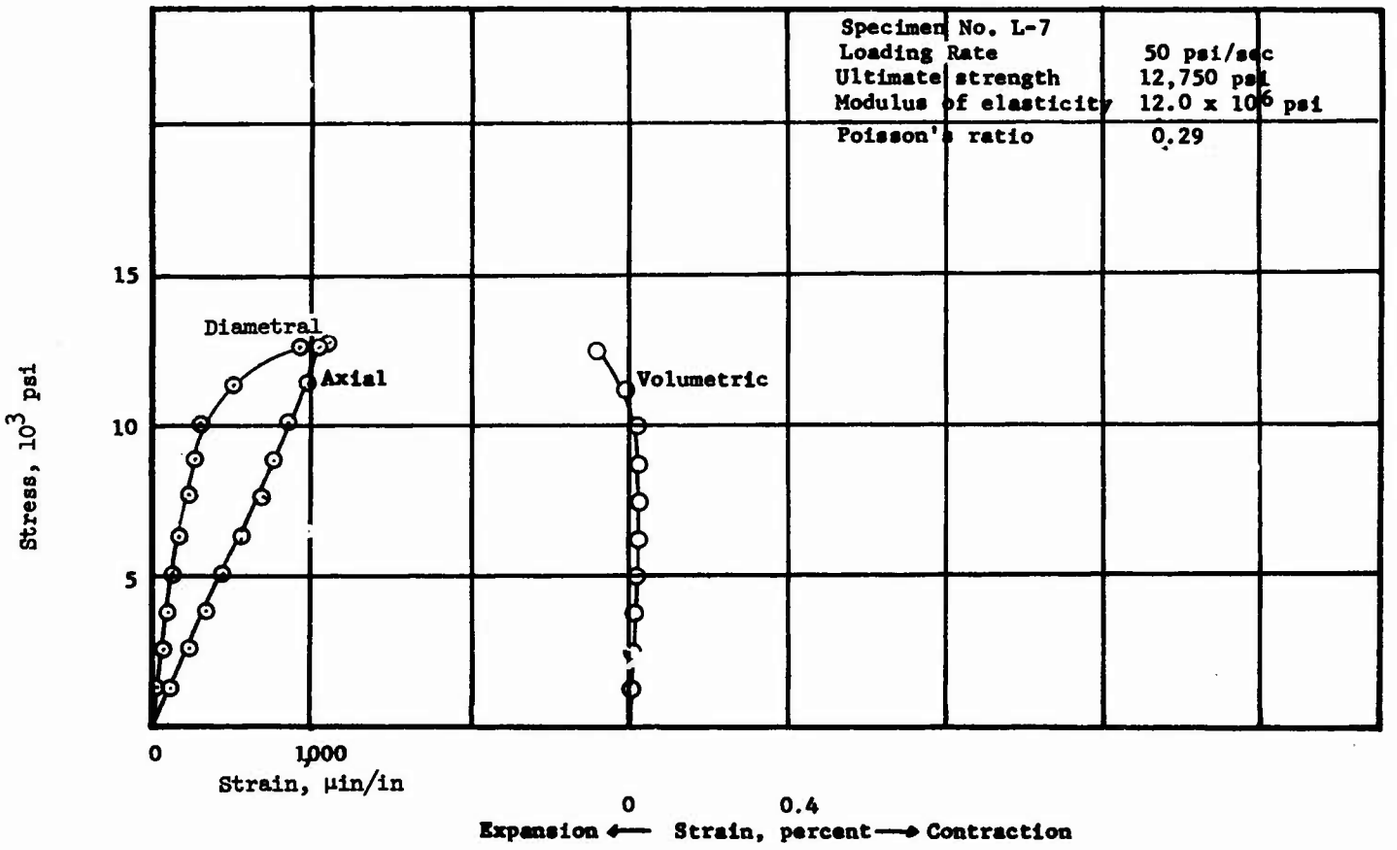

Figure 3.25 Stress versus strain curves for limestone Specimen L-7.

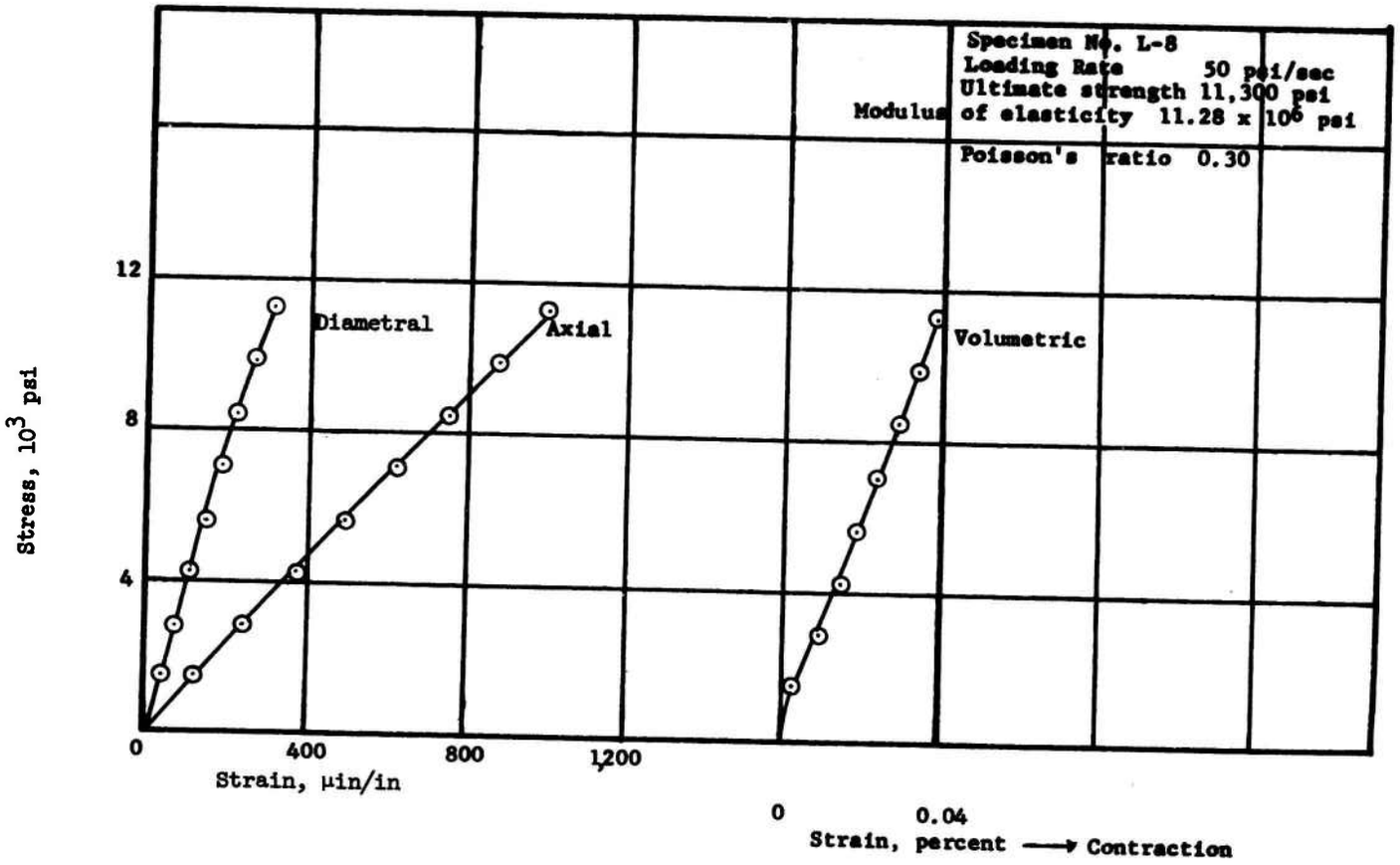

Figure 3.26 Stress versus strain curves for limestone Specimen L-8.

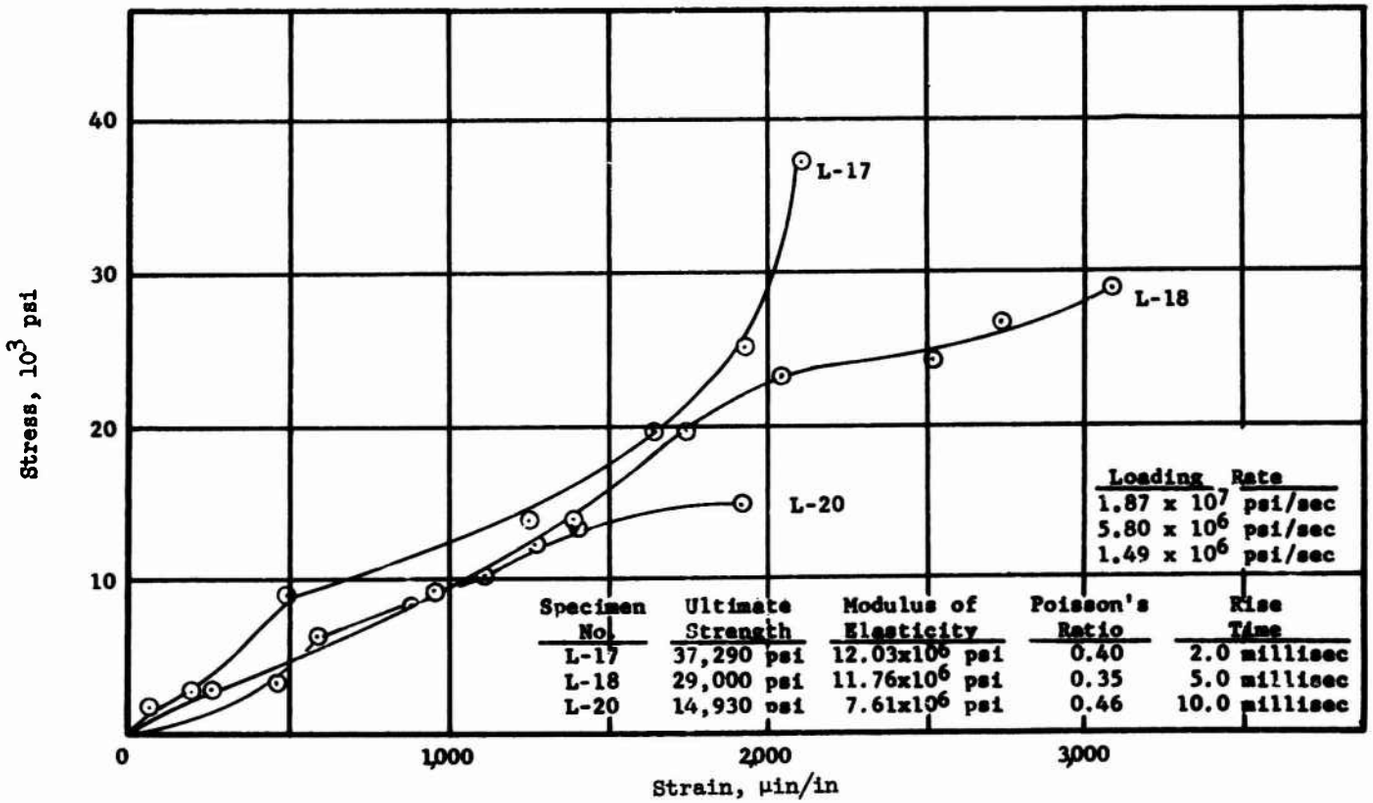

Figure 3.27 Dynamic stress versus strain curves for limestone (200-kip loader) Specimens L-17, L-18, and L-20.

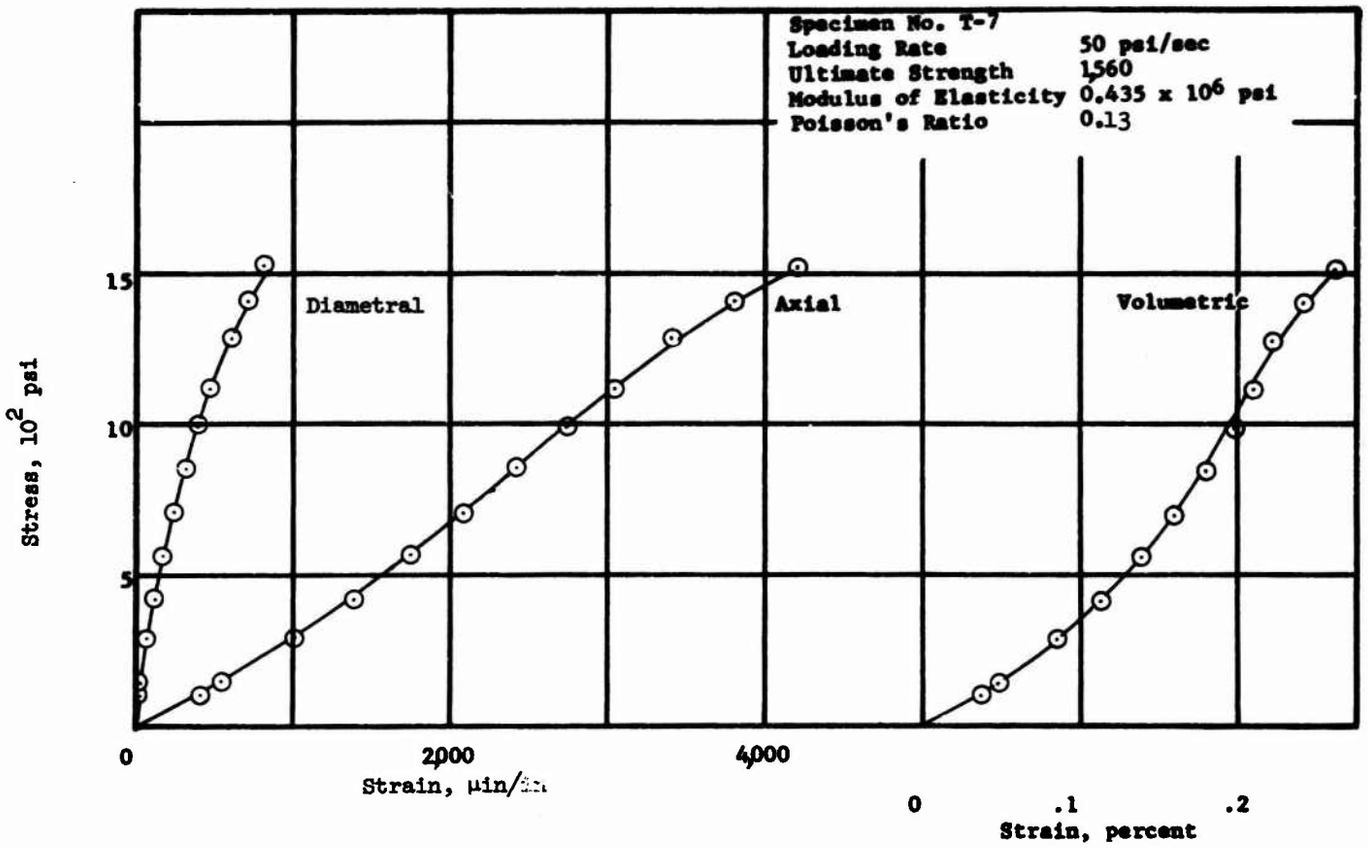

Figure 3.28 Stress versus strain curves for tuff Specimen T-7.

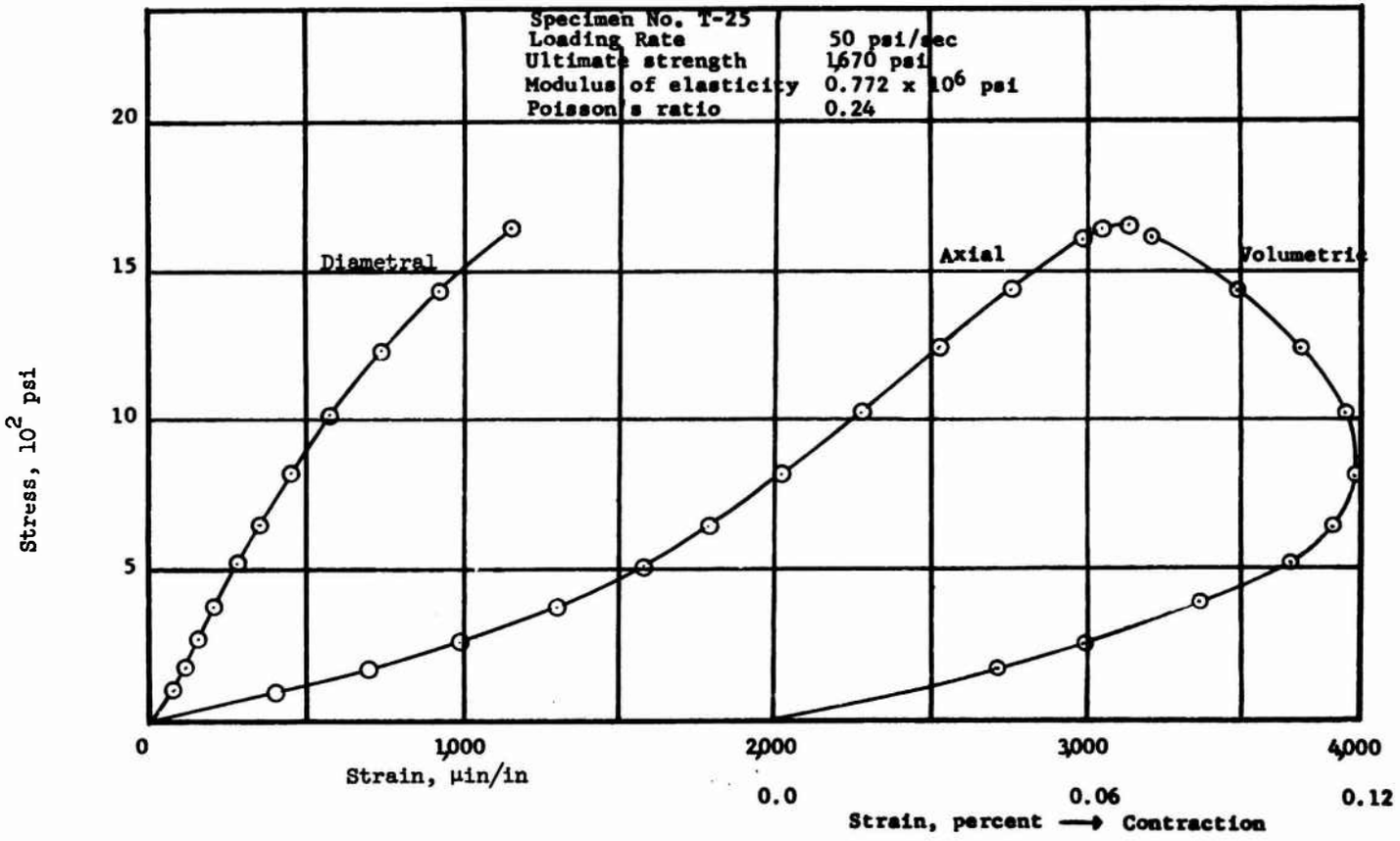

Figure 3.29 Stress versus strain curves for tuff Specimen T-25.

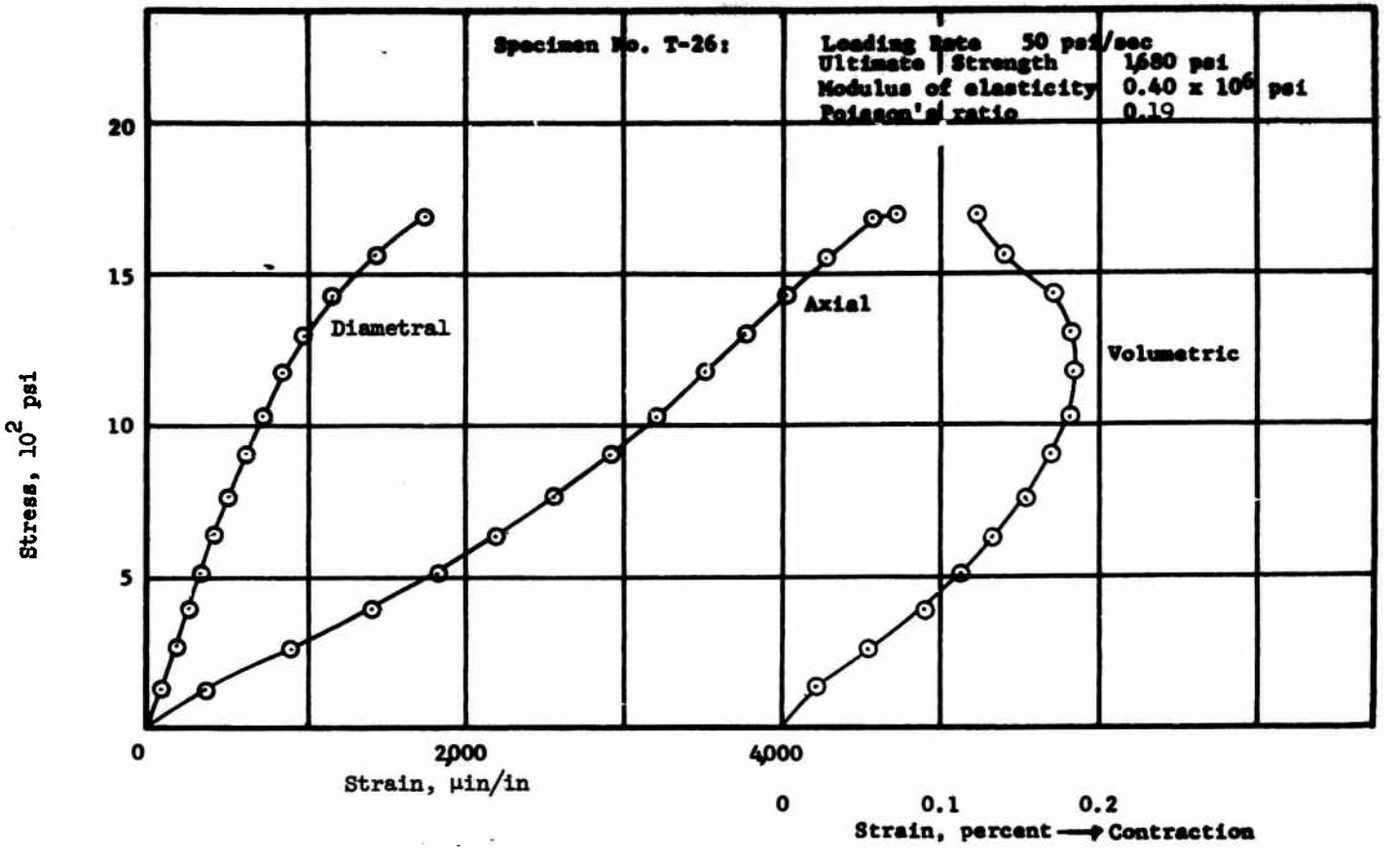

Figure 3.30 Stress versus strain curves for tuff Specimen T-26.

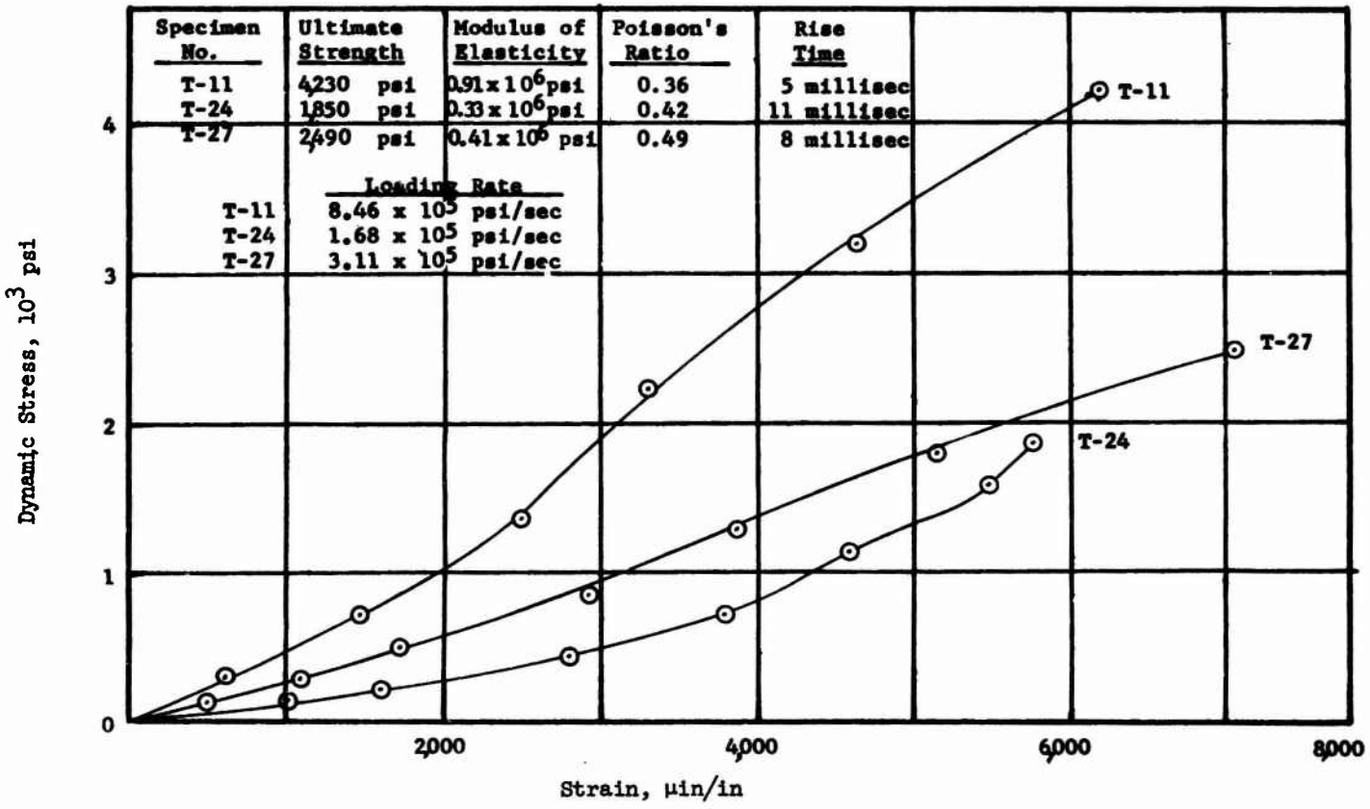

Figure 3.31 Dynamic stress versus strain curves for tuff (drop tower) Specimens T-11, T-24, and T-27.

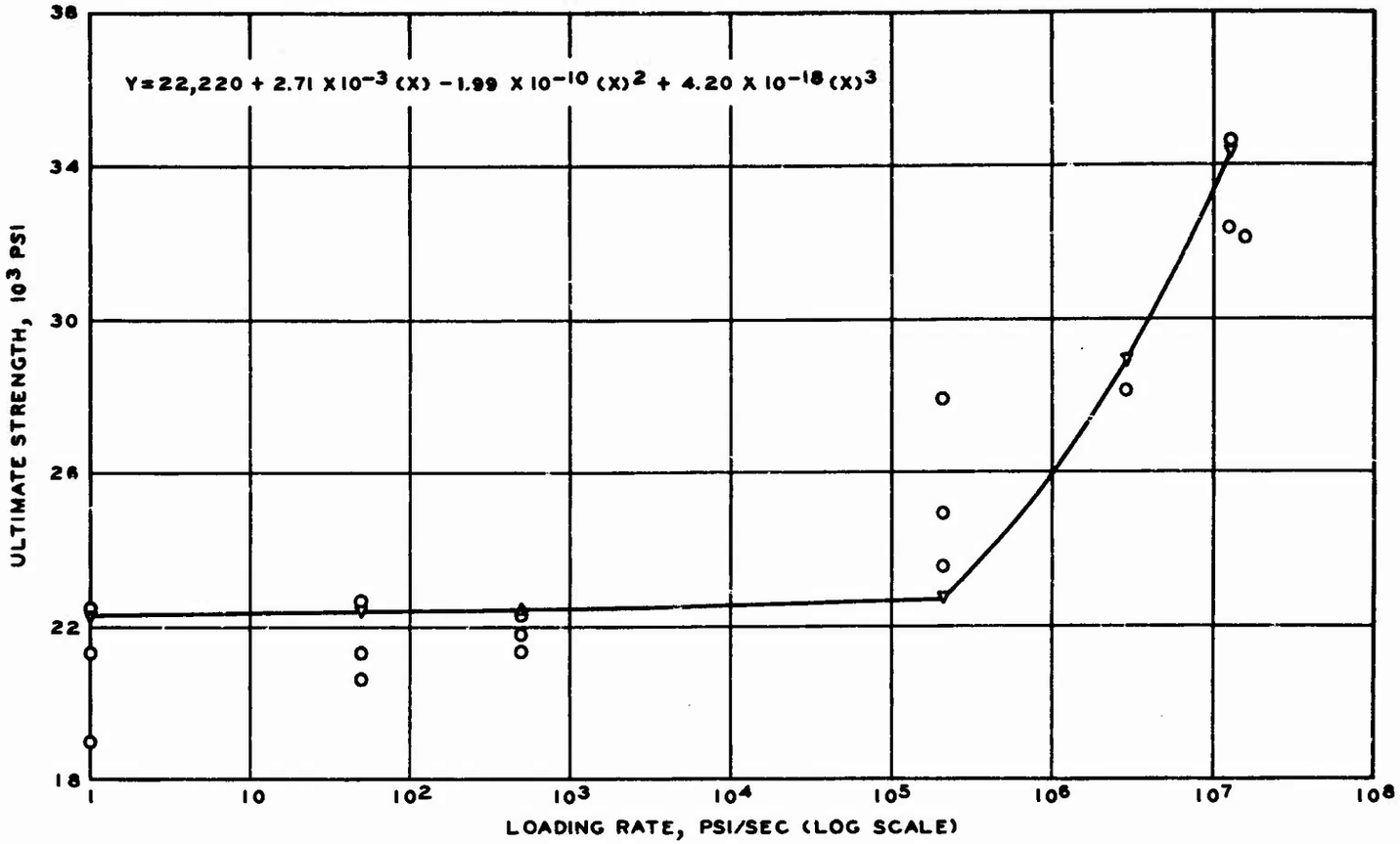

Figure 3.32 Ultimate strength versus loading rate for basalt in unconfined compression.

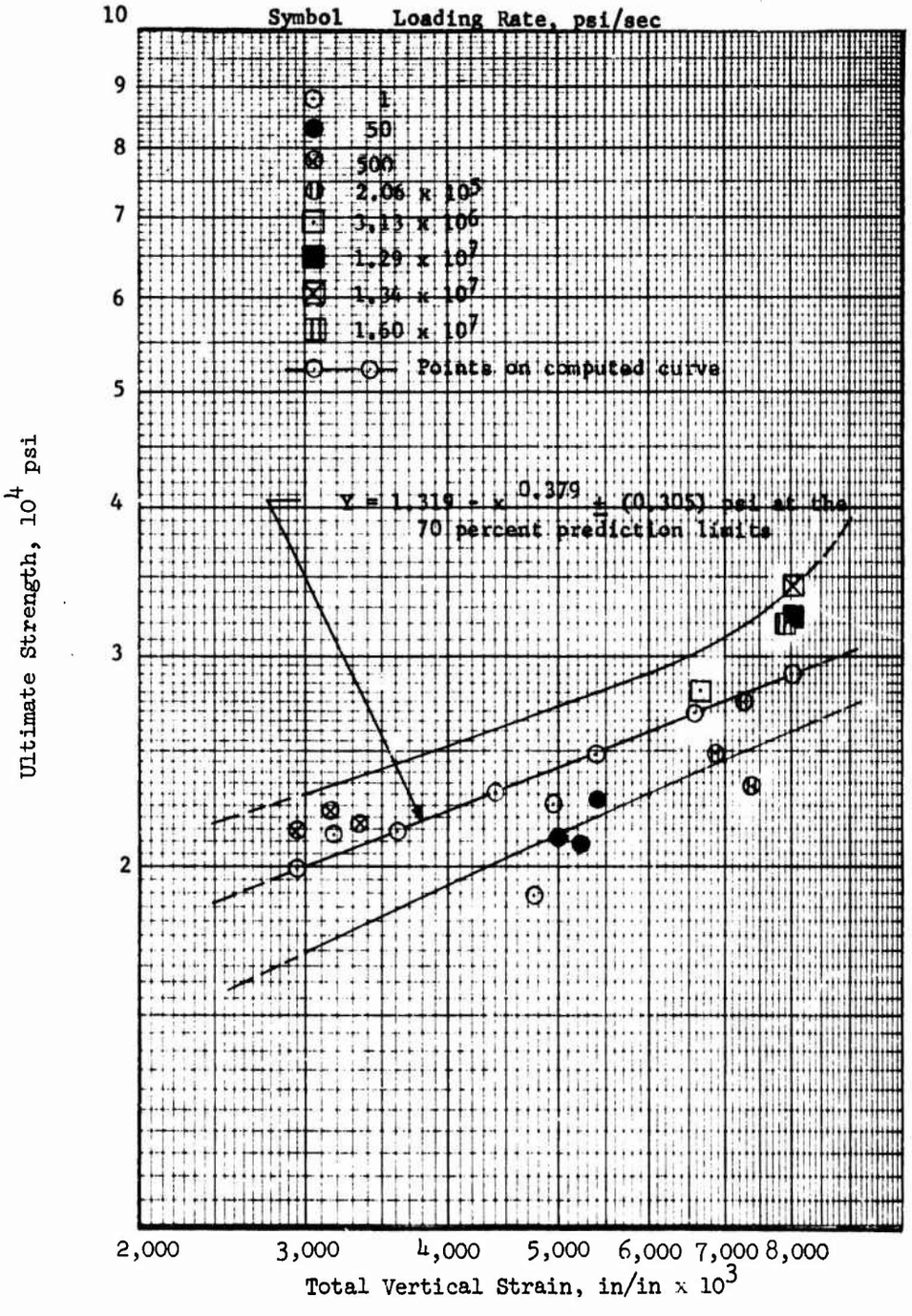

Figure 3.33 Ultimate strength versus total vertical strain at failure for basalt tested in unconfined compression at loading rates from 1 to 1.6×10^7 psi/sec.

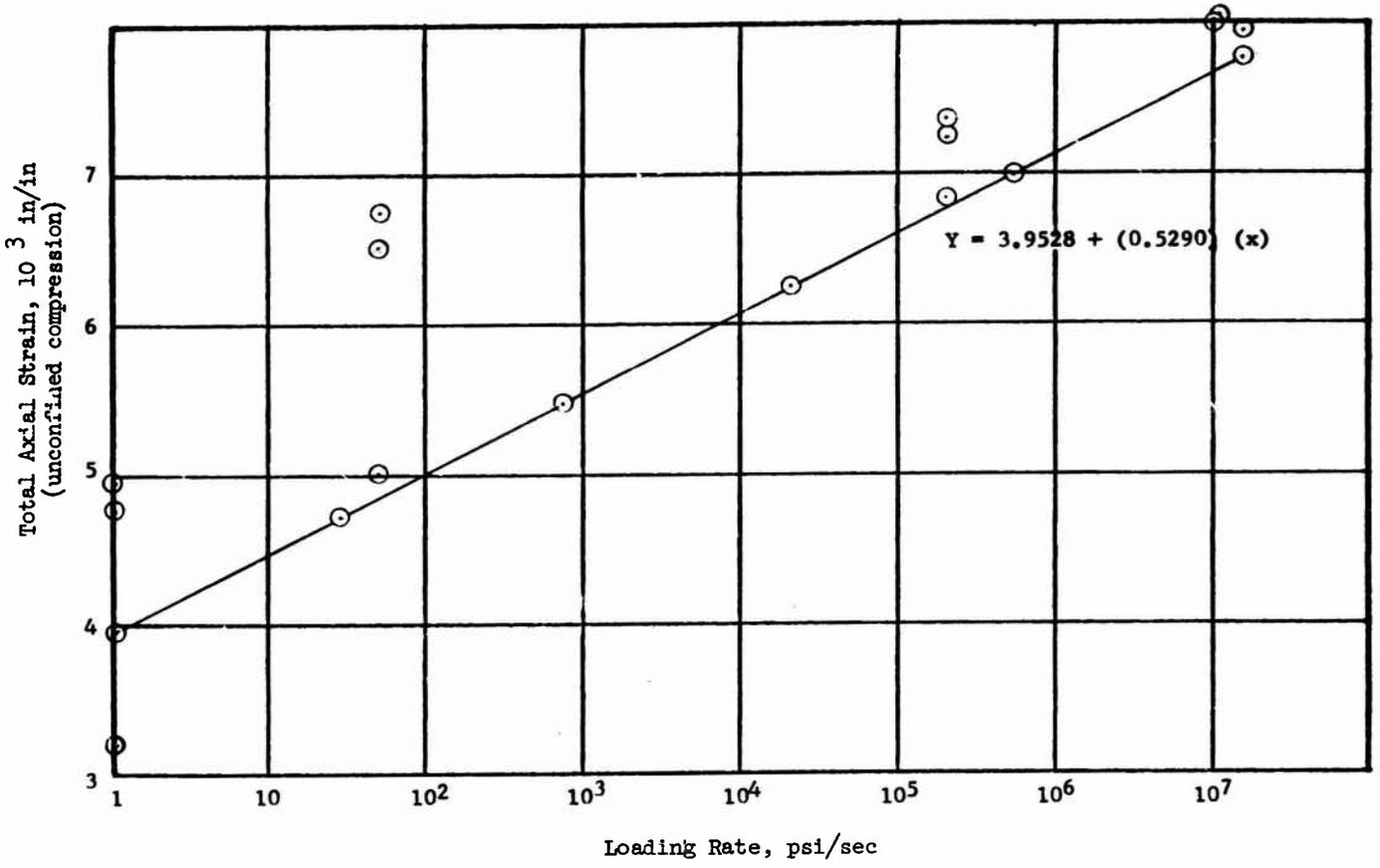

Figure 3.34 Loading rate versus total axial strain at failure for basalt.

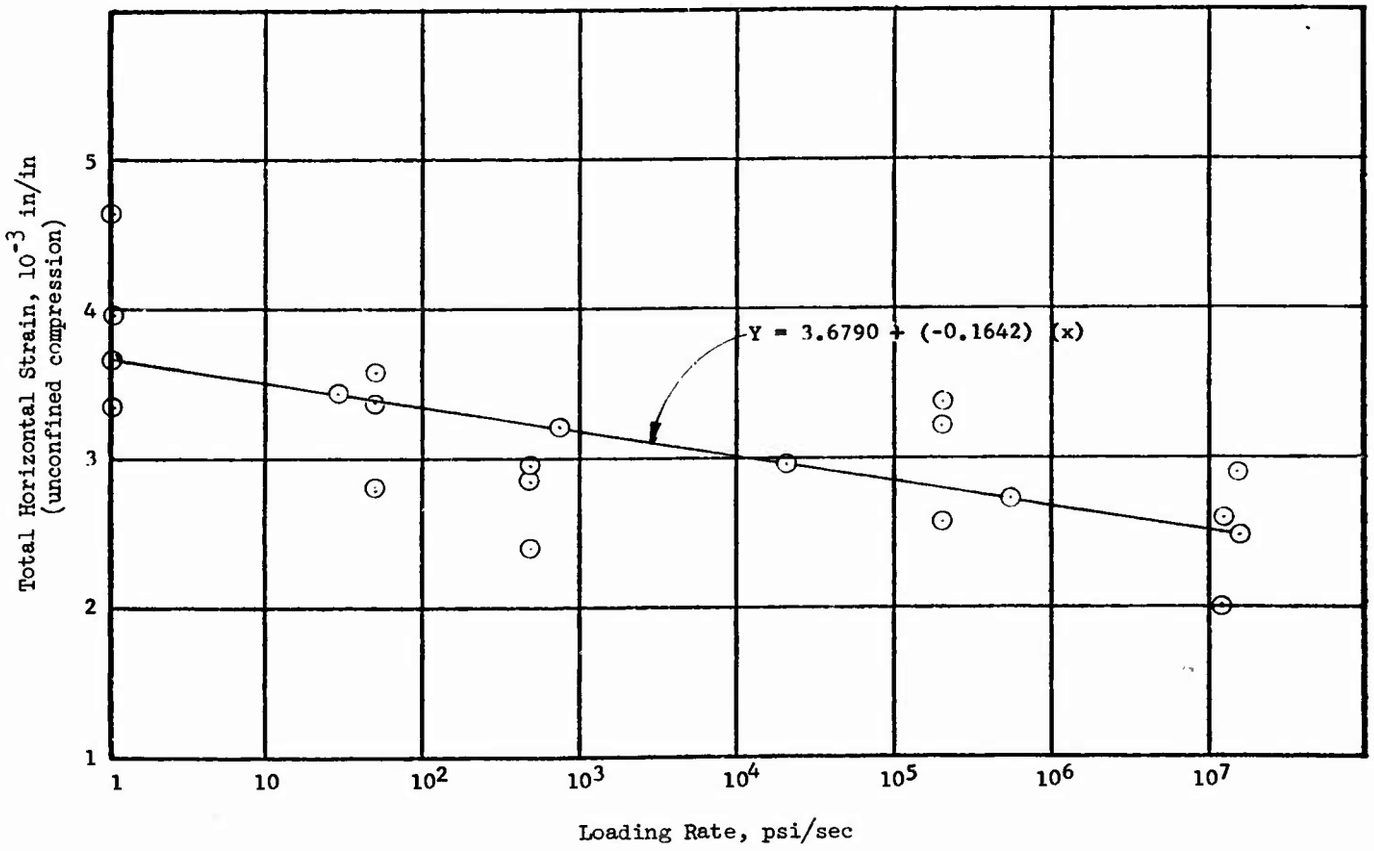

Figure 3.35 Loading rate versus total horizontal strain at failure for basalt.

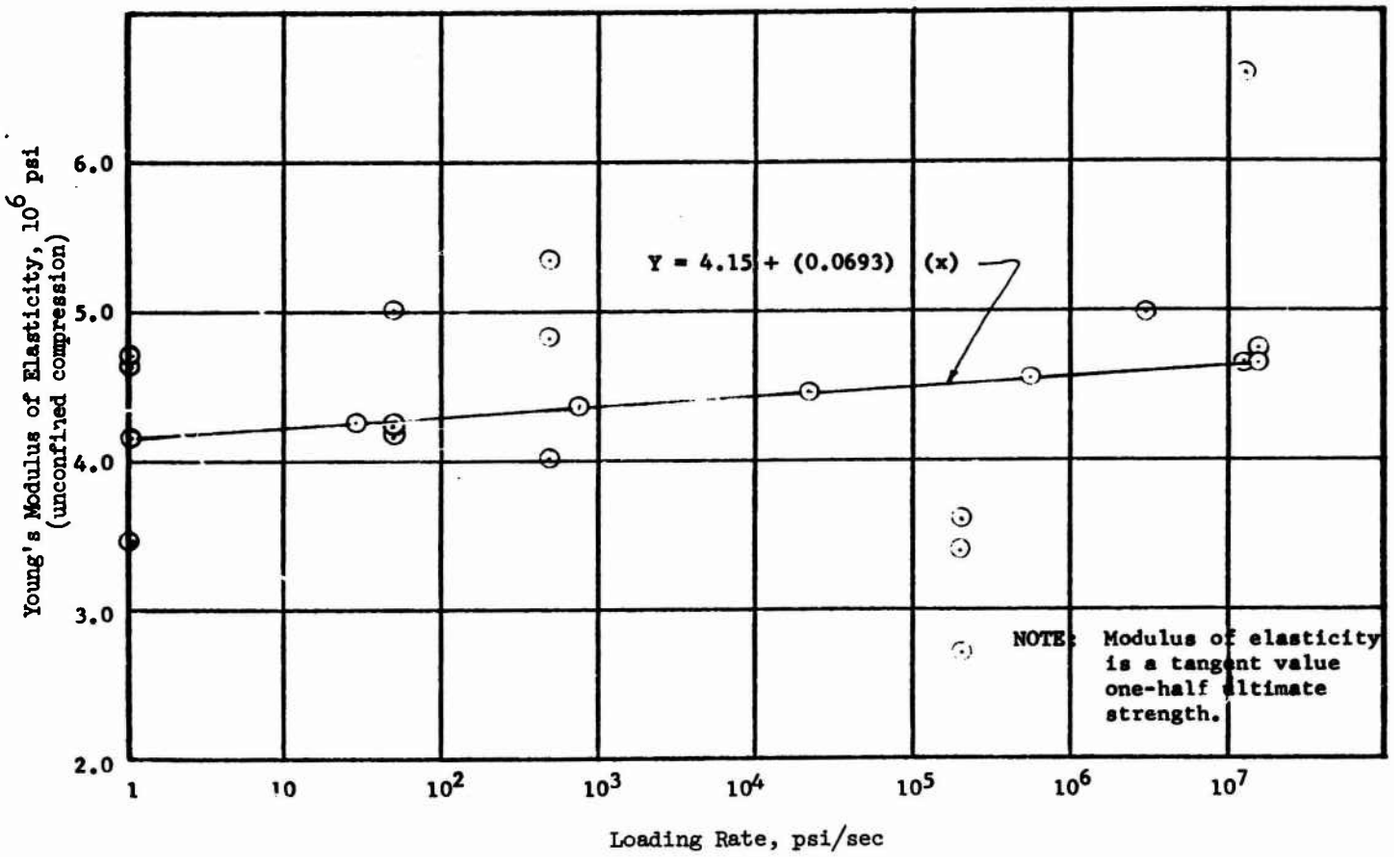

Figure 3.36 Loading rate versus modulus of elasticity for basalt.

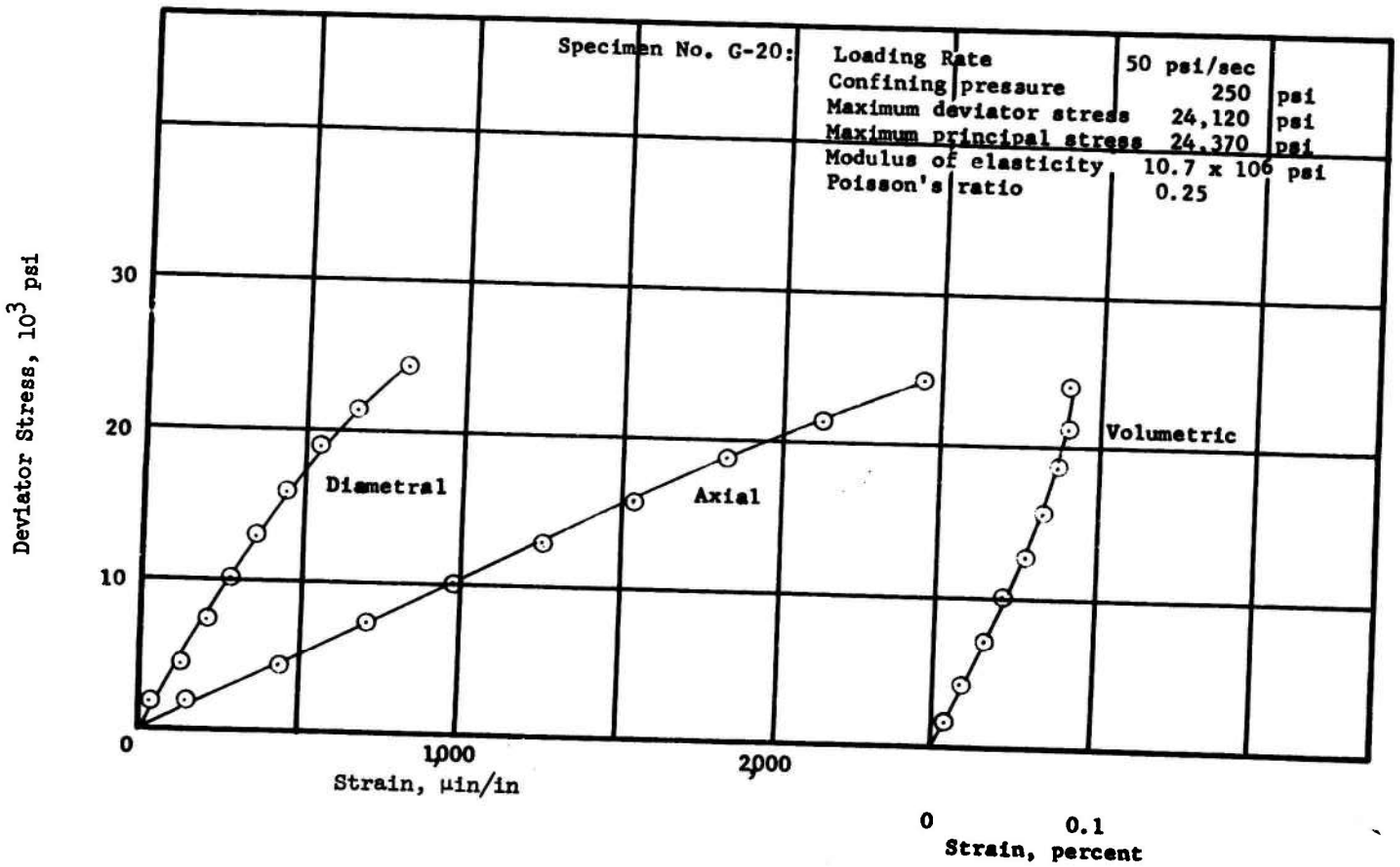

Figure 3.37 Deviator stress versus strain curves for granite Specimen G-20.

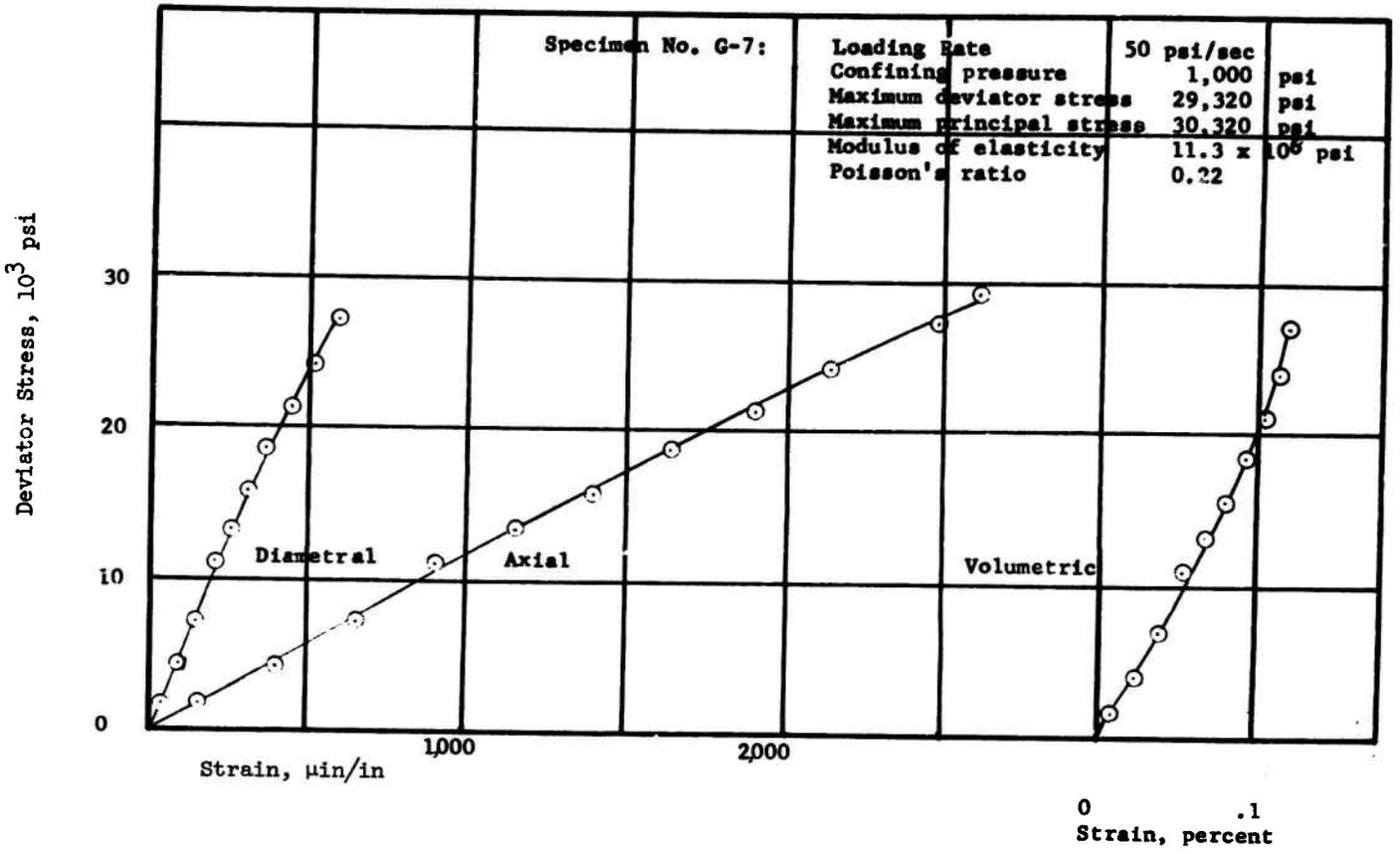

Figure 3.38 Deviator stress versus strain curves for granite Specimen G-7.

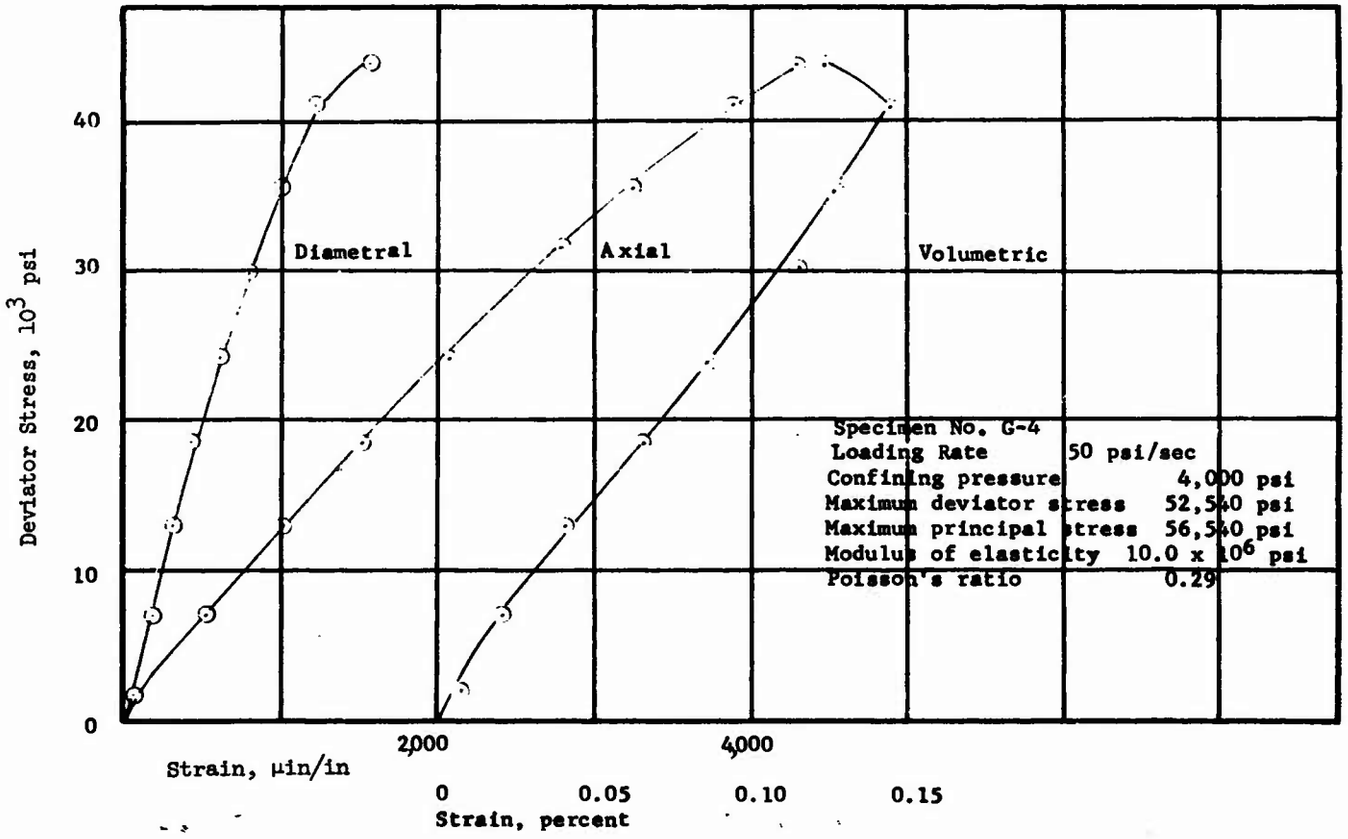

Figure 3.39 Deviator stress versus strain curves for granite Specimen G-4.

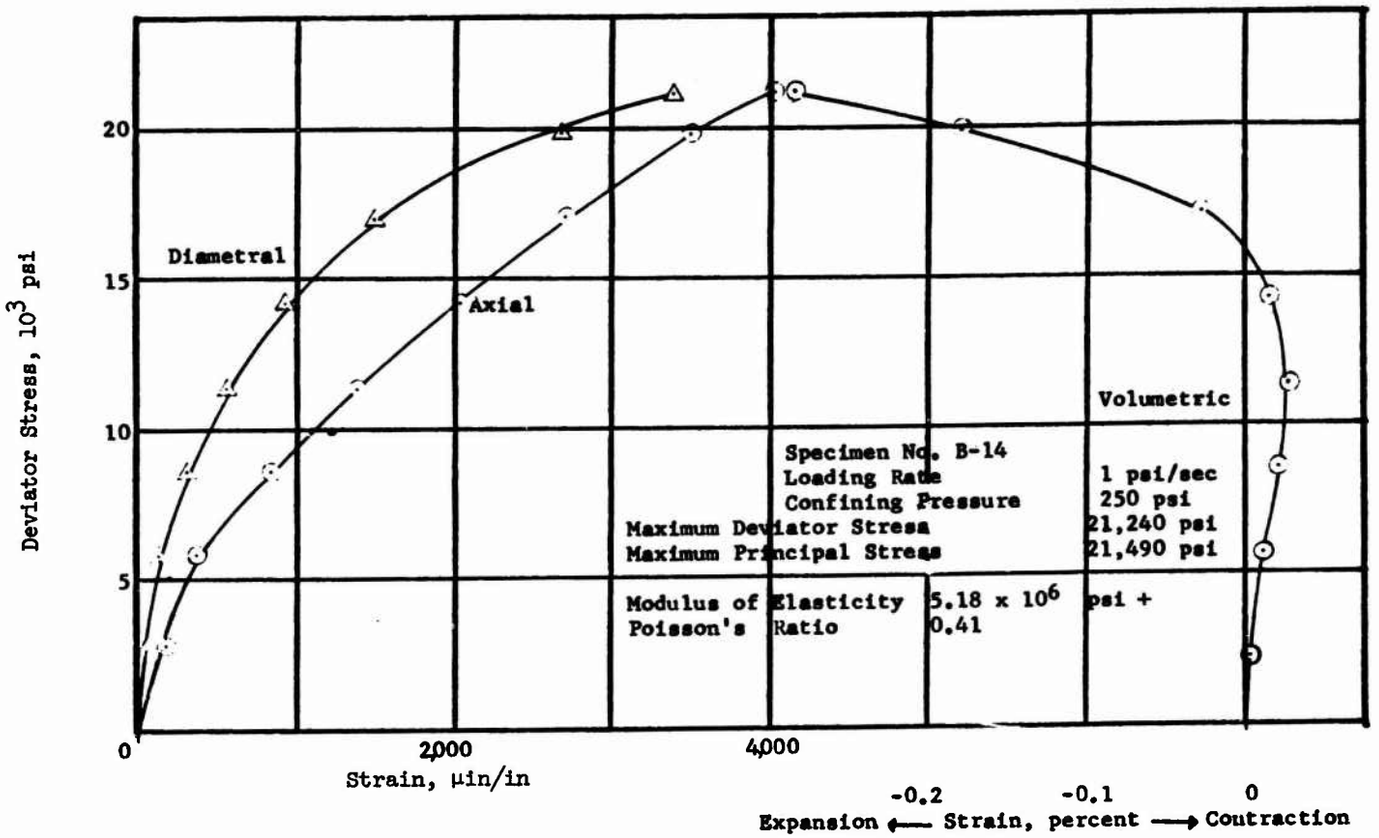

Figure 3.40 Deviator stress versus strain curves for basalt Specimen B-14.

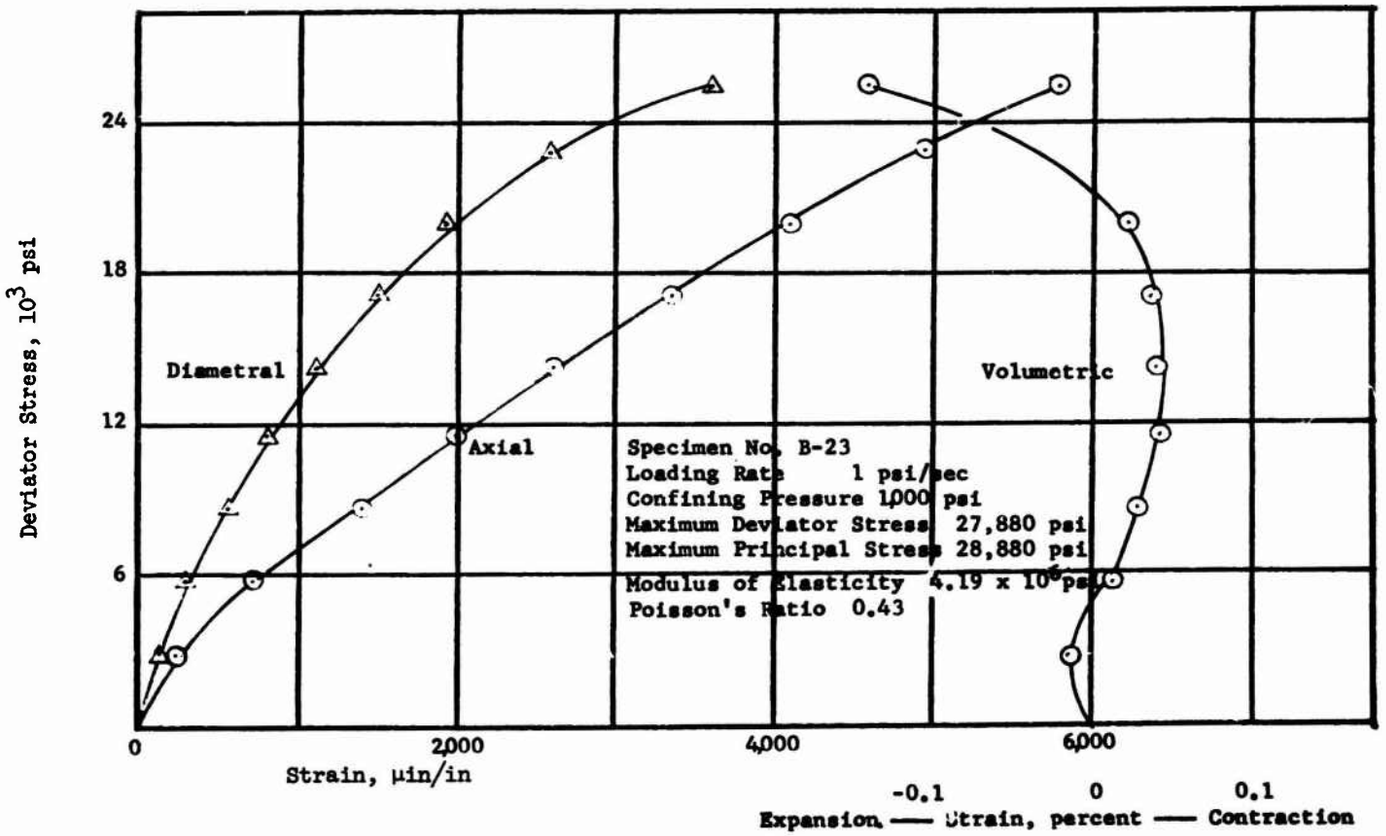

Figure 3.41 Deviator stress versus strain curves for basalt Specimen B-23.

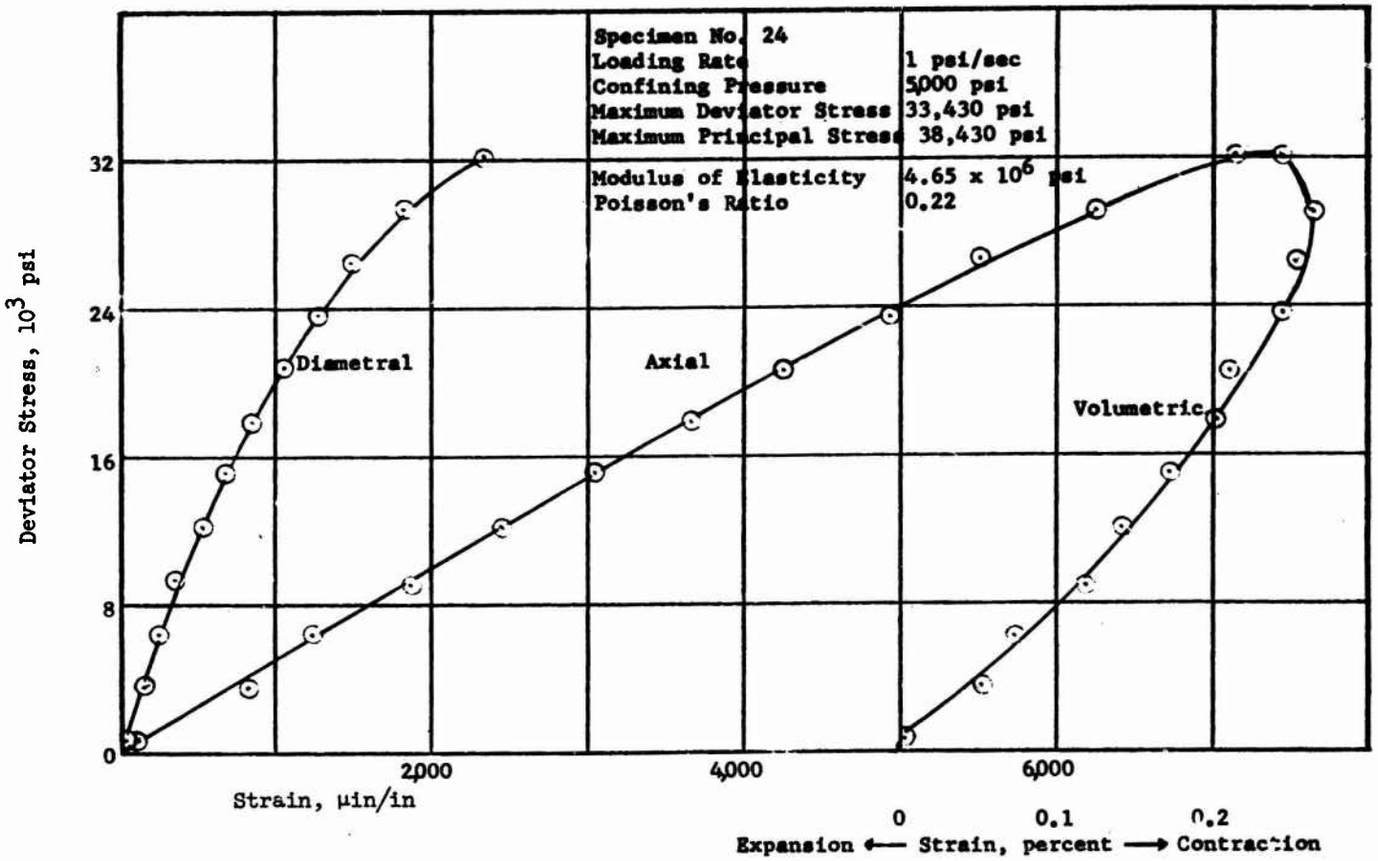

Figure 3.42 Deviator stress versus strain curves for basalt Specimen 24.

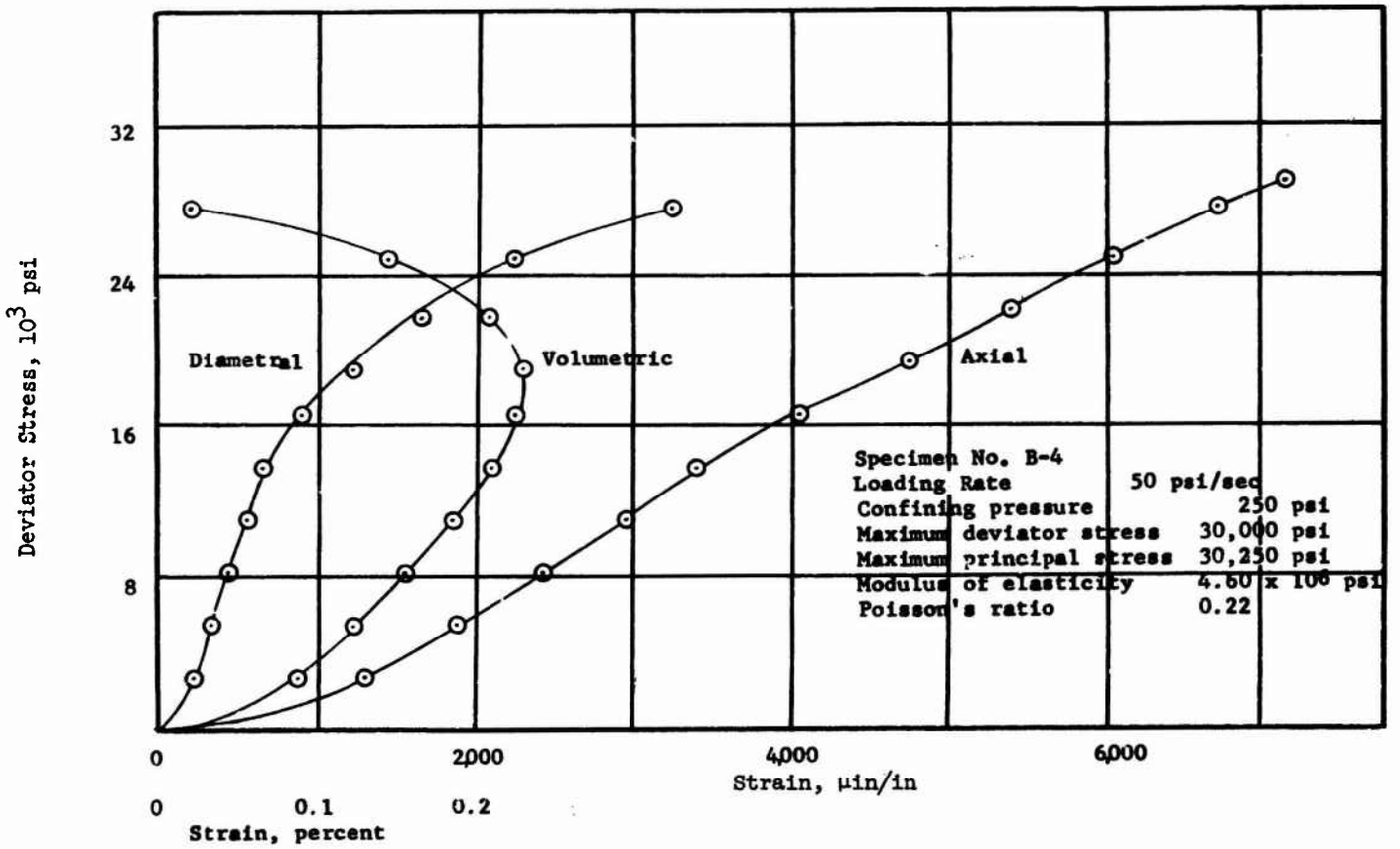

Figure 3.43 Deviator stress versus strain curves for basalt Specimen B-4.

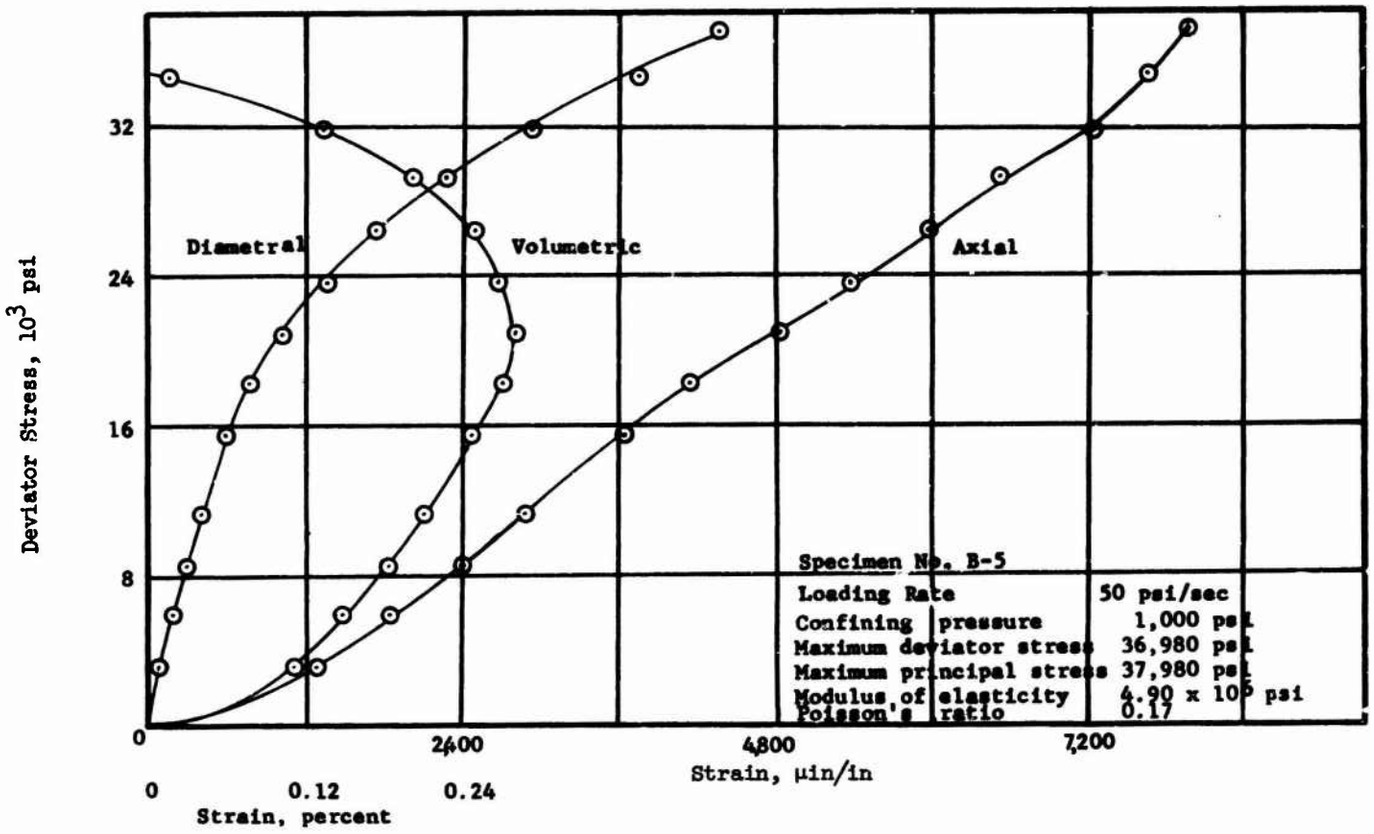

Figure 3.44 Deviator stress versus strain curves for basalt Specimen B-5.

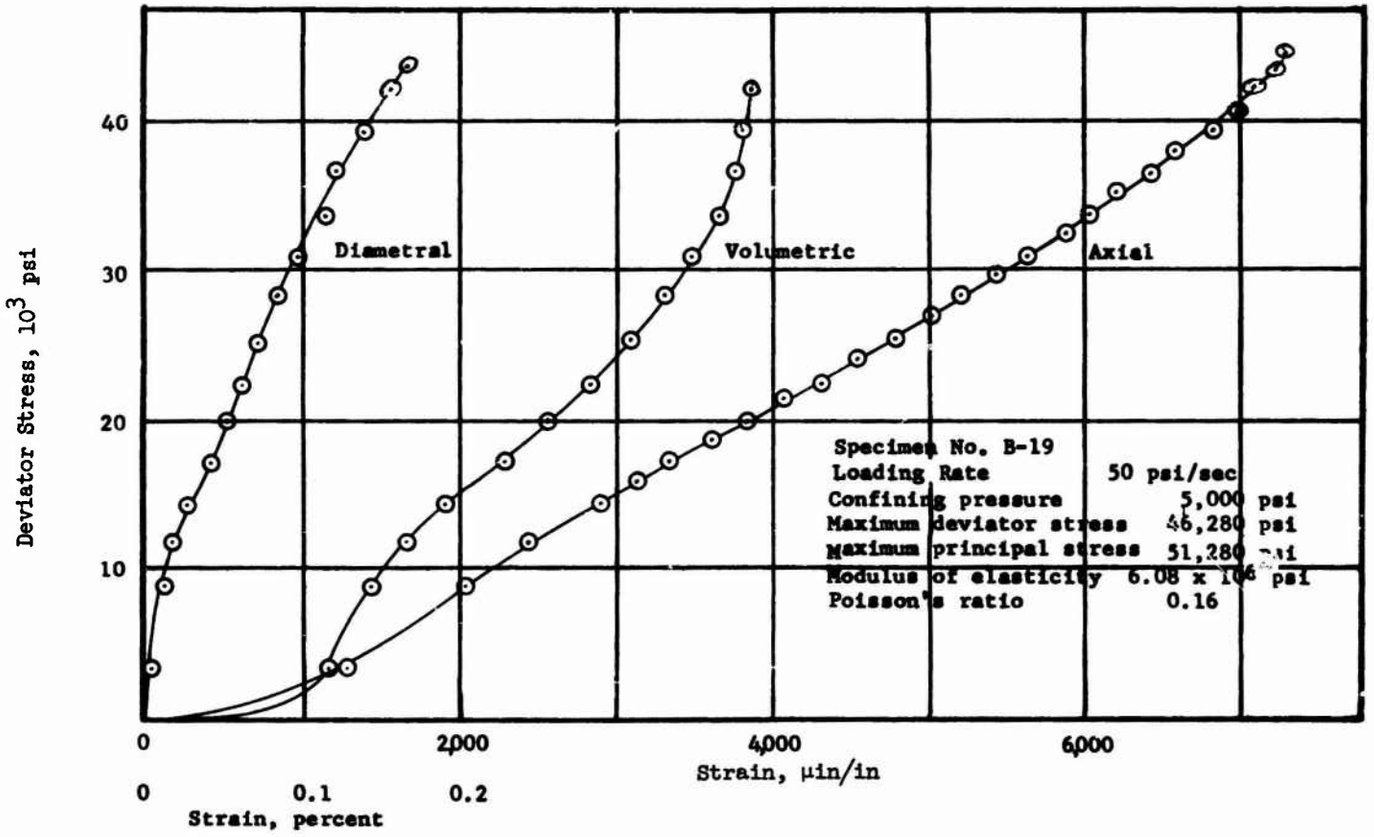

Figure 3.45 Deviator stress versus strain curves for basalt Specimen B-19.

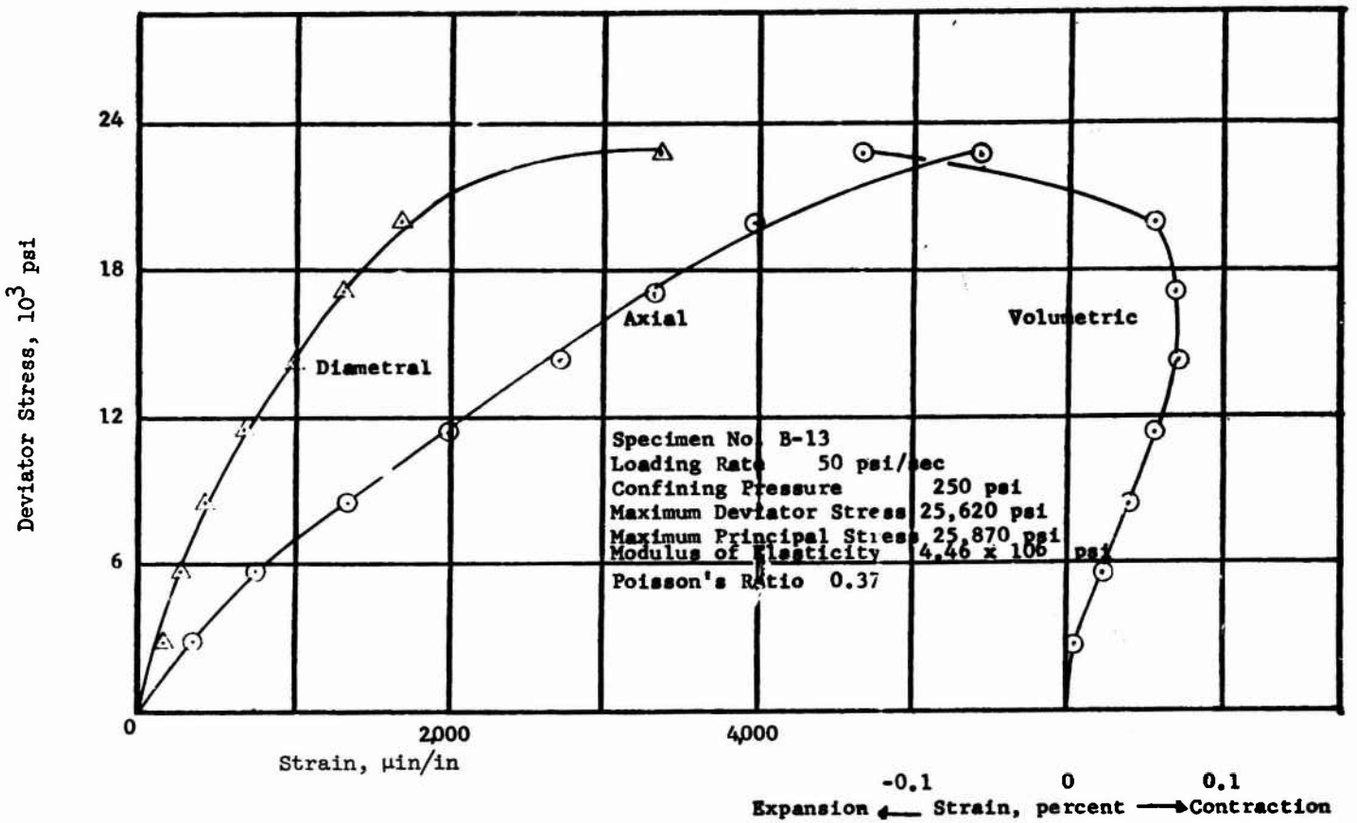

Figure 3.46 Deviator stress versus strain curves for basalt Specimen B-13.

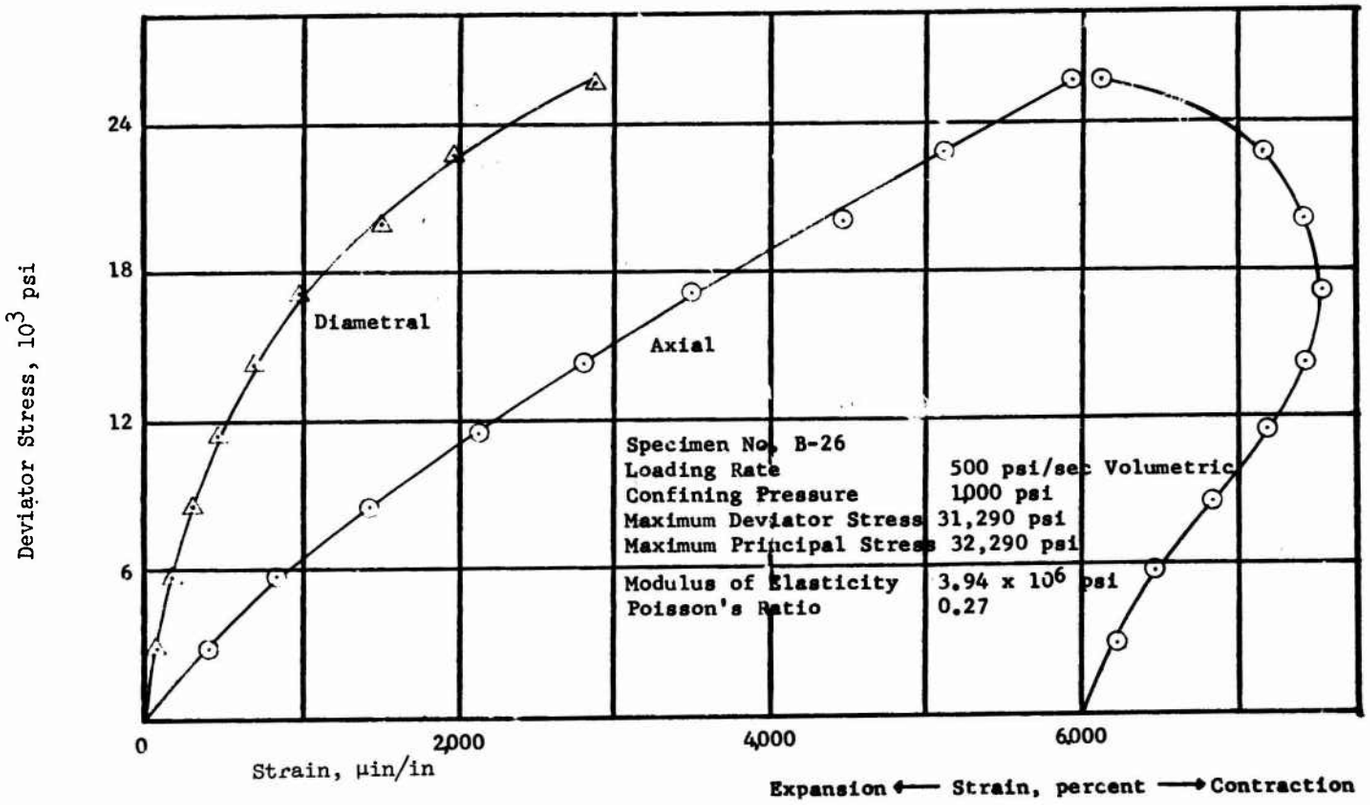

Figure 3.47 Deviator stress versus strain curves for basalt Specimen B-26.

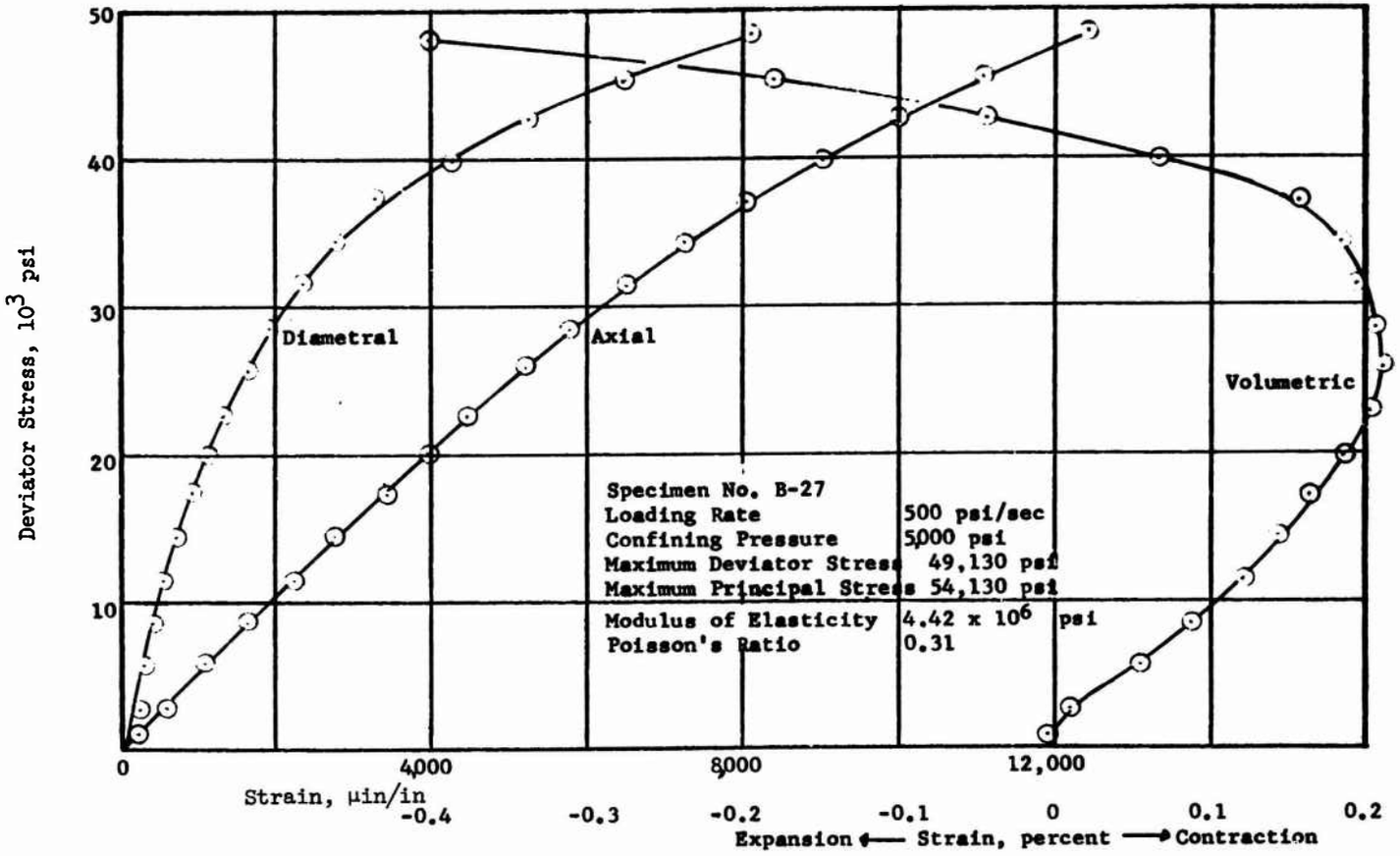

Figure 3.48 Deviator stress versus strain curves for basalt Specimen B-27.

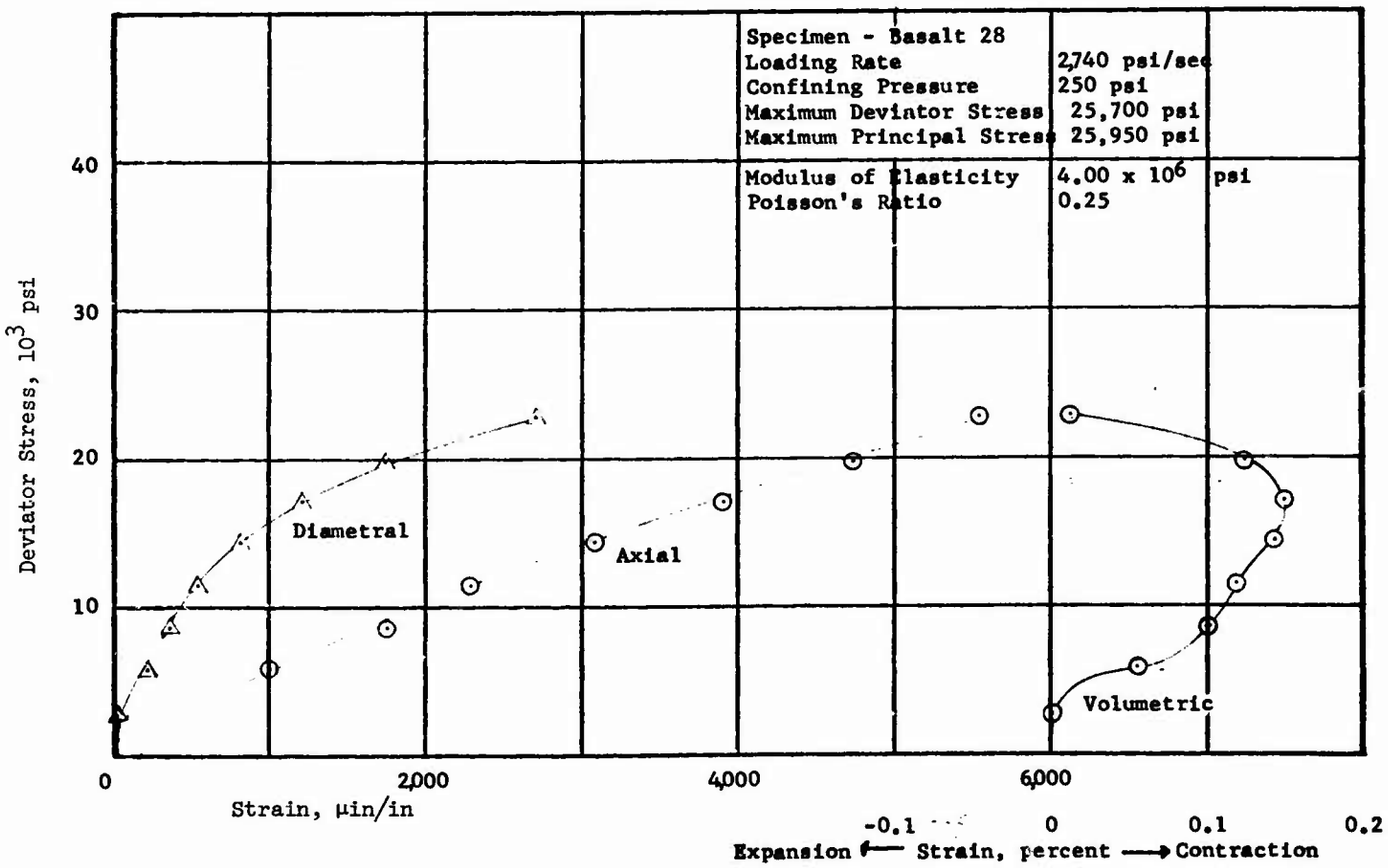

Figure 3.49 Deviator stress versus strain curves for basalt Specimen 28.

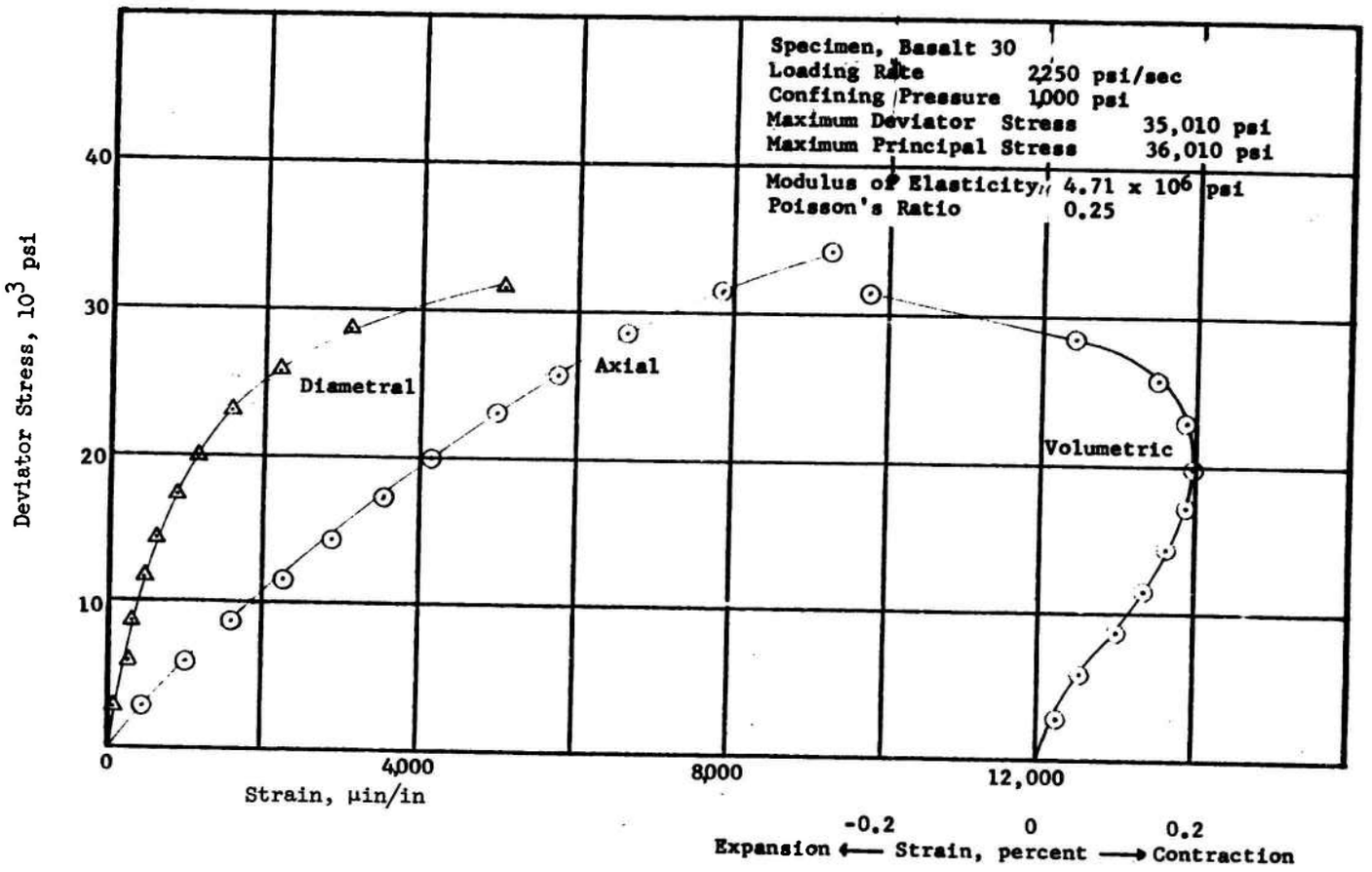

Figure 3.50 Deviator stress versus strain curves for basalt Specimen 30.

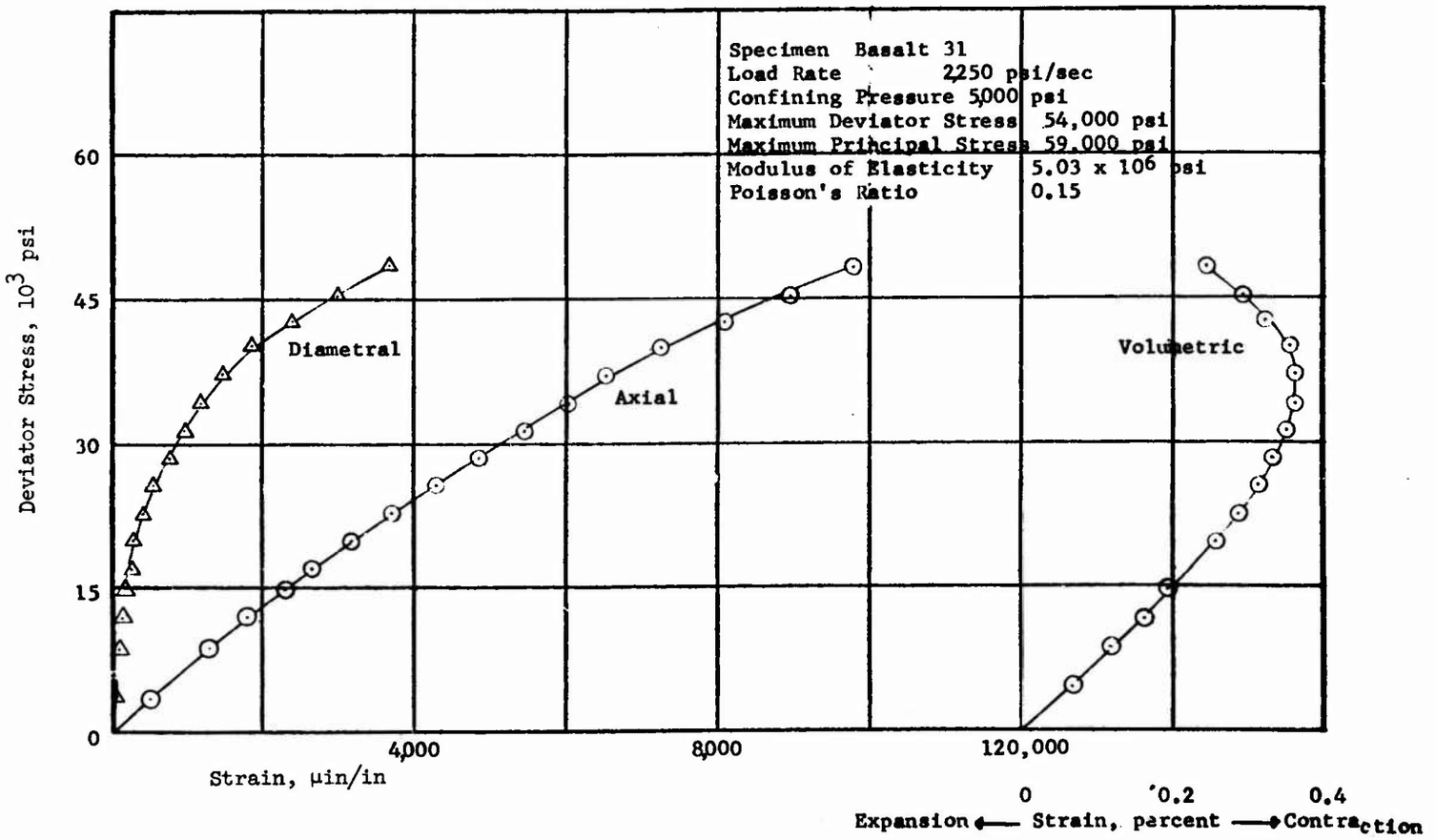

Figure 3.51 Deviator stress versus strain curves for basalt Specimen 31.

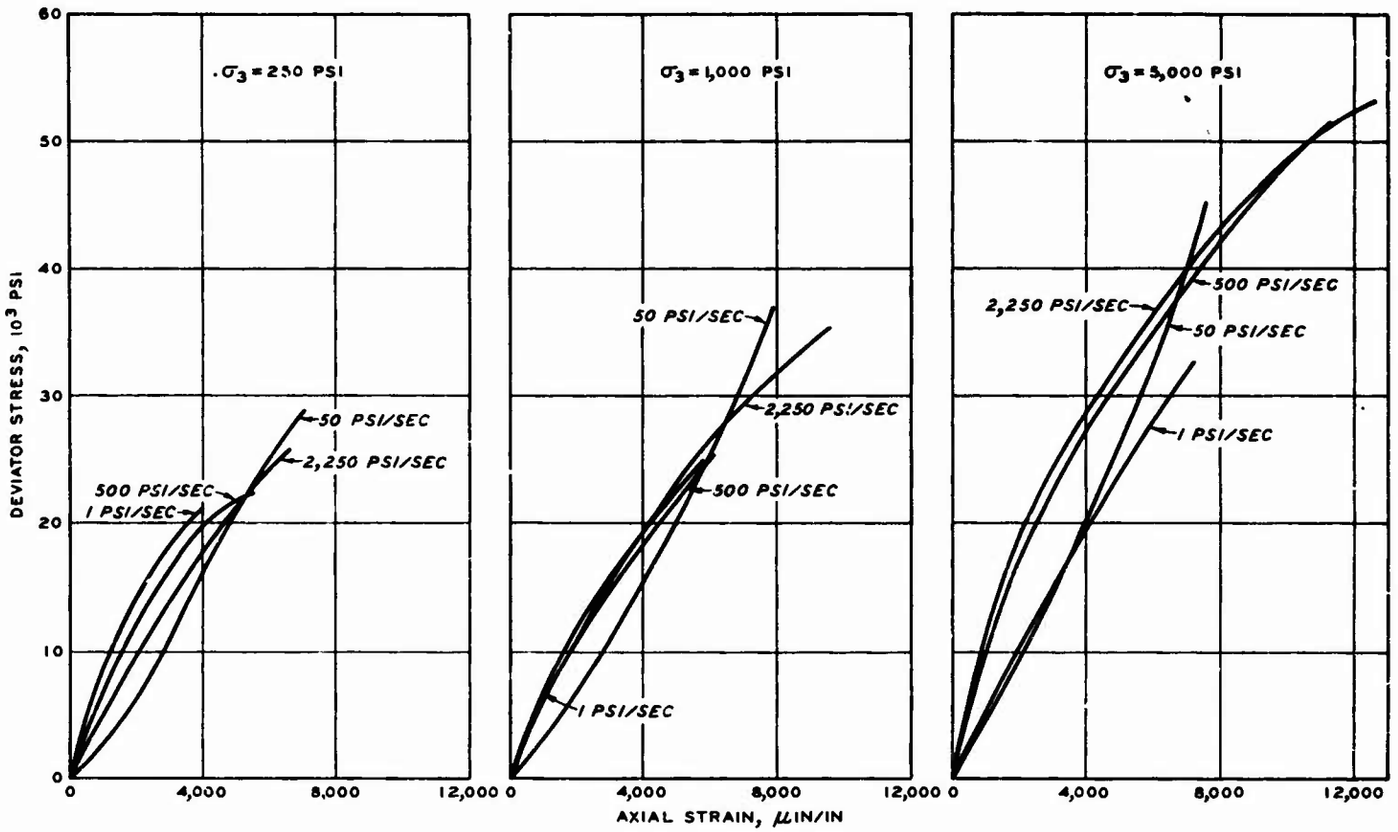

Figure 3.52 Increase in deviator stress and axial strain with increase in loading rate at confining pressures σ_3 of 250, 1,000, and 5,000 psi for basalt.

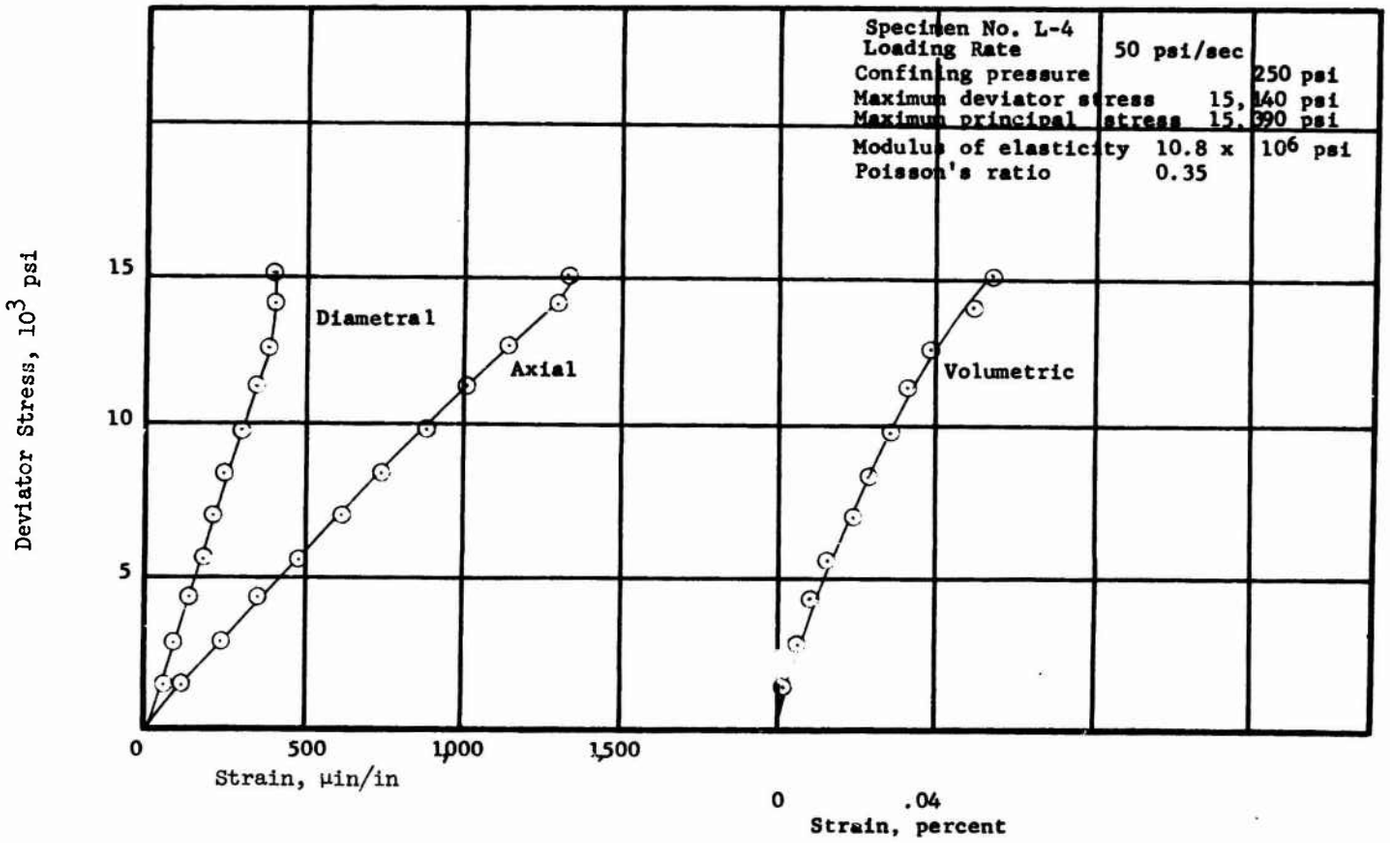

Figure 3.53 Deviator stress versus strain curves for limestone Specimen L-4.

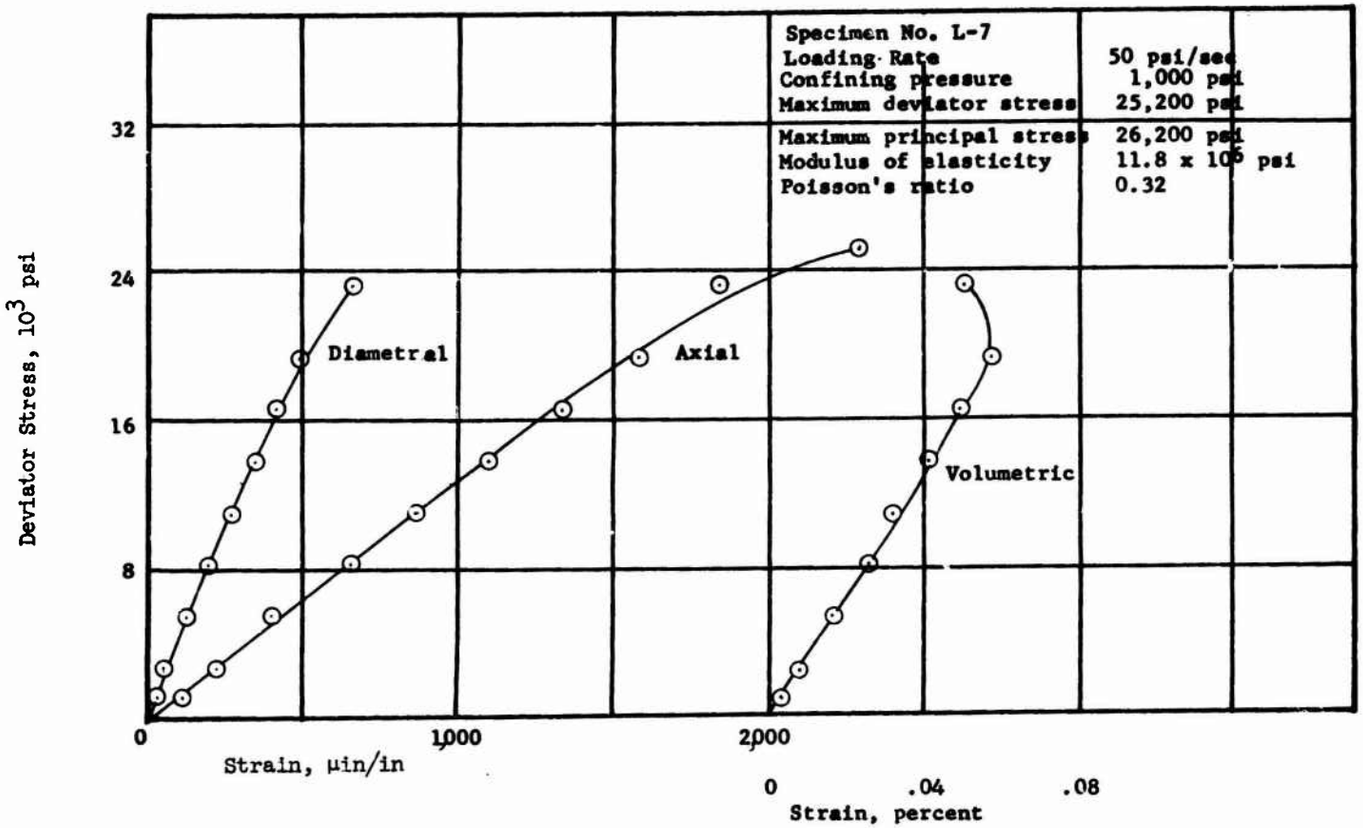

Figure 3.54 Deviator stress versus strain curves for limestone Specimen L-7.

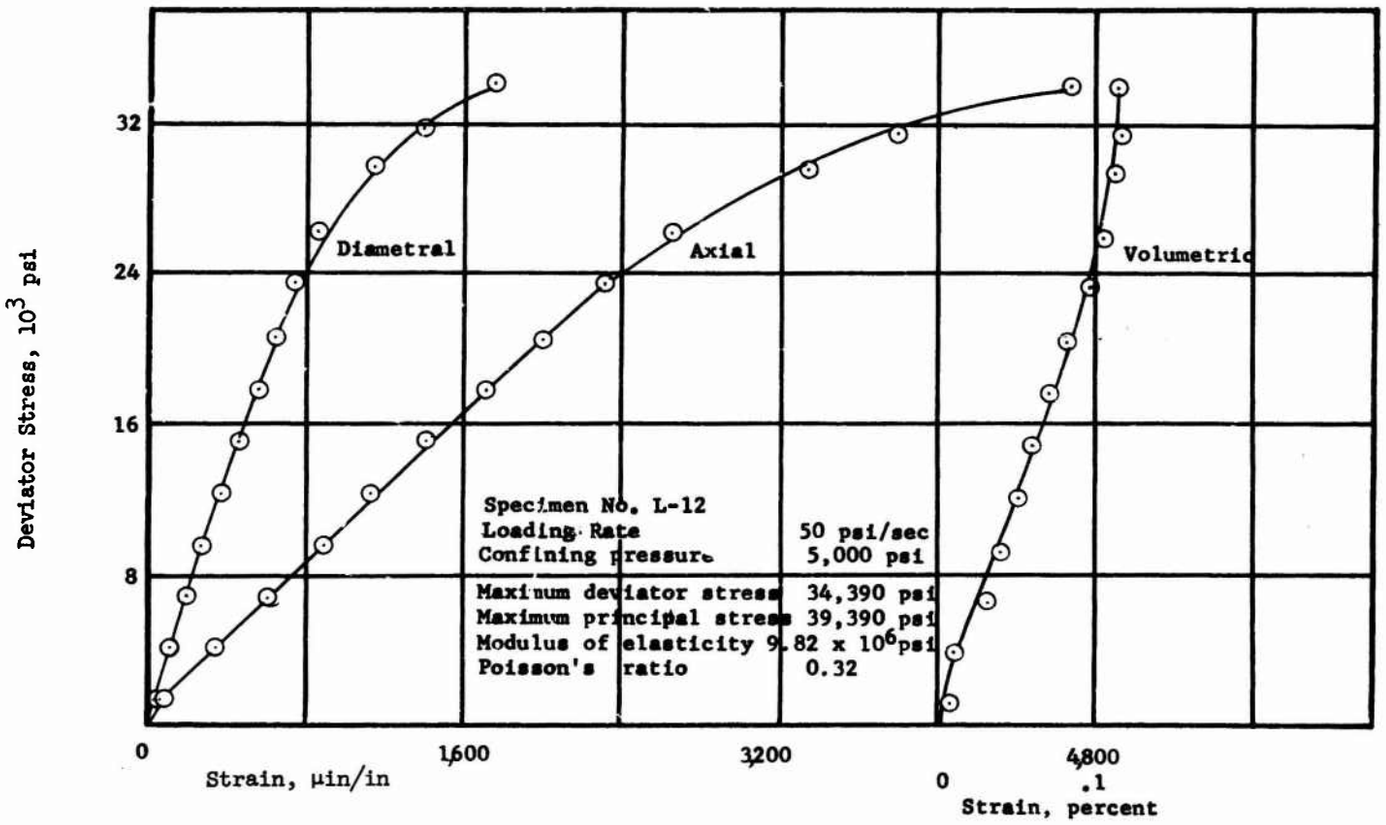

Figure 3.55 Deviator stress versus strain curves for limestone Specimen L-12.

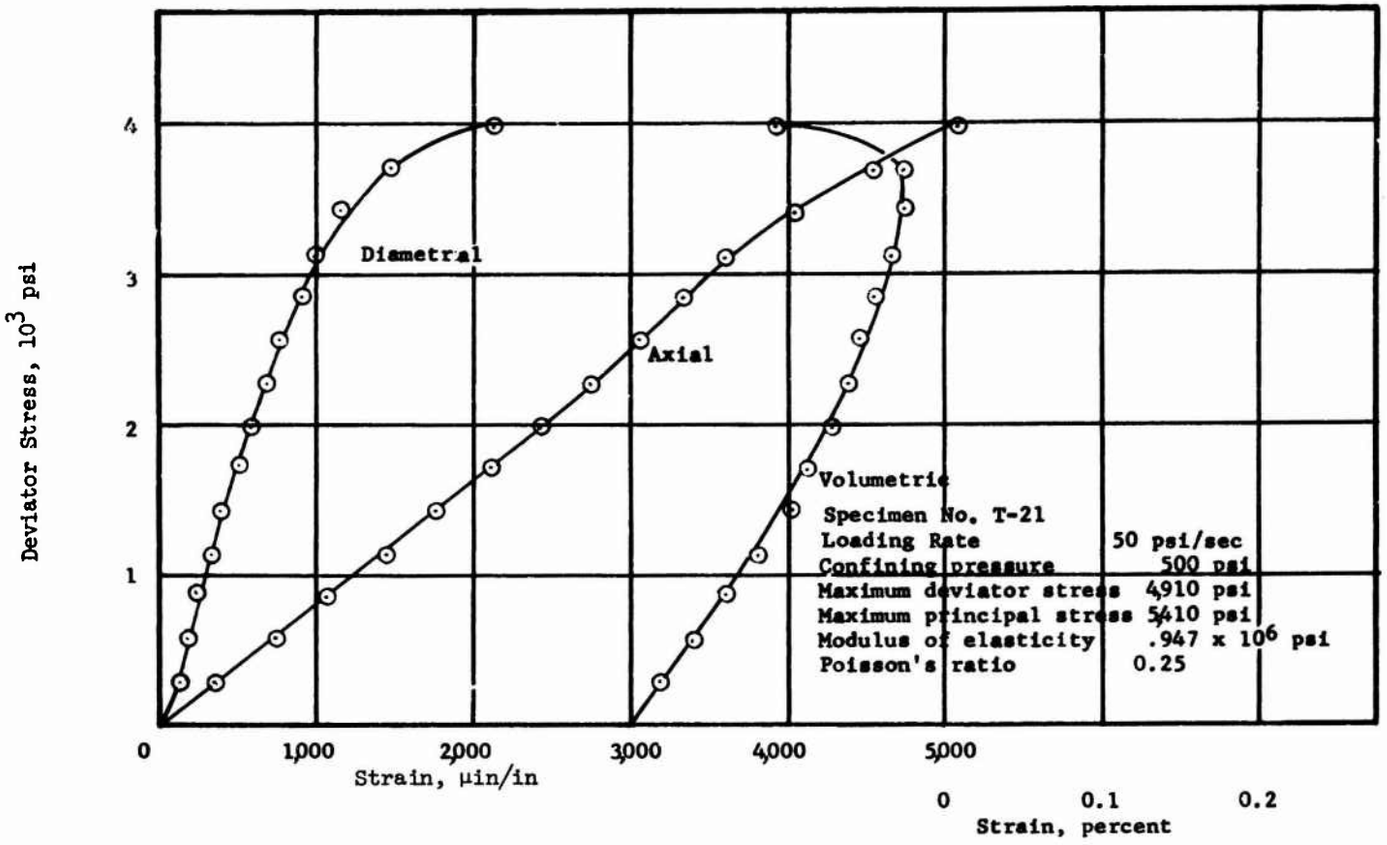

Figure 3.56 Deviator stress versus strain curves for tuff Specimen T-21.

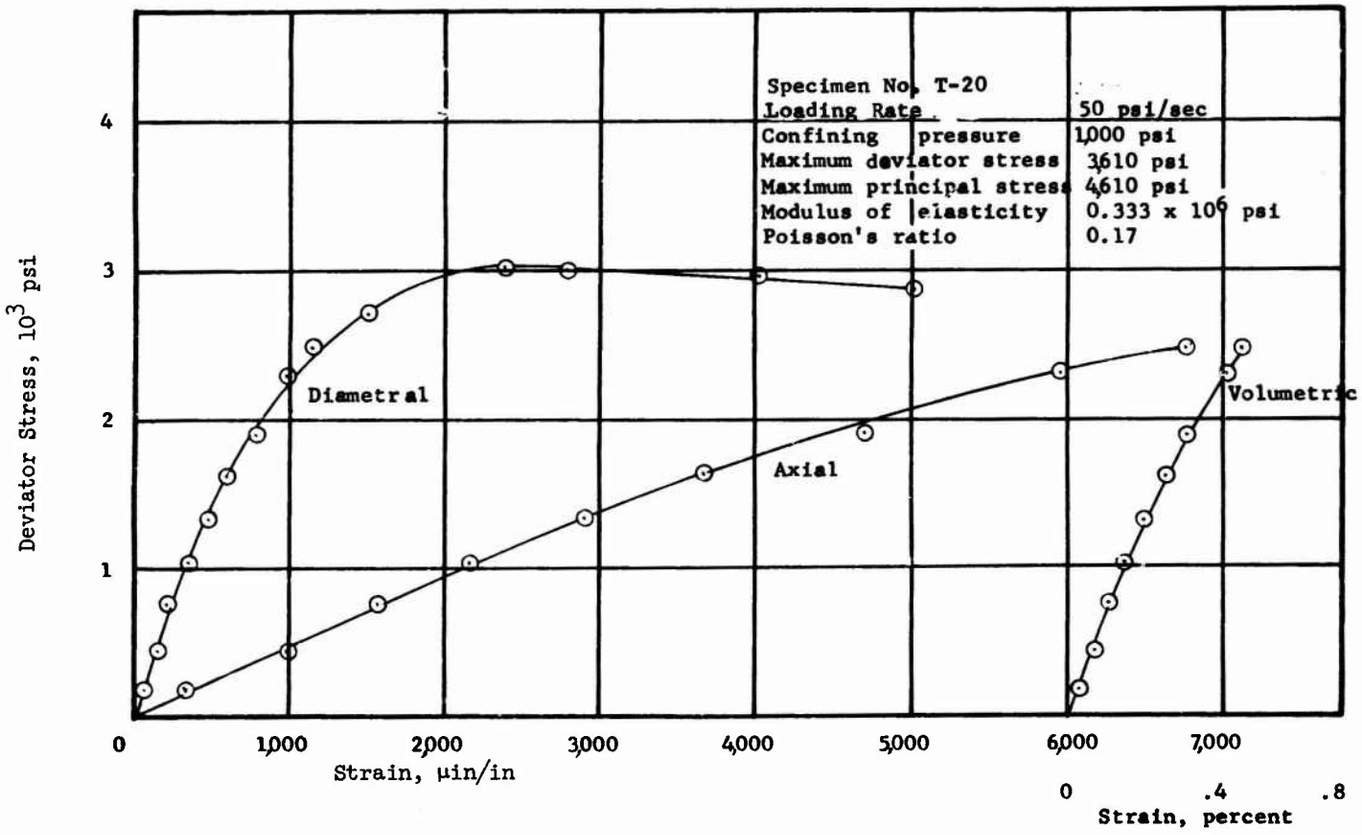

Figure 3.57 Deviator stress versus strain curves for tuff Specimen T-20.

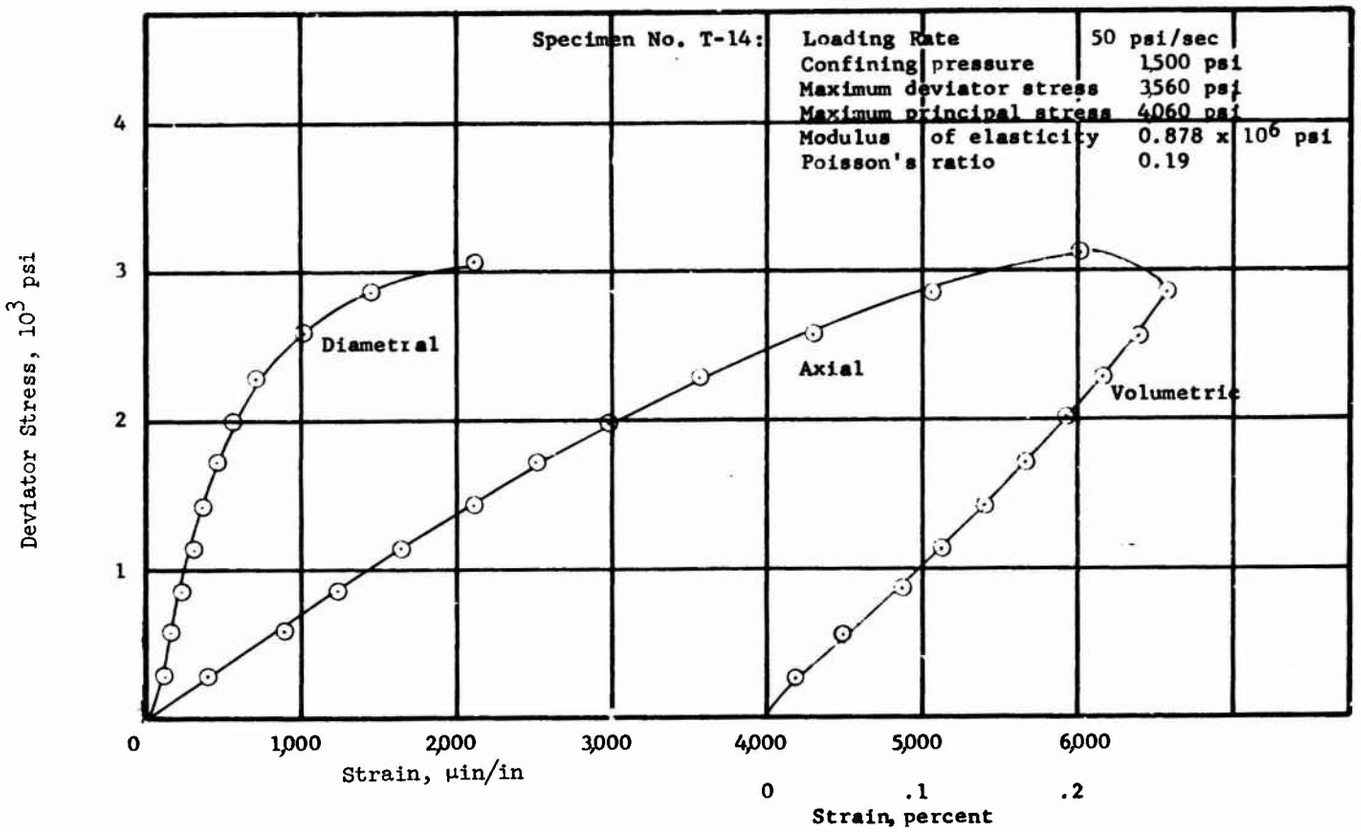

Figure 3.58 Deviator stress versus strain curves for tuff Specimen T-14.

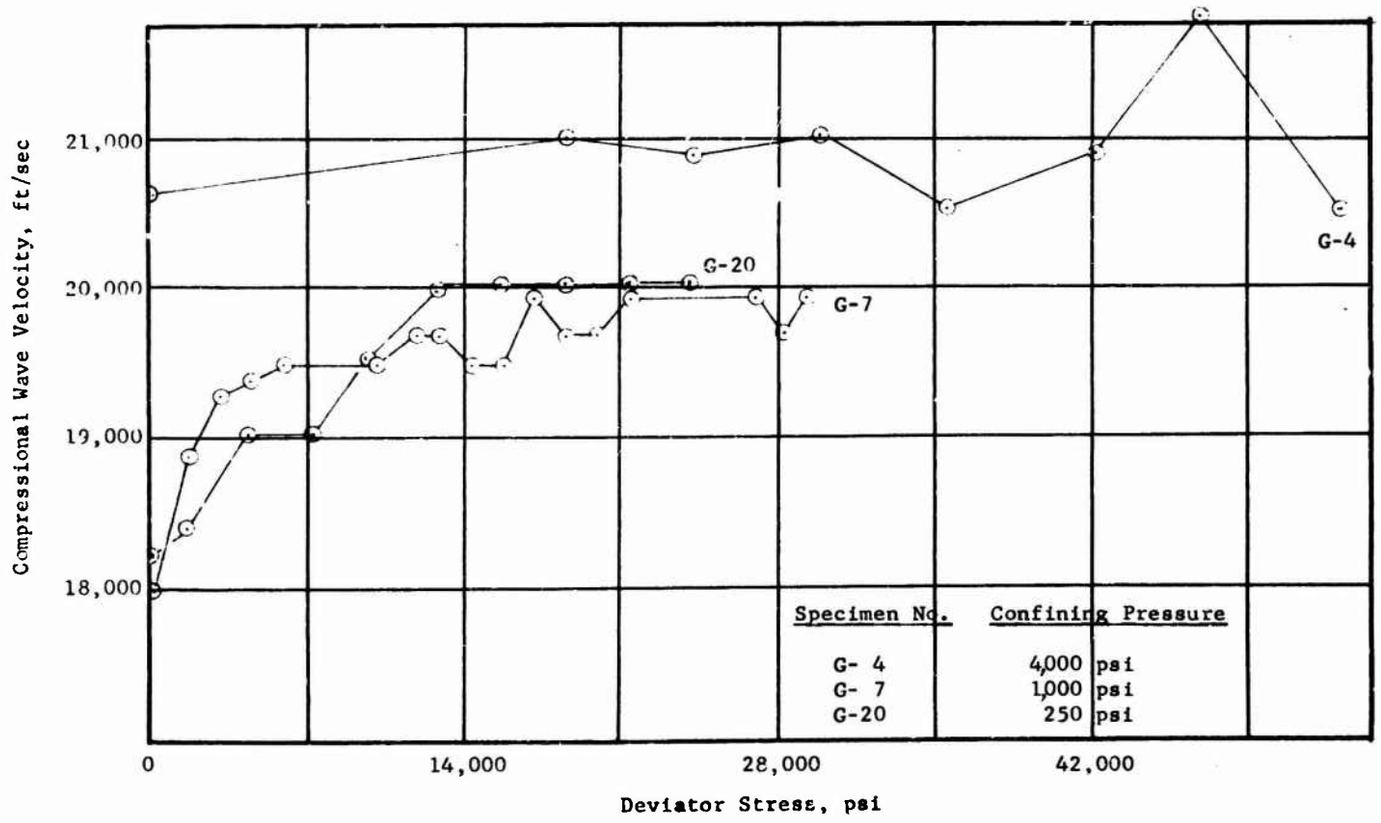

Figure .59 Compressional wave velocity versus deviator stress for granite.

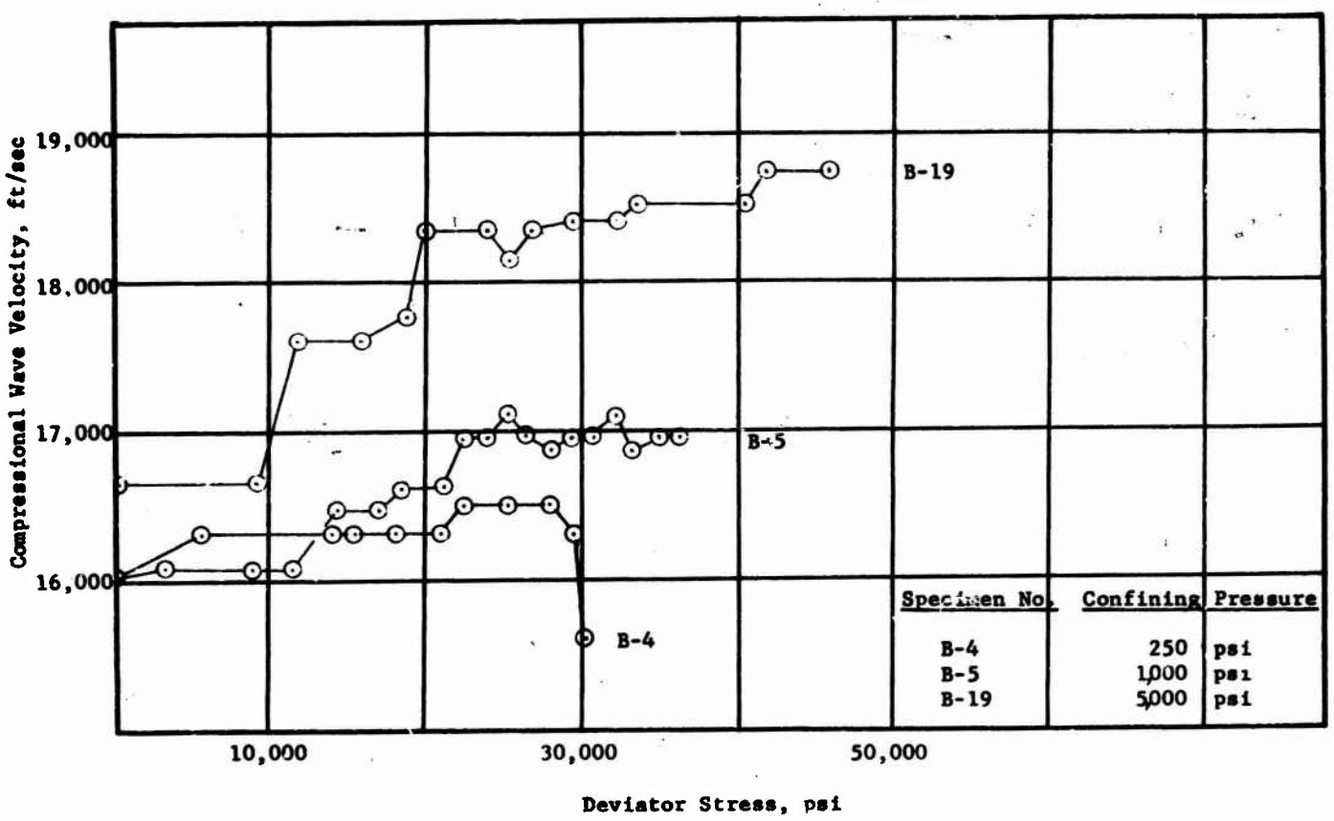

Figure 3.60 Compressional wave velocity versus deviator stress for basalt.

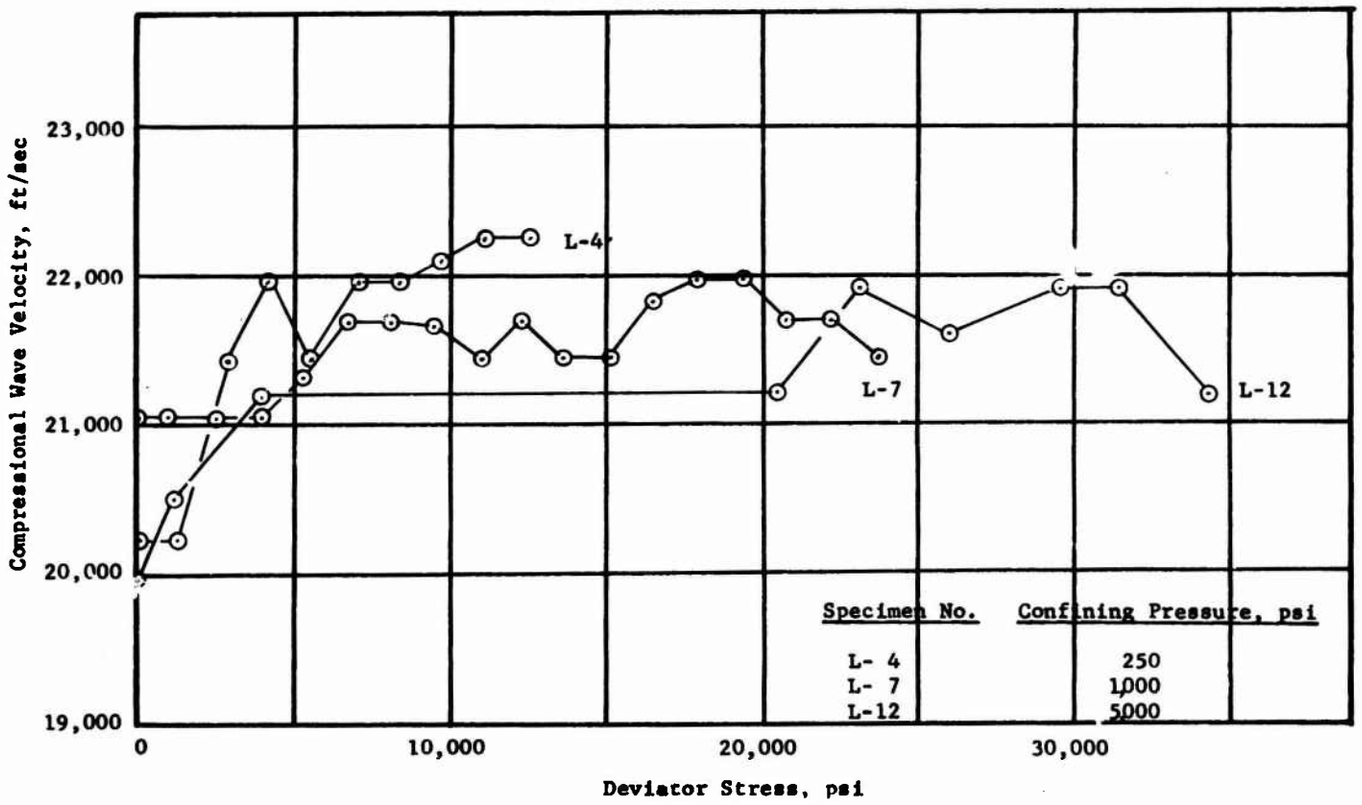

Figure 3.61 Compressional wave velocity versus deviator stress for limestone.

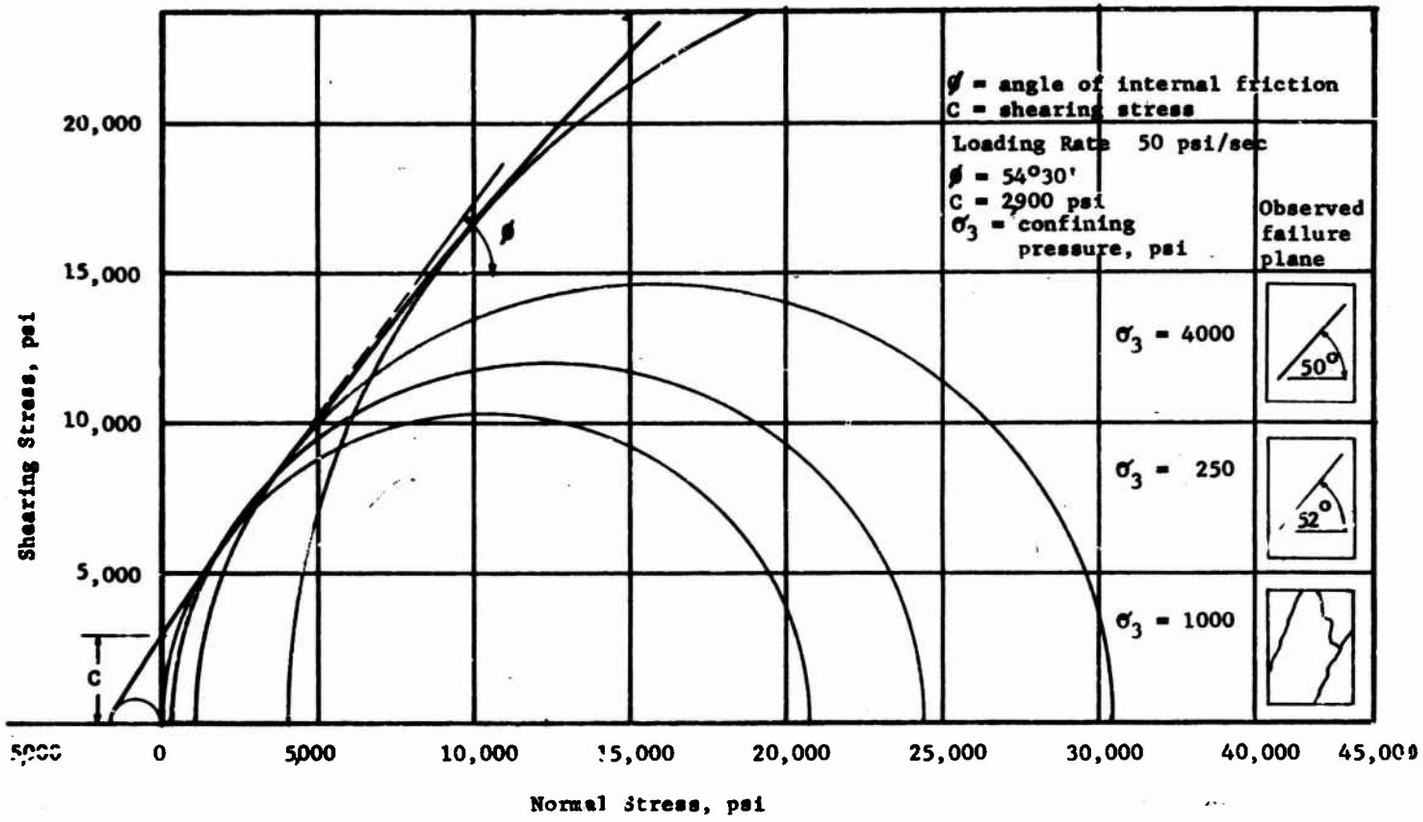

Figure 3.62 Mohr circles for granite.

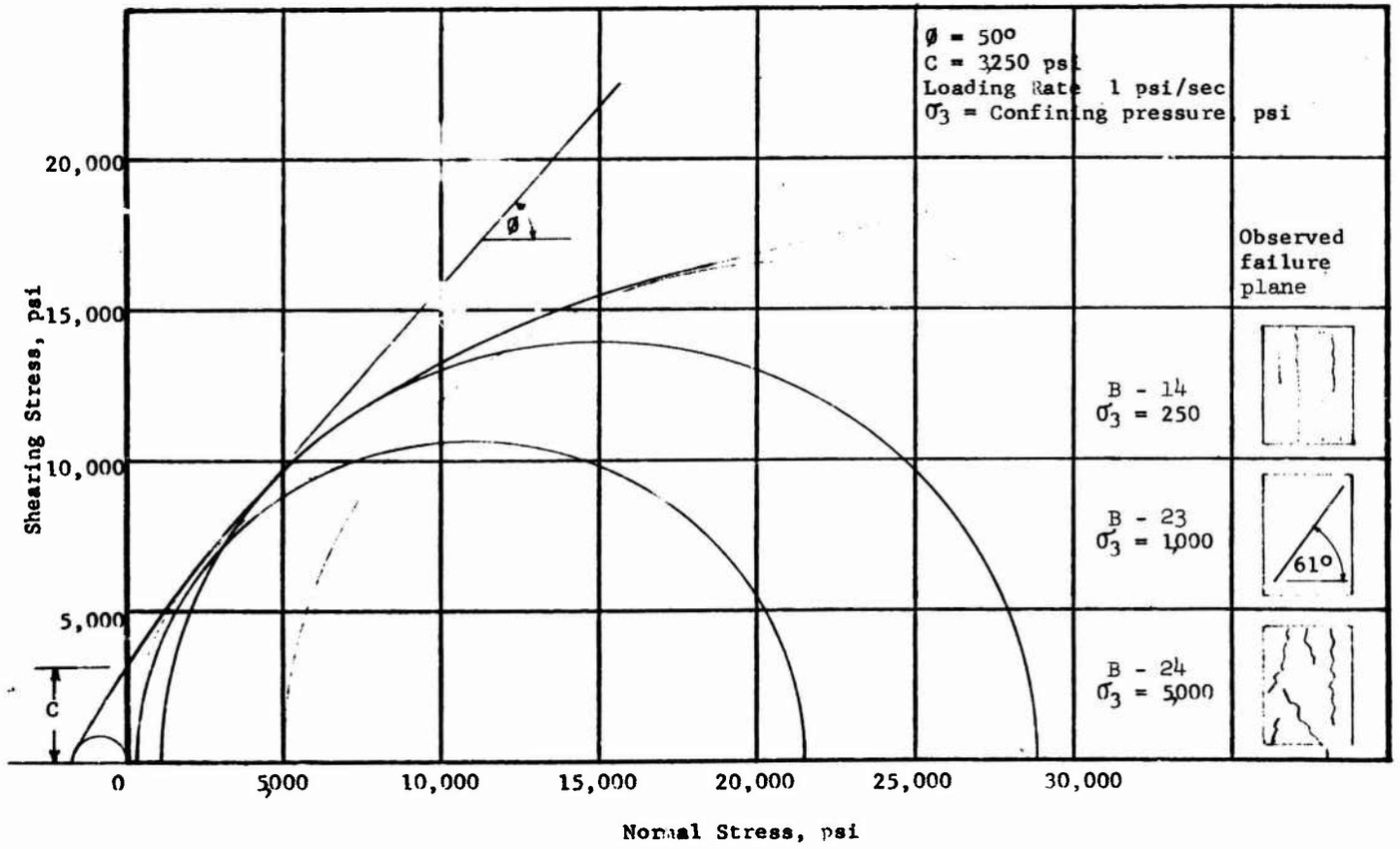

Figure 3.63 Mohr circles for basalt tested at loading rate of 1 psi/sec.

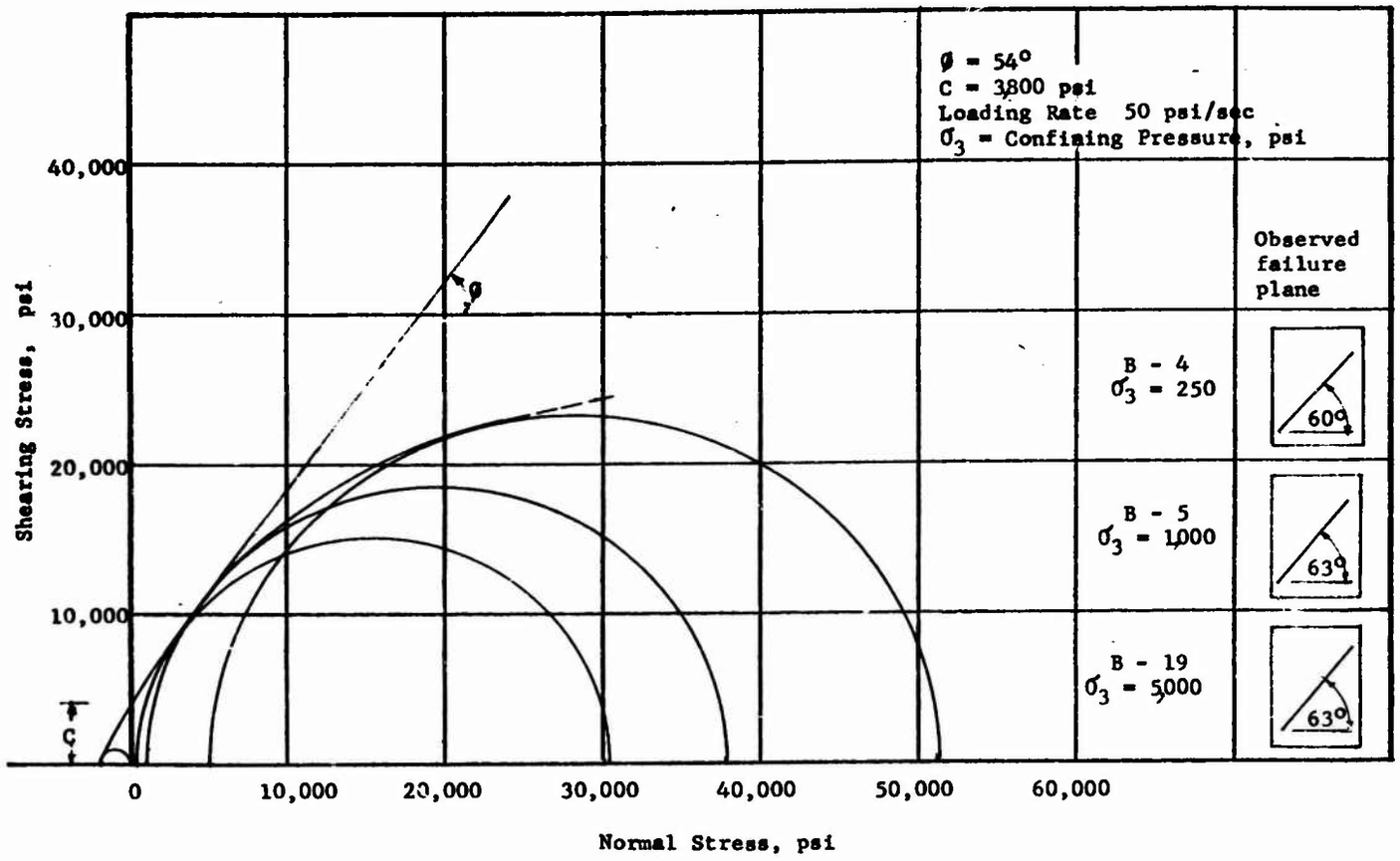

Figure 3.64 Mohr circles for basalt tested at loading rate of 50 psi/sec.

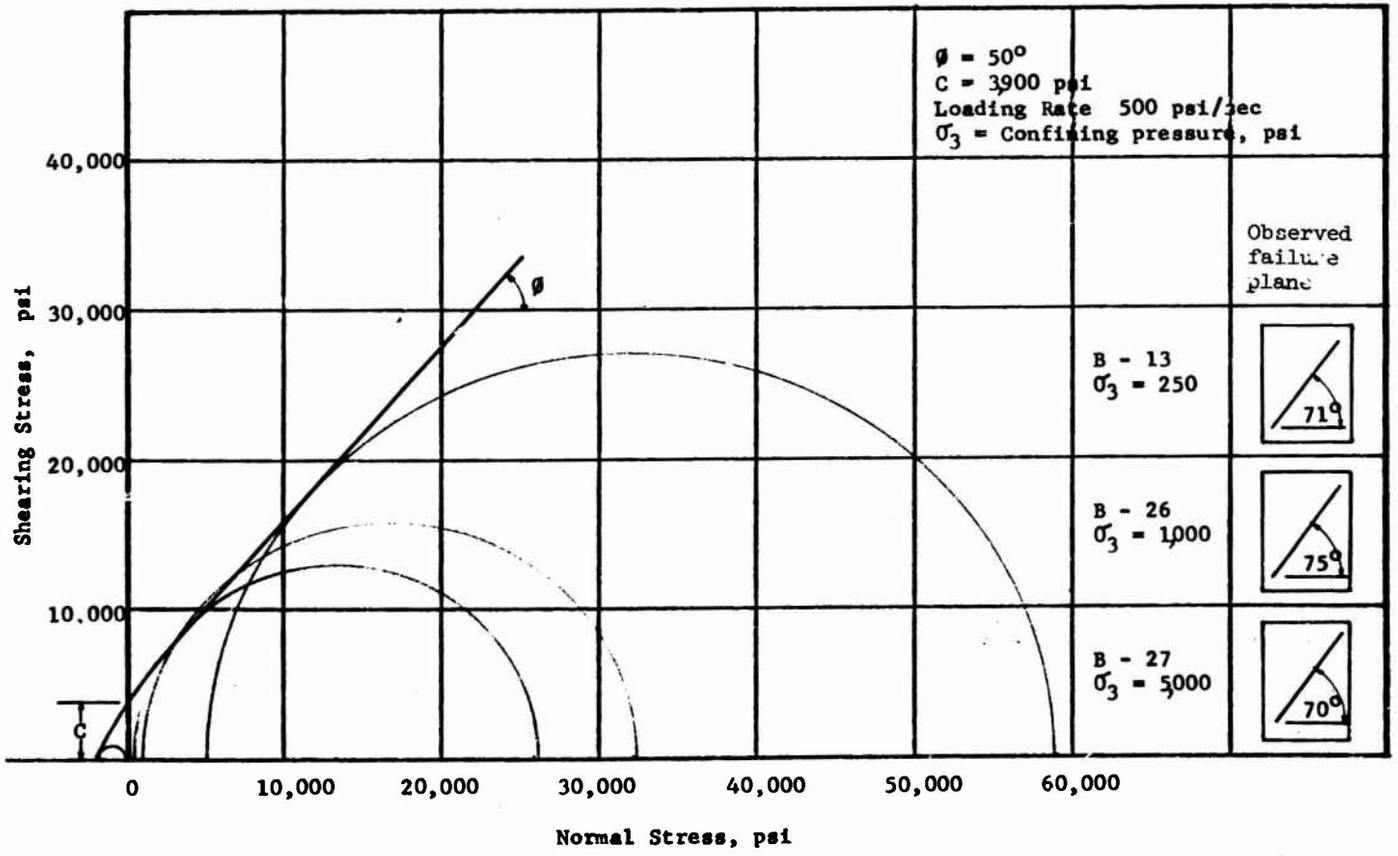

Figure 3.65 Mohr circles for basalt tested at loading rate of 500 psi/sec.

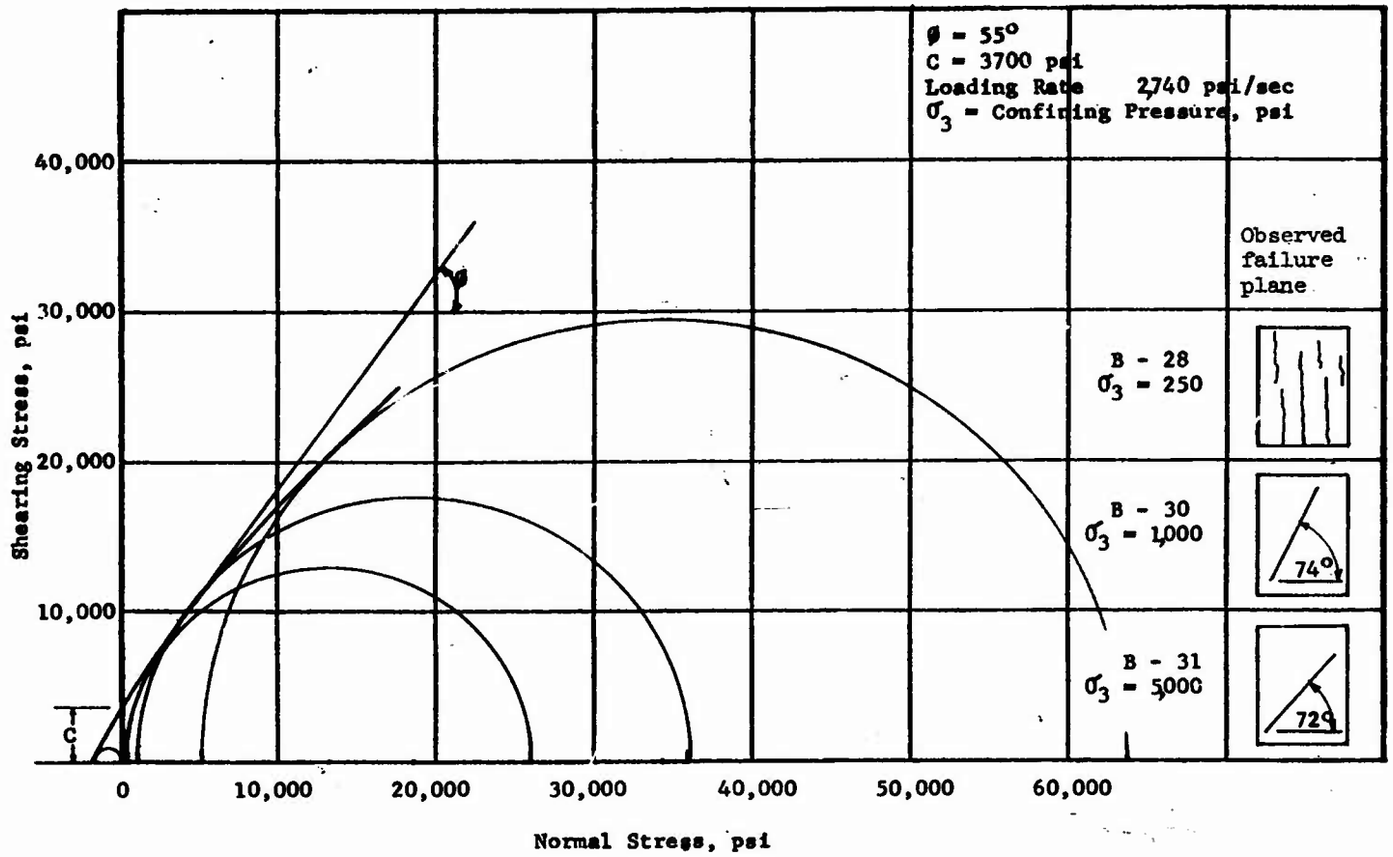

Figure 3.66 Mohr circles for basalt tested at loading rate of 2,740 psi/sec.

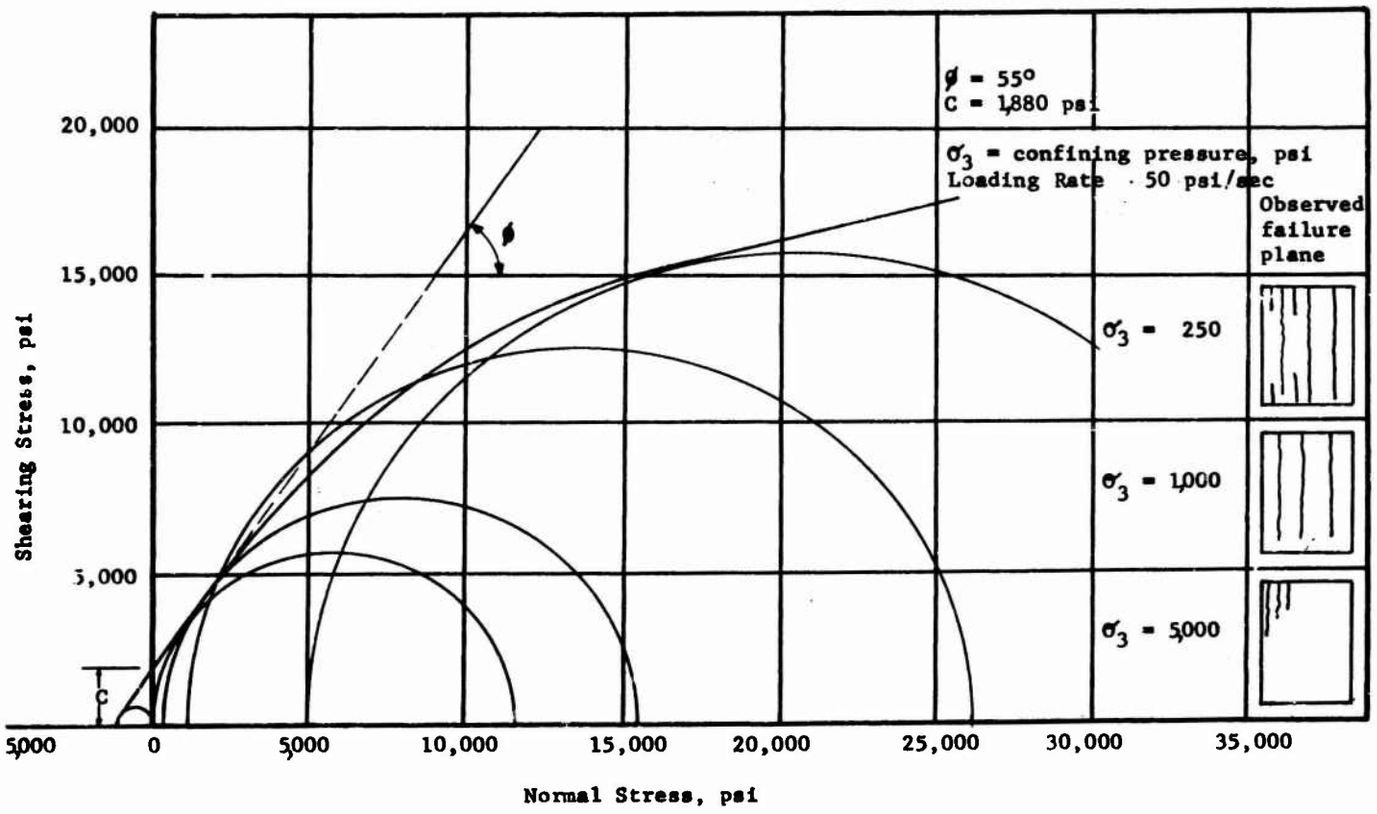

Figure 3.67 Mohr circles for limestone.

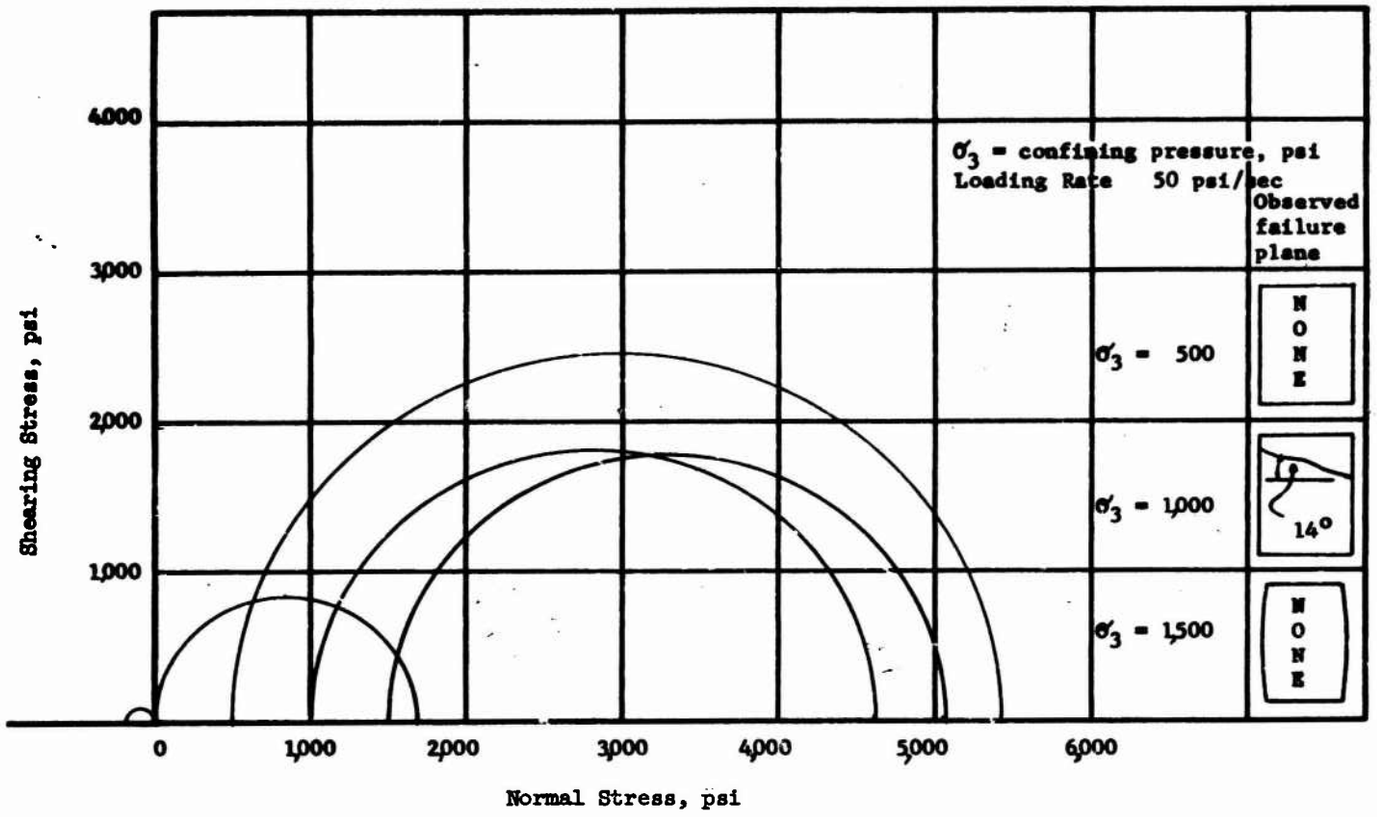

Figure 3.68 Mohr circles for tuff.

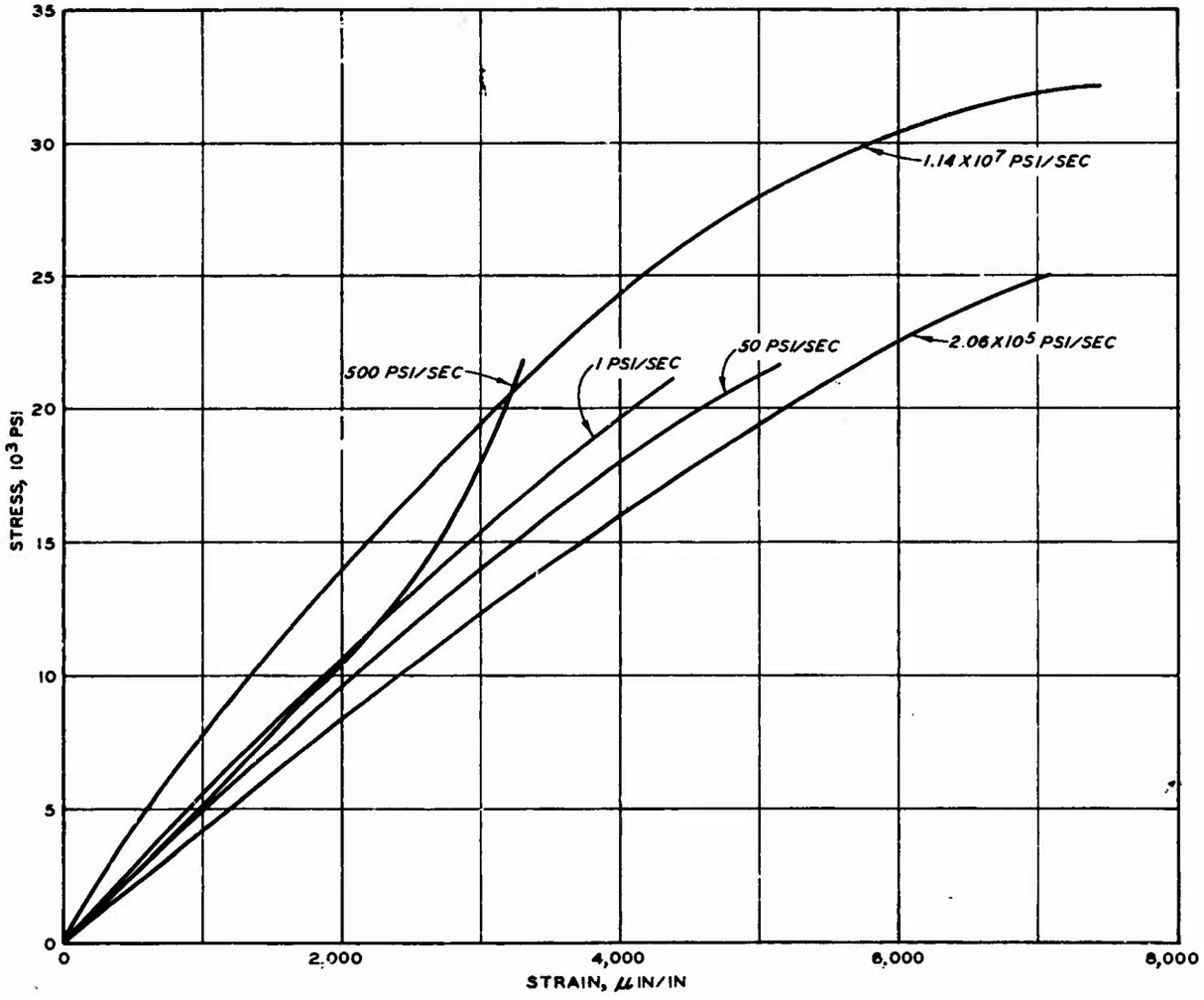

Figure 3.69 Average stress-strain curves for basalt at various rates of loading showin increase in ultimate strength and strain at failure.

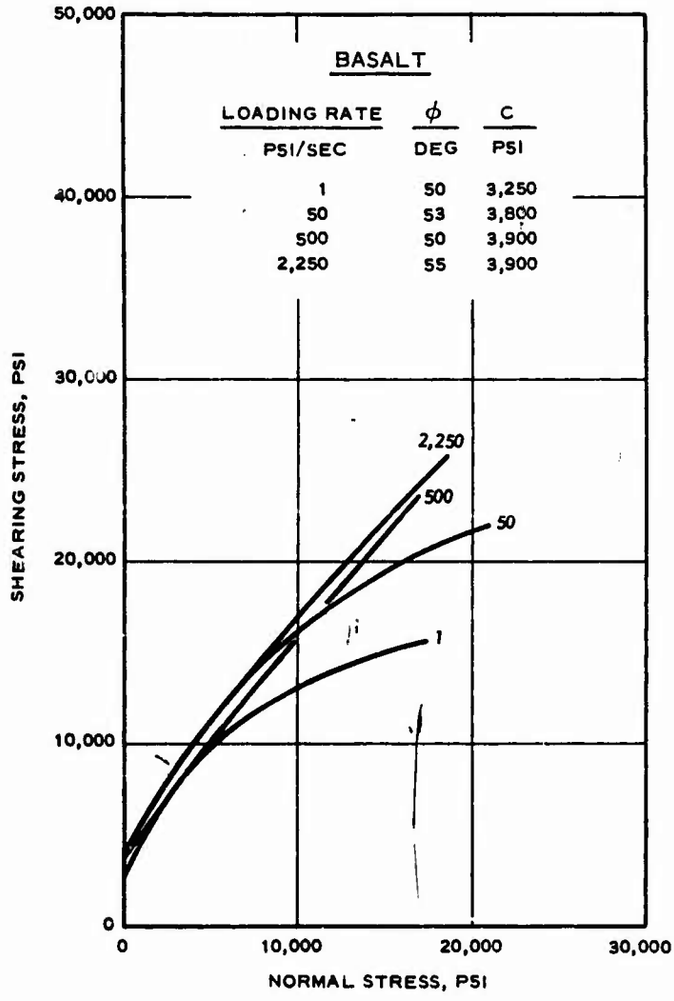

Figure 3.70 Mohr envelope at various loading rates for basalt.

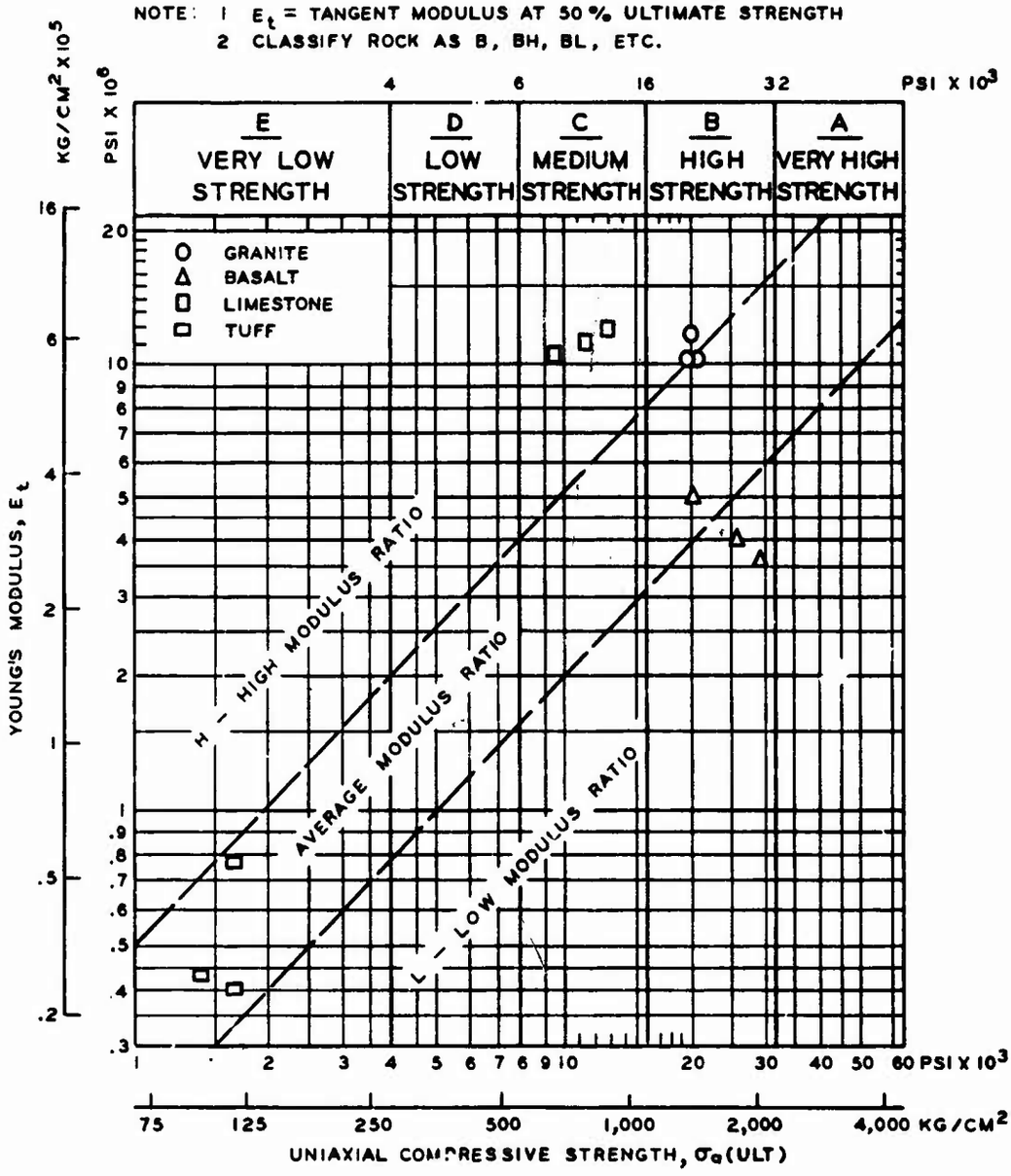

Figure 3.71 Engineering classification for intact rock at a loading rate of 50 psi/sec.

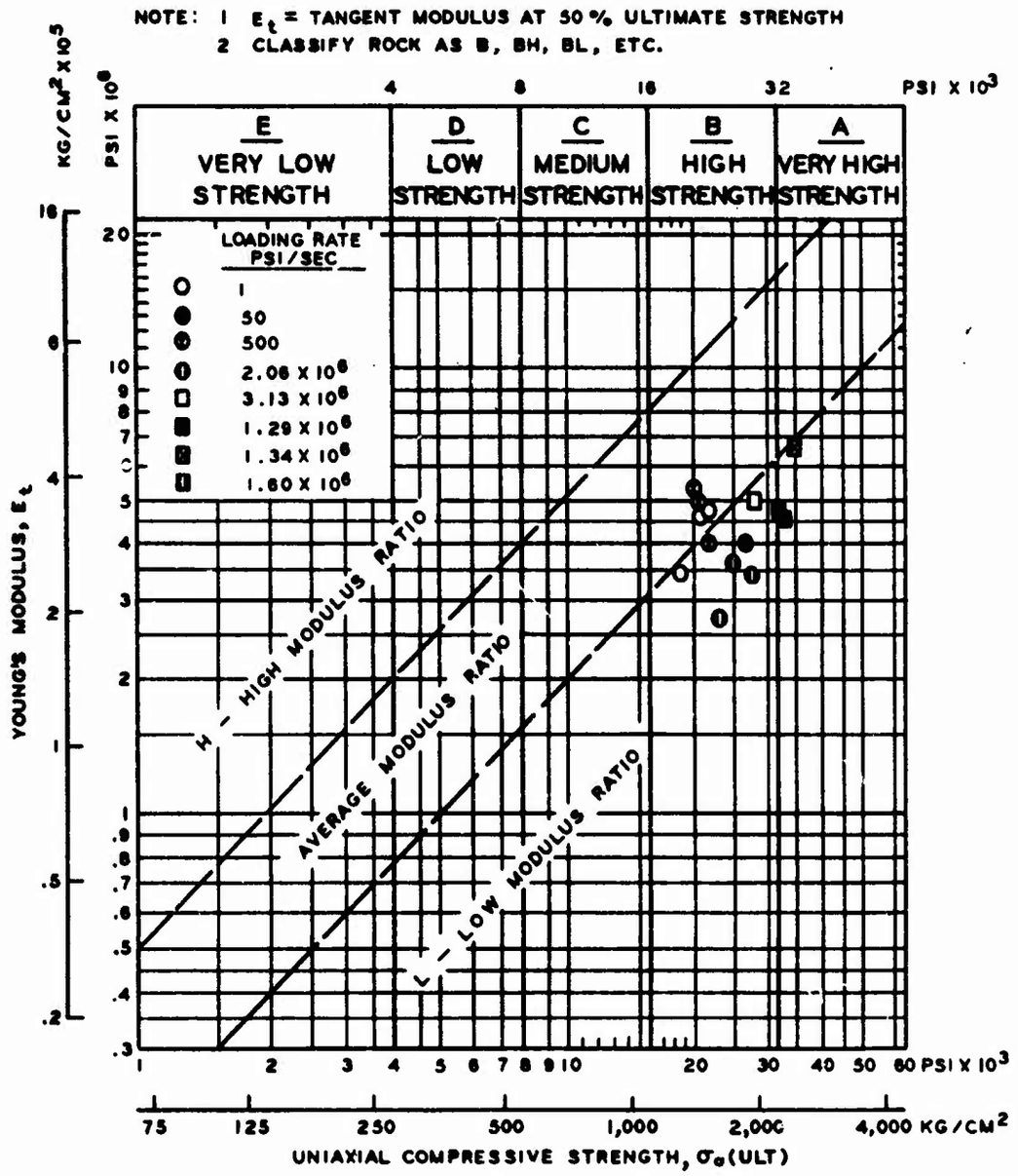

Figure 3.72 Engineering classification for intact rock at a rapid loading rate of >50 psi/sec.

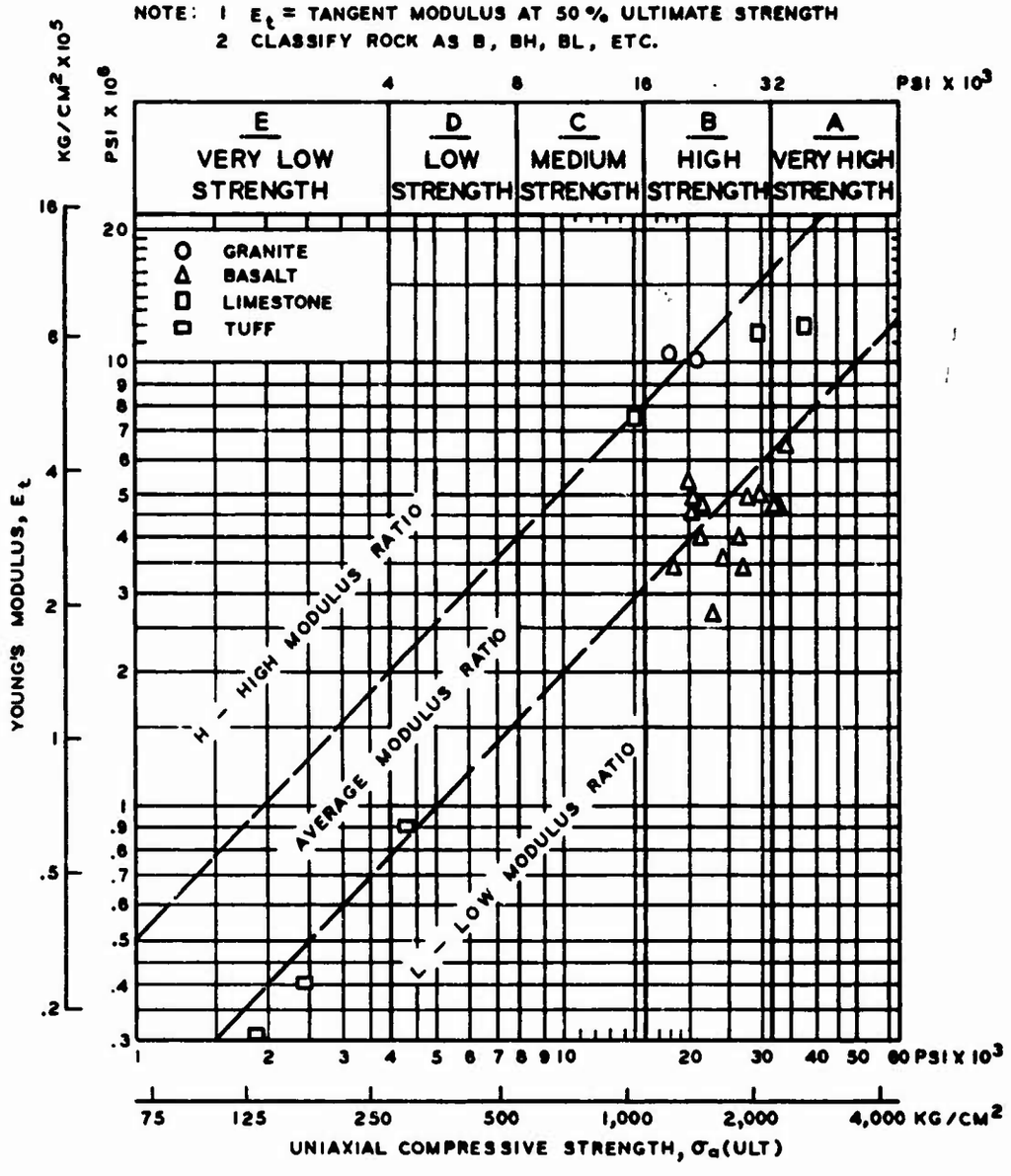

Figure 3.73 Engineering classification for intact rock for basalt at loading rates from 1 to 16 x 10^6 psi/sec.

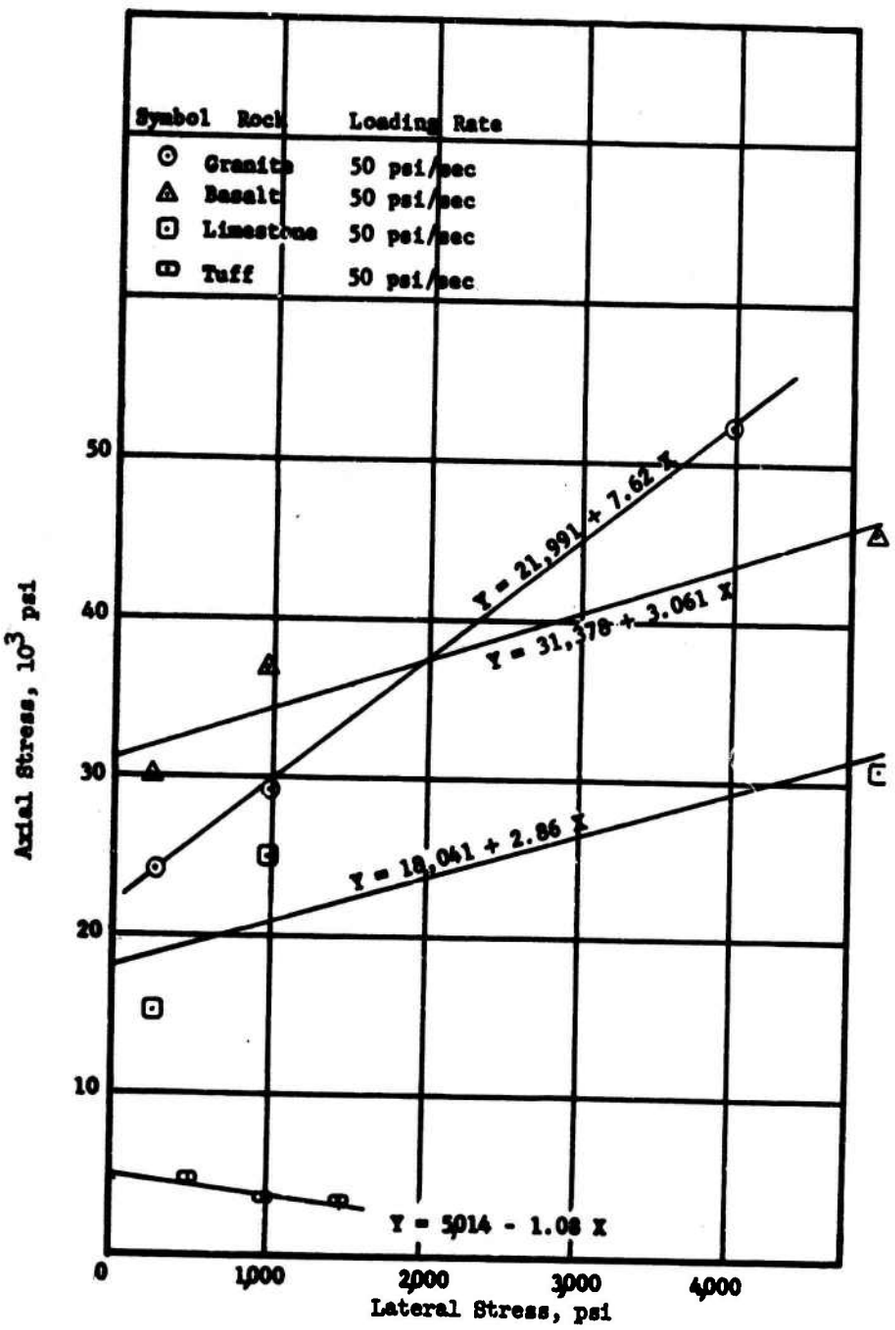

Figure 3.74 Relation of axial stress to lateral stress at failure in triaxial compression tests of rock cores.

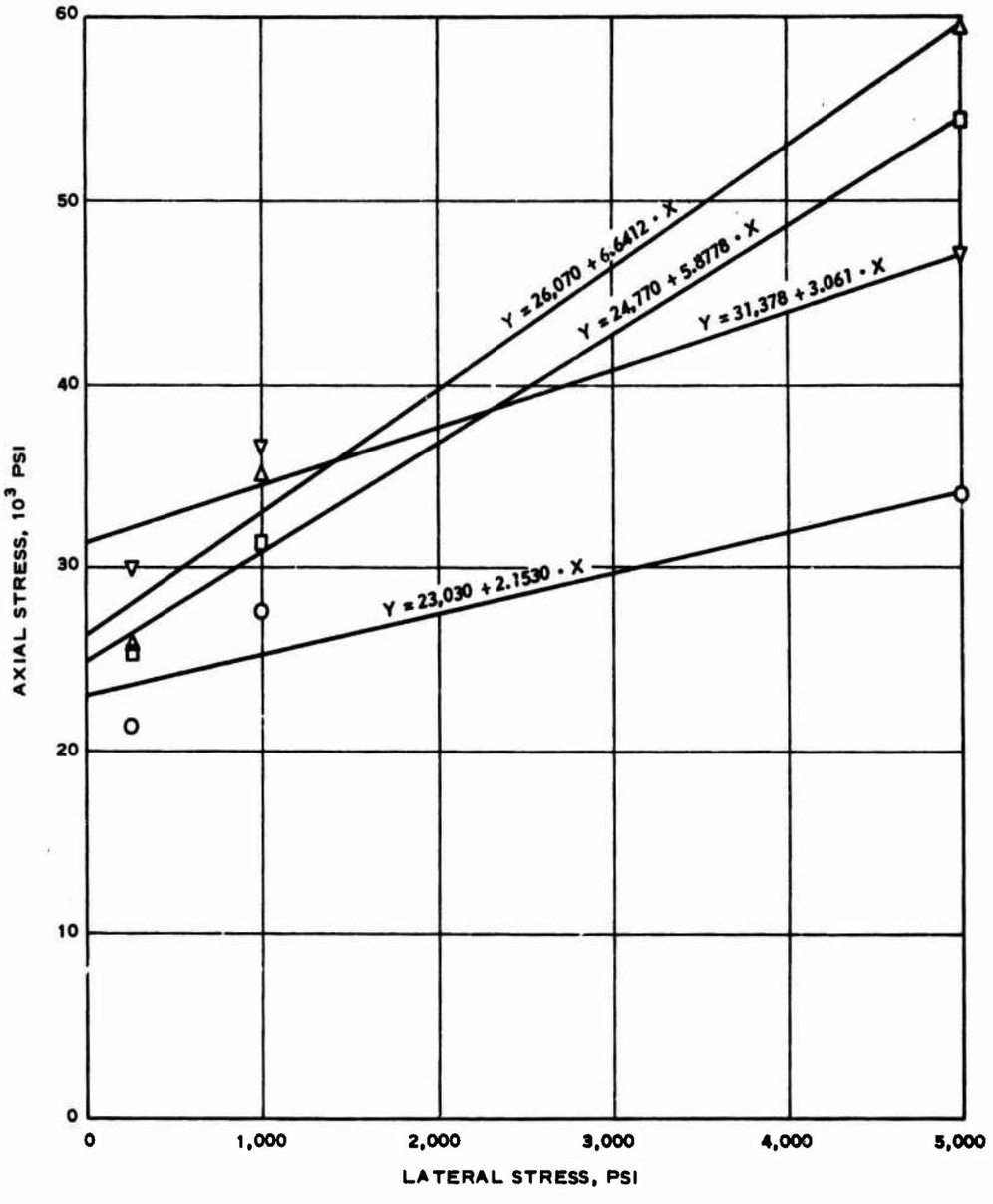

Figure 3.75 Relation of axial stress to lateral stress at failure in triaxial compression at different loading rates for basalt.

CHAPTER 4

CONCLUSIONS AND RECOMMENDATIONS

4.1 CONCLUSIONS

On the basis of results obtained from the various slow and rapid tests of rocks of four types, the following conclusions are drawn:

1. Nondestructive tests, such as specific gravity, porosity, and compressional wave velocity tests, indicate that all rock specimens within each type were uniform.

2. Results of unconfined compressive testing show that as the rate of loading increases, the ultimate strength of the rock increases. For the basalt rock, the total axial strain and the Young's modulus of elasticity, as well as the ultimate compressive strength, increase at rates of loading from 1 to 1.60×10^7 psi/sec. However, the total diametral strain decreased with increased rates of loading.

3. The difference in the unconfined compressive strength between the slow and the rapid rates of loading for the rocks tested varied considerably. The dynamic compressive strength factor f'_{cd} for the granite was less than 1; for the basalt, 1.35; for the limestone, 1.52; and for the tuff, 1.74.

4. Results of triaxial compression tests on basalt show that the maximum deviator stress $\sigma_1 - \sigma_3$ and total axial strain increase as both confining pressure and loading rates increase. Loading rates

have a pronounced effect on maximum deviator stress with lateral pressures up to 5,000 psi. Apparently, however, loading rates up to 2,250 psi/sec do not have a significant effect on the angle of internal friction ϕ and the cohesion c of basalt at confining pressures up to 5,000 psi. Mohr's theory of failure fits the basalt rock quite well for $\ddot{\epsilon}$ and σ_3 used in this investigation.

5. The compressional wave velocity of rock is affected by increases in both the applied axial stress and confining pressure. Velocities recorded in the direction of applied stress increase sharply within about one-half of the maximum deviator stress and then generally level off until failure.

4.2 RECOMMENDATIONS

It is recommended that additional limestone and tuff rock be tested under various loading rates to determine the validity of the f'_{cd} presented in this report.

Based on information obtained from the literature search and on the results of the triaxial tests reported herein, it is recommended that the effects of pore pressure be taken into account if porous rock with a high water content (such as tuff) is tested in the future under triaxial conditions.

REFERENCES

1. A. Kuman, F. E. Hausser, and J. E. Dorr; "The Effect of Stress Rate and Temperature on the Strength of Rocks"; Publisher Unknown; Unclassified.

2. R. L. Stowe; "Dynamic Properties of Granodiorite, Project Pile Driver"; Engineering Mechanics Division Specialty Conference Proceedings, American Society of Civil Engineers, 12-14 October 1966 (abstract only); Unclassified.

3. H. C. Heard; "Effect of Large Changes in Strain Rate in the Experimental Deformation of Yule Marble"; Journal of Geology, 1963, Vol. 71, Pages 162-195; Unclassified.

4. R. G. Wuerker; "Influence of Stress Rate and Other Factors on the Strength and Elastic Properties of Rocks"; Quarterly of the Colorado School of Mines, July 1959, Vol. 54, No. 3, Pages 3-31; Unclassified.

5. F. D. Adams and J. T. Nicholson; "An Experimental Investigation into the Flow of Marble"; Philosophical Transactions of the Royal Society of London, 1901, Ser. A, Vol 195, Pages 363-401; Unclassified.

6. J. Handin; "Strength and Plasticity"; Publication No. 99,

1956; Pages 1-15; Shell Development Company Exploration and Production Research; Unclassified.

7. J. Handin and R. V. Hager, Jr.; "Experimental Deformation of Sedimentary Rocks Under Confining Pressure; Tests at Room Temperature on Dry Samples"; Bulletin of the American Association of Petroleum Geologists, 1957, Vol. 41, No. 1, Pages 1-50; Unclassified.

8. T. von Kārmān; "Strength Tests Under Triaxial Pressure"; Zeilschrift des Vereines Deutscher Ingenieune, 1911, Vol. 55, No. 42, Pages 1749-1757 (in German); Unclassified.

9. N. J. Price; "A Study of Rock Properties in Conditions of Triaxial Stress"; Proceedings, Conference on Mechanical Properties of Non-Metallic Brittle Materials, 1958, Page 106; Butterworth, London; Unclassified.

10. D. W. Hobbs; "A Study of the Behavior of a Broken Rock Under Triaxial Compression, and Its Application to Mine Roadways"; International Journal Rock Mechanics Mining Sciences, 1966, Vol. 3; Pergamon Press, Ltd.; Unclassified.

11. K. Mogi; "Deformation and Fracture of Rocks Under Confining Pressure (1) Compression Tests on Dry Rock Sample"; Bulletin of the Earthquake Research Institute, September 1964, Vol. 42, Part 3, Pages 491-514; Unclassified.

12. K. S. Lane and W. J. Heck; "Triaxial Testing for Strength of Rock Joints"; Proceedings, Sixth Symposium on Rock Mechanics, 1964, Pages 98-108; Missouri University, Rolla, Missouri; Unclassified.

13. F. Birch and R. B. Dow; "Compressibility of Rocks and Glasses at High Temperatures and Pressures: Seismological Application"; Bulletin of the Geological Society of America, August 1936, Vol. 47, Pages 1235-1255; Unclassified.

14. M. S. Paterson; "Triaxial Testing of Materials at Pressures up to 10,000 kg./sq.cm. (150,000 lb./sq.in.)"; The Journal, Institution of Engineers, Australia, January-February 1964, Vol. 36, No. 1-2, Pages 23-29; Unclassified.

15. M. C. Redmond; "Laboratory Tests of Foundation Rock Cores, Morrow Park Damsite, Colorado River Storage Project"; Report No. C-1157, 9 September 1965; Bureau of Reclamation, Denver, Colorado; Unclassified.

16. F. Birch and D. Bancroft; "The Effect of Pressure on the Rigidity of Rock"; Journal of Geology, 1938, Vol. 46, Pages 59-87 and 113-141; Unclassified.

17. D. Bancroft; "An Electronic Interval-Timer for Laboratory Seismometry"; Transactions, American Geophysics Union, 1940, Part II, Pages 695-696; Unclassified.

18. D. S. Hughes and H. J. Jones; "Variations of Elastic Moduli of Igneous Rocks with Pressure and Temperature"; Bulletin of the Geological Society of America, 1950, Vol. 61, Pages 843-856; Unclassified.

19. D. S. Hughes and H. J. Cross; "Elastic Wave Velocities in Rocks at High Pressures and Temperatures"; Geophysics, 1951, Vol. 16, No. 4, Pages 577-593; Unclassified.

20. D. S. Hughes and J. L. Kelly; "Variation of Elastic Wave Velocity with Saturation in Sandstone"; Geophysics, 1952, Vol. 17, No. 4, Pages 739-752; Unclassified.

21. D. S. Hughes and C. Maurette; "Variation of Elastic Wave Velocities in Granites with Pressure and Temperature"; Geophysics, 1956, Vol. 21, No. 2, Pages 277-284; Unclassified.

22. M. R. J. Wyllie, A. R. Gregory, and L. W. Gardner; "Elastic Wave Velocities in Heterogeneous and Porous Media"; Geophysics, 1956, Vol. 21, No. 1, Pages 41-70; Unclassified.

23. M. R. J. Wyllie, A. R. Gregory, and G. H. F. Gardner; "An Experimental Investigation of Factors Affecting Elastic Wave Velocities in Porous Media"; Geophysics, 1958, Vol 23, Pages 459-493; Unclassified.

24. M. P. Volarovich and D. B. Balashov; "Study of Velocities of Elastic Waves in Samples of Rock Under Pressures up to 5000 kg/cm^2"; Bulletin, Academy of Science, USSR (Izvestiya, Akademiya Nauk, SSSR), Geophysics Ser. (English ed.), 1957, Vol. 3, Pages 56-69; Unclassified.

25. F. Birch; "The Velocity of Compressional Waves in Rock to 10 Kilobars", Part 1; Journal of Geophysical Research, April 1960, Vol. 65, No. 4, Pages 1083-1102; Unclassified.

26. F. Birch; "The Velocity of Compressional Waves in Rock to 10 Kilobars", Part 2; Journal of Geophysical Research, July 1961, Vol. 66, No. 7, Pages 2199-2224; Unclassified.

27. S. Matsushima; "Variation of the Elastic Wave Velocities of Rocks in the Process of Deformation and Fracture Under High Pressure"; Bulletin No. 32, March 1960; Kyoto University, Disaster Prevention Research Institute, Japan; Unclassified.

28. R. H. Bergman and R. A. Shahbender; "Effect of Statically Applied Stresses on the Velocity of Propagation of Ultrasonic Waves"; Journal of Applied Physics, 1958, Vol. 29, No. 12, Pages 1736-1738; Unclassified.

29. G. Simmons; "Velocity of Compressional Waves in Various Minerals at Pressures to 10 Kilobars"; Journal of Geophysical

Research, March 1964, Vol. 69, No. 6, Pages 1117-1121; Unclassified.

30. G. Baron, P. Habib, and P. Morlier; "Effect of Stresses and Deformations on Velocity of Sound in Rock"; Fourth International Conference on Strata Control and Rock Mechanics, 4-8 May 1964; Columbia University, New York; Unclassified.

31. J. S. Rinehart, J. Fortin, and L. Burgin; "Propagation Velocity of Longitudinal Waves in Rocks; Effect of State of Stress, Stress Level of the Wave, Water Content, Porosity, Temperature, Stratification and Texture"; Mining Engineering Series, Rock Mechanics, Third Technical Session; Publishing Date Unknown; Unclassified.

32. D. U. Deere and R. P. Miller; "Engineering Classification and Index Properties for Intact Rock"; Technical Report No. AFWL-TR-65-116, December 1966; University of Illinois, Urbana, Illinois; Unclassified.

33. S. J. Shand; "Eruptive Rocks; Their Genesis, Composition, Classification, and Their Relation to Ore-Deposits"; Third Edition, 1947; John Wiley and Sons, Inc., New York; Unclassified.

34. U. S. Army Engineer Waterways Experiment Station, CE; "Handbook for Concrete and Cement"; August 1949 (with quarterly supplements); Vicksburg, Mississippi; Unclassified.

35. L. Obert; "Static Stress Determinations"; Project 3.6, Operation Nougat, Shot Hard Hat, POR 1804, 12 April 1963; U. S. Bureau of Mines, College Park, Maryland; Unclassified.

36. R. L. Stowe; "Operation Flint Lock, Shot Pile Driver; Report 2, Physical Properties of Granodiorite from Operation Pile Driver" (in preparation); U. S. Army Engineer Waterways Experiment Station, CE, Vicksburg, Mississippi; Unclassified.

37. B. L. Atchley and H. C. Furr; "Strength and Energy Absorption Capabilities of Plain Concrete Under Dynamic and Static Loadings"; American Concrete Institute, Proceedings, November 1967, Vol. 64, No. 11, Pages 745-756; Unclassified.

38. D. Watstein; "Effect of Straining Rate on the Compressive Strength and Elastic Properties of Concrete"; American Concrete Institute, Proceedings, April 1953, Vol. 49, No. 8, Pages 729-744; Unclassified.

39. D. L. Neumann and H. W. Heslin, Jr.; "A GE-225 Computer Program for Simple Linear and Curvilinear Regression Analyses (Method of Least Squares)"; Miscellaneous Paper No. 5-667, July 1964; U. S. Army Engineer Waterways Experiment Station, CE, Vicksburg, Mississippi; Unclassified.

Unclassified
Security Classification

DOCUMENT CONTROL DATA - R & D

(Security classification of title, body of abstract and indexing annotation must be entered when the overall report is classified)

1. ORIGINATING ACTIVITY (Corporate author)
U. S. Army Engineer Waterways Experiment Station
Vicksburg, Mississippi

2a. REPORT SECURITY CLASSIFICATION
Unclassified

2b. GROUP

3. REPORT TITLE
STRENGTH AND DEFORMATION PROPERTIES OF GRANITE, BASALT, LIMESTONE, AND TUFF AT VARIOUS LOADING RATES

4. DESCRIPTIVE NOTES (Type of report and inclusive dates)
Final report

5. AUTHOR(S) (First name, middle initial, last name)
Richard L. Stowe

6. REPORT DATE	7a. TOTAL NO. OF PAGES	7b. NO. OF REFS
January 1969	161	39

8a. CONTRACT OR GRANT NO.	9a. ORIGINATOR'S REPORT NUMBER(S)
b. PROJECT NO. NWER Subtask 13.191A	Miscellaneous Paper C-69-1
c.	9b. OTHER REPORT NO(S) (Any other numbers that may be assigned this report)
d.	

10. DISTRIBUTION STATEMENT
This document has been approved for public release and sale; its distribution is unlimited.

11. SUPPLEMENTARY NOTES	12. SPONSORING MILITARY ACTIVITY
	Defense Atomic Support Agency Washington, D. C.

13. ABSTRACT

The objective of the work reported herein was to determine the strength and stress-strain characteristics of rocks of four types under various rates of loading. This was accomplished by conducting slow (specimens loaded at rates of less than 2,251 psi/sec) and rapid (specimens loaded at rates greater than 2,251 psi/sec) unconfined compression tests, tensile splitting tests, and triaxial compression tests utilizing confining pressures ranging from 250 to 5,000 psi. Granite, basalt, limestone, and tuff from the Atomic Energy Commission's Nevada Test Site, Mercury, Nevada, were used in this program. Nondestructive tests such as specific gravity, porosity, and compressional wave velocity were conducted on all specimens to determine homogeneity of each rock. Results of nondestructive tests indicated that the rock within each rock type was quite uniform. Results of the unconfined compressive strength tests on basalt indicated that as the loading rate was increased from 1 to 1.60 x 10^7 psi/sec, ultimate strength, total axial strain, and Young's modulus of elasticity increased. Total diametral strain decreased as loading rate was increased. Results of triaxial tests indicated that the maximum deviator stress and total axial strain increased as the confining pressure and loading rates were increased. Apparently, loading rates from 1 to 2,250 psi/sec do not have a significant effect on the angle of internal friction and cohesion of basalt at confining pressures up to 5,000 psi. Compressional wave velocities recorded in the direction of applied stress increased sharply within about one-half of the maximum deviator stress and then generally remained constant to failure. The difference in the unconfined compressive strength between the slow and the rapid rates of loading for the rocks tested varied considerably. The dynamic compressive strength

DD Form 1 NOV 68 1473 REPLACES DD FORM 1473, 1 JAN 64, WHICH IS OBSOLETE FOR ARMY USE.

Unclassified
Security Classification

factor for the granite was less than 1; for the basalt, 1.35; for the limestone, 1.52; and for the tuff, 1.74. The compressional wave velocity of rock is affected by increases in both the applied axial stress and confining pressure. Velocities recorded in the direction of applied stress increase sharply within about one-half of the maximum deviator stress and then generally level off until failure.

KEY WORDS	LINK A		LINK B		LINK C	
	ROLE	WT	ROLE	WT	ROLE	WT
Granite						
Basalt						
Limestone						
Tuff						
Rock properties						